University of Calgary

PRISM Repository **https://prism.ucalgary.ca**

The Vault Open Theses and Dissertations

2014-08-15

Vascular Reactivity by Blood Oxygen Level Dependent Functional MRI in Cerebral Amyloid Angiopathy: Comparison with Alzheimer's Disease and Assessment of Longitudinal Change

Switzer, Aaron

Switzer, A. (2014). Vascular Reactivity by Blood Oxygen Level Dependent Functional MRI in Cerebral Amyloid Angiopathy: Comparison with Alzheimer's Disease and Assessment of Longitudinal Change (Master's thesis, University of Calgary, Calgary, Canada). Retrieved from https://prism.ucalgary.ca. doi:10.11575/PRISM/28634

http://hdl.handle.net/11023/1687

Downloaded from PRISM Repository, University of Calgary

UNIVERSITY OF CALGARY

Vascular Reactivity by Blood Oxygen Level Dependent Functional MRI in Cerebral Amyloid Angiopathy: Comparison with Alzheimer's Disease and Assessment of Longitudinal Change

by

Aaron Ross Switzer

A THESIS

SUBMITTED TO THE FACULTY OF GRADUATE STUDIES

IN PARTIAL FULFILMENT OF THE REQUIREMENTS FOR THE

DEGREE OF MASTER OF SCIENCE

GRADUATE PROGRAM IN NEUROSCIENCE

CALGARY, ALBERTA

August, 2014

© AARON SWITZER 2014

Abstract

Cerebral amyloid angiopathy (CAA) refers to the deposition of Abeta (Aβ) peptides in the brains small blood vessels leading to hemorrhagic stroke and cognitive impairment. Aβ is toxic to smooth muscle cells and impairs blood flow regulation. Reduced blood oxygen level dependent (BOLD) signal amplitude in response to a visual fMRI task has recently been implicated as a surrogate marker for impaired vascular reactivity in CAA. There have been no studies investigating how the BOLD amplitude changes in other Aβ diseases that present with CAA (Alzheimer's disease (AD) or mild cognitive impairment (MCI)), or how it changes over time in CAA. BOLD amplitudes were lowest in CAA compared to controls but were not lower in MCI or AD. BOLD amplitudes decreased over 1-year in CAA but not in controls. These results provide more evidence for the use of BOLD amplitudes as a measure of impaired vascular reactivity in CAA.

Acknowledgements

I would like to acknowledge those that were instrumental in the completion of the studies in this thesis. First, I would like to thank everyone in the Smith lab for offering assistance, support, and for contributing to a fun and encouraging work environment. Thanks to Dr. Cheryl McCreary, Anna Charlton, Karyn Fischer, Dr. Saima Batool, Rachel Wang, Angela Zwiers, Dr. Shivanand Patil, Dr. Steven Peters, Catherine Collins, Aaron Peterson, Dr. Randall Stafford, and Lindsay Litowski.

Thank you to everyone in the Seaman Family MR Center for always being available to help and provide support. The collaborative work environment of the center definitely enriched my graduate school experience.

Thank you to Dr. Paolo Federico and Dr. Cheryl McCreary for being members of my supervisory committee. Thank you for providing a fresh perspective as I worked through my project and especially for your support along the way.

Many thanks to the lab of Dr. Bradley Goodyear; especially to Alireza Sojoudi for always being available and willing to answer all of my questions regarding FSL, statistics, and just fMRI in general. Special thanks to my co-supervisor Dr. Bradley Goodyear: for mentoring and encouraging me, and for your invaluable input regarding my project.

To my supervisor Dr. Eric Smith: thank you for the time and effort you spent on my project, and thank you for investing your confidence in me and entrusting your data to me. Thank you for providing encouragement and guidance, and for imparting your vast knowledge of small vessel diseases (and more) unto me. You were a great supervisor; thank you for making my graduate school experience outstanding.

To my grandparents, William and Lillian Woods.

Table of Contents

Abstract ii
Acknowledgements iii
Table of Contents v
List of Tables vii
List of Figures and Illustrations viii
List of Symbols, Abbreviations and Nomenclature xi

CHAPTER ONE: INTRODUCTION 1
1.1 Beta Amyloid Pathogenesis 3
1.2 Alzheimer's Disease – Clinical Characteristics 6
1.3 Cerebral Amyloid Angiopathy – Clinical Characteristics 10
1.4 Biomarkers of CAA 17
1.4.1 Hemorrhagic Markers 18
1.4.2 White Matter Change Markers 19
1.4.3 Non-Hemorrhagic Markers 21
1.4.4 Molecular Imaging of Beta-Amyloid 22
1.4.5 Markers of Vascular Function 22
1.5 Vascular reactivity 23
1.6 Functional MRI and the Blood Oxygen Level Dependent Signal 25
1.7 Vascular Reactivity in CAA and AD 27
1.8 Hypotheses 31
1.8.1 Specific Aims 32
1.9 Scientific Contributions and Publication Record 32

CHAPTER TWO: CROSS-SECTIONAL DIFFERENCES IN FMRI BLOOD OXYGEN LEVEL DEPENDENT SIGNAL IN CEREBRAL AMYLOID ANGIOPATHY AND ALZHEIMER'S DISEASE 35
2.1 Introduction 35
Methods 37
2.1.1 Study Population 37
2.1.2 Measurements 38
2.1.2.1 MRI Parameters 38
2.1.2.2 Visual Task 39
2.1.2.3 Visual Evoked Potentials 39
2.1.3 Image Processing 41
2.1.3.1 fMRI Preprocessing 41
2.1.3.2 First-Level fMRI Analysis 41
2.1.3.3 Isolating the 200 Most Active Voxels and BOLD % Signal Change Calculation 42
2.1.3.4 Higher-level fMRI Analysis 44
2.1.3.5 Quantification of WMH Volumes 44
2.1.3.6 Classification of Microbleeds 45
2.1.4 Statistical Analysis 45
2.2 Results 46
2.2.1 Demographics 46

2.2.2 BOLD Amplitude Responses 47
2.2.3 Higher-level fMRI Analysis 48
2.2.4 WMH Volumes and Cerebral Microbleed Counts 48
2.2.5 Multivariable-adjusted Analyses of the Association between Group Status and fMRI BOLD Amplitude, Controlling for Other Factors....51
2.3 Discussion....51
2.4 Conclusion 56

CHAPTER THREE: LONGITUDINAL DECREASE IN FMRI BLOOD OXYGEN LEVEL DEPENDENT SIGNAL IN CEREBRAL AMYLOID ANGIOPATHY 57
3.1 Introduction....57
3.2 Methods 58
3.2.1 Study Population 58
3.2.2 Measurements....58
3.2.3 Image Processing....59
3.2.3.1 fMRI Preprocessing 59
3.2.3.2 Isolating the 200 Most Active Voxels and BOLD % Signal Change Calculation 59
3.2.3.3 Higher Level Analysis 59
3.2.3.4 DICE Coefficient of Overlap....60
3.2.3.5 Calculating BOLD Amplitudes with an Anatomical ROI 61
3.2.3.6 Calculating WMH Volumes and Counting Cerebral Microbleeds....61
3.2.4 Statistical Analysis 62
3.3 Results....63
3.3.1 Demographics....63
3.3.2 BOLD Amplitude Changes 64
3.3.3 Longitudinal WMH Volume and Cerebral Microbleed Count Changes....67
3.4 Discussion....68
3.5 Conclusions....73

CHAPTER FOUR: CONCLUSION AND FUTURE DIRECTIONS....74
4.1 Summary of Results....74
4.2 Overall Conclusions....76
4.3 Future Directions 78
4.4 Implications for Clinical Care....80

REFERENCES: 81

List of Tables

Table 1.1 Boston Criteria for the diagnosis of cerebral amyloid angiopathy 16

Table 2.1 Study inclusion and exclusion criteria 37

Table 2.2 Clinical features of the study populations..... 46

Table 2.3 General linear model results controlling for group, age, and hypertension..... 52

Table 2.4 General linear model results controlling for group age, hypertension, and WMH volume..... 52

Table 3.1 Clinical features of the study populations..... 64

Table 3.2 Mixed model linear regression results. 67

Table 3.3 Microbleeds at baseline and follow-up in CAA. 69

List of Figures and Illustrations

Figure 1.1 The proteolytic cleavage of the amyloid precursor protein. A) APP is processed via the non-amyloidogenic pathway. APP is cleaved by α-secretase, resulting in the excreted sAPPα and membrane bound C83 proteins. Next, γ-secretase cleaves C83, resulting in extracellular P3 and intracellular CTFγ excretion. B) APP is processed via the amyloidogenic pathway. First, APP is cleaved by β-secretase, resulting in the excreted sAPPβ and membrane bound C99 proteins. Following, γ-secretase cleaves C99 resulting in the intracellular CTFγ and extracellular, pathogenic Aβ peptides. This figure is based on information by Zhange *et al.,* 2013.[15] 3

Figure 1.2 Pathogenesis of the amyloid precursor protein in Alzhiemer's Disease and Cerebral Amyloid Angiopathy. APP is cleaved by β- and γ- secretases to produce either $A\beta_{(1-40)}$ or $A\beta_{(1-42)}$. Aβ can be eliminated by proteolytic degradation, crossing the BBB, or through perivascular clearance. In high concentrations, $A\beta_{(1-42)}$ forms oligomers and fibrils with other $A\beta_{(1-42)}$ peptides, which further aggregate into beta-amyloid plaques that deposit into the brains parenchyma. $A\beta_{(1-40)}$ accumulates in the perivascular spaces and deposit in the walls of cerebral small vessels..... 5

Figure 1.3 Cerebral microbleeds on T2*-weighted GRE and SWI axial images. Arrows indicate small, round signal voids classified as cerebral microbleeds. Images taken from a single patient with CAA from the study outlined in this thesis. 19

Figure 1.4 White matter hyperintensities as indicated by hyperintense signal on T2-weighted FLAIR axial images. Panels A, B, and C exhibit mild, moderate, and severe cases of WMH, respectively. Single arrow indicates periventricular lesions and double arrows indicate subcortical lesions. Images taken from 3 patients with CAA from the study outlined in this thesis. 20

Figure 1.5 Blood oxygen level dependent signal in response to a brief neural stimulus..... 27

Figure 1.6 BOLD responses to a visual stimulus task in 31 patients with CAA and 27 healthy controls. Data was extracted from the baseline fMRI visits of participants in the study outlined in this thesis. 29

Figure 2.1 fMRI visual stimulus task. A. 8-Hz contrast reversing checkerboard stimulus for 40 seconds. B. Fixation cross for 40 seconds. 39

Figure 2.2 Typical VEP waveform. The letter N refers to a negative trough and the letter P refers to a positive peak. There are 2 N troughs at 75 ms (N75) and 145 ms (P145) following stimulus onset, and 1 P peak 100 ms (P100) following stimulus onset. The difference between the N75 and P100 signal values is defined as the P100 amplitude ($P100_{amp}$). The time between the stimulus onset and the peak of P100 is defined as the P100 latency ($P100_{latency}$) 40

Figure 2.3. fMRI convolution. The block design representing the neural stimulus based on the fMRI paradigm is convolved with the hemodynamic response function and results in the predicted BOLD signal. 43

Figure 2.4 BOLD amplitudes for healthy controls, MCI, AD, and CAA. CAA BOLD amplitudes were significantly lower than healthy controls. MCI BOLD amplitudes were significantly lower than healthy controls. AD BOLD amplitudes were not lower than healthy controls or higher than CAA. Error bars indicate standard deviation. 47

Figure 2.5 Differences in BOLD activation between each patient group and healthy controls. A) For patients with CAA, fMRI activation was significantly lower in a 35.9 cm^3 volume of the primary visual cortex, compared to healthy controls. B) For patients with MCI, fMRI activation was significantly lower in a 13.3 cm^3 volume of the primary visual cortex, compared to healthy controls. C) For patients with AD, fMRI activation was significantly lower in a 6.6 cm^3 volume of the primary visual cortex, compared to healthy controls. Areas of activation were cluster corrected to $z>2.3$ with a significance of $p<0.05$. 49

Figure 2.6 Differences in WMH volumes between healthy controls, MCI, AD, and CAA. CAA WMH volumes were significantly higher than controls, MCI WMH volumes were significantly higher than healthy controls, and AD WMH volumes were borderline significantly higher than healthy controls and borderline significantly lower than CAA. Error bars represent 5% and 95% confidence intervals. For statistical tests, WMH volumes were log transformed and group differences were determined using an ANOVA with Tukey's post-hoc test. 50

Figure 2.7 BOLD amplitude and microbleed analyses in patients with CAA. A) Cerebral microbleed categories in patients with CAA. B) BOLD amplitudes were significantly lower when patients had higher microbleed counts in CAA. Error bars represent standard deviation. Statistical differences were determined using an un-paired t-test. 50

Figure 3.1 Examples of DICE coefficient overlap analyses. A) The 200 most active voxels mask from each time point almost overlapped completely showing that the anatomical area of activation was relatively consistent across time in a healthy control. B) The 200 most active voxels mask from each time point did not overlap completely showing that the anatomical area of activation varied over time in a patient with CAA. 61

Figure 3.2 Anatomically defined ROI for sensitivity analysis. The ROI was a modified version of the Visual Cortex V1 structure from the Juelich Histological atlas. Mean BOLD amplitudes were extracted from all voxels within the anatomical ROI to normalize the longitudinal sampling of voxels. 62

Figure 3.3 Longitudinal BOLD amplitude changes in response to a visual fMRI task. A) BOLD amplitudes did not change over time in healthy controls ($2.54 \pm 0.58\%$ vs. $2.76 \pm 0.59\%$, $p=0.08$). B) BOLD amplitudes decreased over time in CAA ($1.98 \pm 0.87\%$ vs. $1.64 \pm 0.77\%$, $p=0.04$). Coloured markers denote mean BOLD amplitude and error bars represent standard deviations. Significance was determined by paired t-test. 65

Figure 3.4 Absolute longitudinal difference in BOLD amplitude. There was a significant difference between patients with CAA and healthy controls in BOLD (difference $-0.34 \pm$

0.71% vs. 0.21 ± 0.48% respectively, p=0.007). Error bars represent standard deviations. Significance was determined by unpaired t-test. 65

Figure 3.5 Longitudinal change in BOLD activation. fMRI activation was significantly lower at follow-up within the primary visual cortex in patients with CAA and are shown in blue. fMRI activation was significantly higher in the peri-insular regions, shown in red, which was unexpected and may be due to data outliers. Areas of activation were cluster corrected to $z>2.3$ with a significance of $p<0.05$. 66

Figure 3.6 Relationships between WMH volumes and time or BOLD amplitude change in CAA. A) Longitudinal changes in WMH volumes. WMH volume increased over time (median 1.44 mL, interquartile range -0.56 to 9.25 mL, p=0.017). Triangles denote mean BOLD amplitude and error bars represent standard deviations. B) Relationship between absolute longitudinal difference in BOLD amplitudes and WMH volume progression in CAA. Longitudinal decrease in BOLD amplitude in the visual cortex was not correlated with WMH volume increase over time (r=0.08, p=0.72). WMH volume data was log transformed and significance was determined by Spearman correlation coefficient. 68

Figure 3.7 Relationships between baseline microbleed counts and baseline BOLD amplitude or BOLD change over time in CAA. A) Patients with more microbleeds at baseline had low BOLD amplitudes at baseline (2.54 ± 0.69% vs. 1.57 ± 0.78%, p=0.009). B) Patients with more microbleeds at baseline was not associated with greater BOLD loss over time (difference -0.19 ± 0.74%, p=0.56). Error bars represent standard deviations..... 69

List of Symbols, Abbreviations and Nomenclature

Symbol	Definition
AD	Alzheimer's Disease
APOE	Apolipoprotein E
APP	Amyloid Precursor Protein
ATP	Adenosine Triphosphate
Aβ	Abeta
BBB	Blood Brain Barrier
BET	Brain Extraction Tool
BOLD	Blood Oxygen-level Dependent
CAA	Cerebral Amyloid Angiopathy
cAMP	Cyclic Adenosine Monophosphate
CBF	Cerebral Blood Flow
CDR	Clinical Dementia Rating scale
CIPAC	Calgary Image Processing and Analysis Center
CMBs	Cerebral Microbleeds
CT	Computed Tomography
CTFγ	Carboxy-terminal Fragment
DSM-IV-TR	Diagnostic and Statistical Manual of Mental Disorders, fourth edition
DTI	Diffusion Tensor Imaging
DWI	Diffusion Weighted Imaging
FAD	Familial Alzheimer's Disease
FAVR	Functional Assessment of Vascular reactivity
FDG	[^{18}F]Fluorodeoxy Glucose
FEAT	fMRI Expert Analysis Tool
FLAIR	Fluid Attenuated Inversion Recovery
FLAME	FMRIB's Local Analysis of Mixed Effects
fMRI	Functional Magnetic Resonance Imaging
FSL	FMRIB Software Library
FWHM	Full Width Half Maximum
GABA	γ-aminobutyric Acid
GLM	General Linear Model
GRE	Gradient Recalled Echo
GRE-EPI	Gradient-recalled Echo – Echo Planar Imaging
ICHs	Intracranial Hemorrhages
IR-SPGR	Inversion-recovery Spoiled Gradient Recalled
LADIS	The LeukoAriosis and DISability Study
LRP-1	Low-density Lipoprotein receptor-related Protein
MCFLIRT	Motion Correction: FMRIB's Linear Image Registration Tool
MCI	Mild Cognitive Impairment
MMSE	Mini Mental Status Exam
MNI	Montreal Neurological Institute

NADPH	nicotinamide adenine dinucleotide phosphate
NFTs	Neurofibrillary Tangles
NIA	National Institute of Aging
NINCDS-ADRDA	National Institute of Neurological Disorders and Stroke-Alzheimer Disease and Related Disorders
NMDA	N-methyl-D-aspartate
NO	Nitric oxide
PET	Positron Emission Tomography
PiB	Pittsburgh Compound B
PVS	Perivascular Spaces
RAGE	Receptor for Advanced Glycosylation End Products
ROS	Reactive Oxygen Species
sAPPα or β	Soluble Amyloid Precusor Protein α or β
STRIVE	Standards for ReportIng Vascular changes on nEuroimaging
SWI	Susceptibility Weighted Images
TFNE	Transient Focal Neurological Episodes
VEP	Visual Evoked Potentials
WMH	White Matter Hyperintensity

Chapter One: **Introduction**

Over the last 100 years, life expectancy has risen from 40 to 80 years old, and with this increase came the escalation of age-related disease burden. Stroke and dementia have become two of the most common causes of death in Canada. The risk of developing stroke, dementia, or both in men and women aged 65 or older is one in three and one in four, respectively.[1] The most common cause of dementia is Alzheimer's disease (AD).[2]

AD affects nearly 1.5% of the Canadian population according to a study done by the Alzheimer's Society in 2008.[3] AD is defined as the clinical presentation of progressive dementia, including impairment in episodic memory formation and other cognitive domains, and the neuropathological presence of intracellular neurofibrillary tangles (NFTs) and extracellular beta-amyloid plaques causing hippocampal neuritic and synaptic loss.[4] The beta-amyloid plaques result from aberrant processing of the amyloid precursor protein (APP) generating pathogenic Abeta (Aβ) peptides, which further aggregate and deposit into different tissues of the brain.[5] Dementia from AD is preceded by mild cognitive impairment (MCI), a cognitive syndrome where there are clinical concerns about memory and objective evidence of poor performance on memory tests, but essentially preserved social and occupational functioning.[6] Because MCI can have many causes other than AD, much research focuses on determining the cause of MCI, including which cases of MCI are due to AD, and to identify markers that predict decline from MCI to dementia, which occurs in 5-20% of MCI cases per year.[7]

Cerebral amyloid angiopathy (CAA) occurs when beta-amyloid deposits in the media and adventitia of leptomeningeal and cortical arteries, arterioles, and capillaries.[8] CAA clinically manifests as small asymptomatic brain hemorrhages and in severe cases can result in

intracerebral hemorrhagic stroke.[9] CAA has also been associated with other manifestations including transient neurological symptoms, similar to transient ischemic attacks, and cognitive impairment.[10] Most patients with clinically recognized CAA do not have AD, even though both diseases are marked by beta-amyloid accumulation. In persons with AD, CAA is frequently present pathologically but is usually clinically silent—for example, symptomatic hemorrhagic stroke is not common in AD.[11] At present, it is difficult to determine the severity of CAA pathology antemortem. Therefore, there is a push for the development of new biomarkers that can accurately portray the health of CAA-affected vasculature, in order to aid in diagnosis, determine the mechanisms of CAA-related symptoms, and potentially measure the effectiveness of investigational treatments for CAA.

The goal of this thesis is to determine the effectiveness of functional magnetic resonance imaging (fMRI) as a biomarker of vascular reactivity in CAA. Specifically, our aims are: (1) to determine a means of distinguishing CAA from similar disease states such as mild cognitive impairment and AD, by establishing impaired vascular reactivity as a viable biomarker of CAA severity; and (2) to characterize the longitudinal profile of fMRI detected vascular reactivity in CAA. The results from this thesis will provide more evidence for the understanding of impaired vascular reactivity as a disease mechanism for CAA, as well as establish the basis for a novel surrogate marker that could be used to measure CAA severity.

This introductory chapter will review Aβ pathogenesis as it relates to AD and CAA, current biomarkers of CAA severity, the mechanisms behind vascular reactivity, and the physiological basis of the fMRI signal. A review of the scope and specific hypotheses of the thesis will conclude this chapter.

1.1 Beta Amyloid Pathogenesis

APP is an integral transmembrane protein that resides on the surface of glial and neuronal cells.[12] In humans, there are eight different splice variants of APP, ranging from 365-770 amino acids in length.[13] APP is ubiquitously expressed in the brain, and while the exact biological function is not entirely understood, it is thought to be involved in the modulation of synaptic generation, synaptic plasticity, and neurite outgrowth.[14] APP can be proteolytically processed into smaller soluble metabolites that are cleared by two pathways: either the non-amyloidogenic pathway or the amyloidogenic pathway (Figure 1.1).[15] In the non-amyloidogenic pathway, α-secretase cleavage of APP produces extracellular APP α (sAPPα) and membrane-bound C83. The remaining C83 fragment is further processed by γ- secretase, producing the extracellular p3

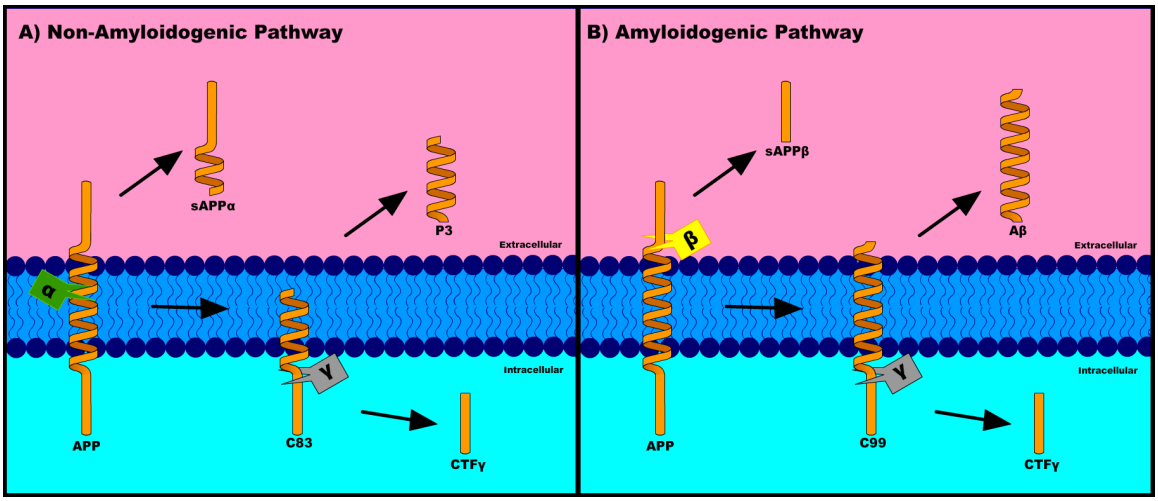

Figure 1.1 The proteolytic cleavage of the amyloid precursor protein. A) APP is processed via the non-amyloidogenic pathway. APP is cleaved by α-secretase, resulting in the excreted sAPPα and membrane bound C83 proteins. Next, γ-secretase cleaves C83, resulting in extracellular P3 and intracellular CTFγ excretion. B) APP is processed via the amyloidogenic pathway. First, APP is cleaved by β-secretase, resulting in the excreted sAPPβ and membrane bound C99 proteins. Following, γ-secretase cleaves C99 resulting in the intracellular CTFγ and extracellular, pathogenic Aβ peptides. This figure is based on information by Zhange *et al.*, 2013.[15]

protein and the intracellular carboxy-terminal fragment (CTFγ). In the amyloidogenic pathway, APP is cleaved by β-secretase resulting in the extracellular sAPPβ and membrane-bound C99. C99 is further processed by γ-secretase to produce CTFγ and the pathogenic Aβ peptide.

Secreted Aβ peptides range in length from 39-42 amino acids, depending on the exact site of γ-secretase cleavage, but the two most common forms are the $A\beta_{(1-40)}$ and $A\beta_{(1-42)}$ peptides.[16] $A\beta_{(1-40)}$ is the most abundant isoform found in the vascular deposits of CAA,[16] and is produced when γ-secretase cleaves APP at the Valanine-40 site of the Aβ region.[17] $A\beta_{(1-42)}$ is more abundant in plaques found in AD,[16] and is produced when γ-secretase cleaves APP at the Alanine-42 site of the Aβ region.[17] Both variants accumulate in the extracellular spaces of the brain (Figure 1.2).[18]

Although the cause of AD is not known, current theories suggest a prominent role for decreased clearance of the potentially toxic Aβ.[19] Possible fates for Aβ include degradation by extracellular proteolytic enzymes, retention in extracellular solution and subsequent removal by perivascular drainage, and expulsion across the blood brain barrier.[20] The endopeptidases insulysin and neprilysin are the enzymes responsible for degrading Aβ. Increased activity of either enzyme has been shown to decrease extracellular levels of Aβ in mouse models.[19] Aβ can dissolve in the interstitial fluids, which move along the basement membrane of adjacent arterioles within the perivascular spaces, and drain into the cervical lymph nodes. Aβ requires specialized carrier molecules to help it cross the blood brain barrier (BBB), which is comprised of capillaries with tightly joined endothelial cells that limit the diffusion of specific molecules from entering the brain.[21] Aβ can bind to either low-density lipoprotein receptor-related protein (LRP-1) or the receptor for advanced glycosylation end products (RAGE), facilitating their

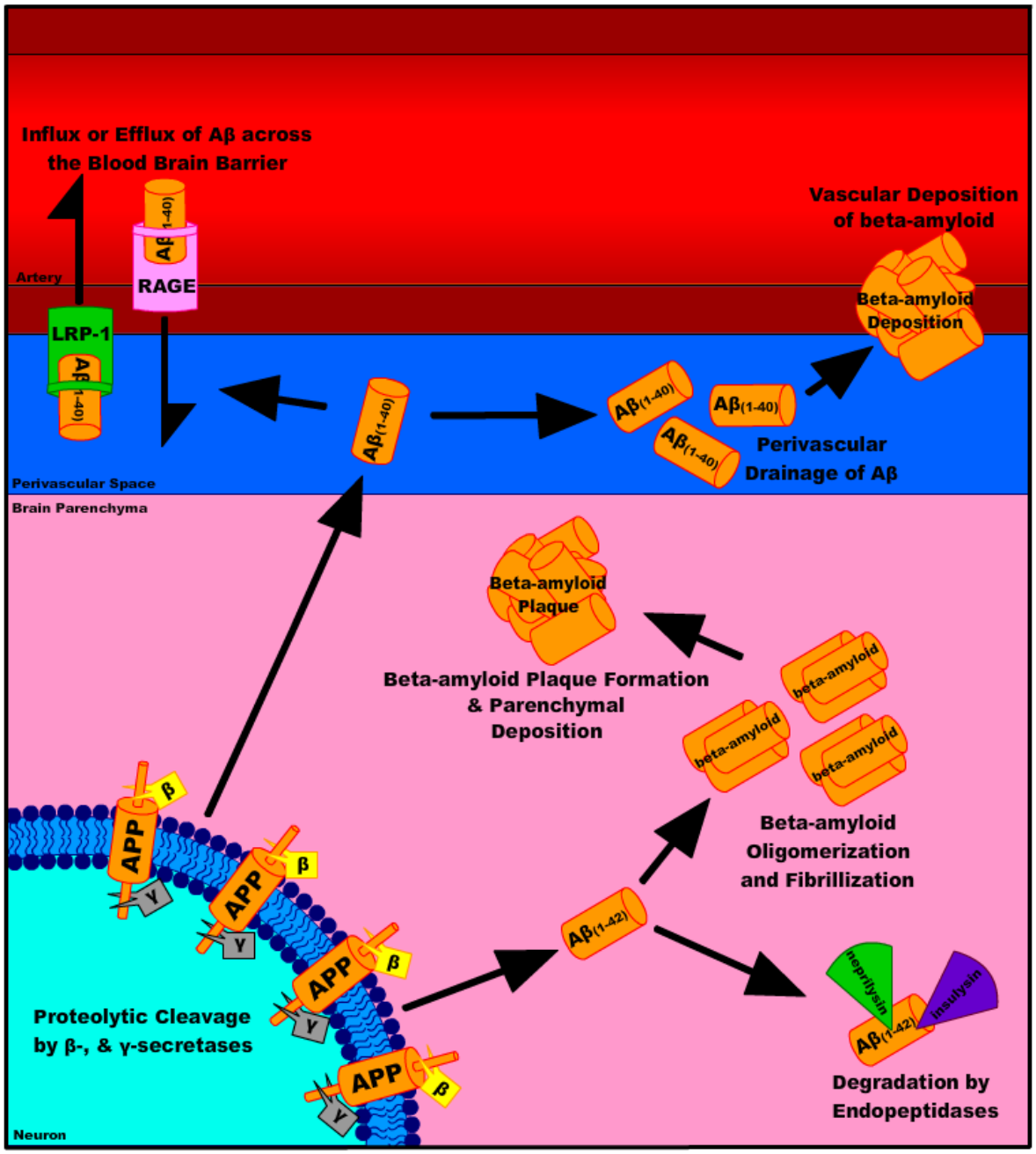

Figure 1.2 Pathogenesis of the amyloid precursor protein in Alzhiemer's Disease and Cerebral Amyloid Angiopathy. APP is cleaved by β- and γ- secretases to produce either $A\beta_{(1-40)}$ or $A\beta_{(1-42)}$. Aβ can be eliminated by proteolytic degradation, crossing the BBB, or through perivascular clearance. In high concentrations, $A\beta_{(1-42)}$ forms oligomers and fibrils with other $A\beta_{(1-42)}$ peptides, which further aggregate into beta-amyloid plaques that deposit into the brains parenchyma. $A\beta_{(1-40)}$ accumulates in the perivascular spaces and deposit in the walls of cerebral small vessels.

efflux and influx, respectively, across the BBB.[19] As the brain ages, each different type of elimination described above begins to break down.[22] When production of Aβ exceeds the brain's ability to clear it, Aβ aggregation and deposition may result.

$A\beta_{(1-42)}$ is less soluble than its shorter $A\beta_{(1-40)}$ counterpart.[18] Both variants have almost the exact same primary structure; however, $A\beta_{(1-40)}$ is more likely to undergo the conformational change required to form β-pleated sheets with other soluble $A\beta_{(1-40)}$ peptides. Both $A\beta_{(1-42)}$ and $A\beta_{(1-40)}$ accumulation can result in oligomerization, fibrillization, and subsequently deposition into the brain tissue as senile plaques or into the vascular media as CAA, respectively.

Beta-amyloid deposits can trigger a number of detrimental events including oxidative stress, alteration of BBB permeability, and release of inflammatory factors, and may indirectly cause cellular toxicity.[23] As previously mentioned, the location of beta-amyloid deposition determines the degree to which AD and CAA are present.[18] The molecular events that determine whether beta-amyloid deposits in the brain (AD) or vasculature (CAA) are not well understood; however, one factor that is known is that the larger less soluble $A\beta_{(1-42)}$ species is more common in the senile plaques than in vascular beta-amyloid deposits. The Aβ in CAA is felt to be mostly derived from neuronal APP processing followed by transport of Aβ to the vessels, without much contribution from local APP synthesis and processing.[22]

1.2 Alzheimer's Disease – Clinical Characteristics

Alzheimer's disease is the most common cause of dementia in the elderly population[2,24]. It is characterized by progressive cognitive decline and the neuropathological presence of NFTs and plaques. While the majority of AD cases occur sporadically, 5% of all cases are caused by autosomal dominant mutations, also known as familial AD (FAD).[17] FAD can result from

mutations in APP, or presenilin 1 and 2 genes.[25] As it is difficult to identify the pathological hallmarks of AD during life, AD diagnosis is primarily clinical and relies on the presence of clinically disabling cognitive symptoms with objective evidence of impairment on cognitive testing.

Alois Alzheimer described the disease that bears his namesake in 1906, based on his observations of a 51 year old patient named Auguste D.[26] Clinically, Ms. D presented with progressive cognitive decline, delusions, hallucinations, and marked psychosocial deficits. Her autopsy showed arteriosclerotic changes, atrophy of brain tissue, and the hallmark beta-amyloid plaques and NFTs. It was not until 1910 that the pathology received its moniker, which was officially coined by Emil Kraepelin under a modified description, excluding delusions, hallucinations, and arteriosclerotic changes from the general definition.

In 2008, the prevalence of AD in Canada was about 1.5% according to the Alzheimer's Society of Canada.[3] There were over 103,700 new cases of AD in 2008, which amounts to one AD diagnosis every 5 minutes. According to the Canadian Institutes of Health Research, the prevalence of AD and related dementias grew to affect 2.2% of the Canadian population in 2011.[27] The economic burden of AD alone in 2011 was $33 billion, which is projected to increase to $293 billion by 2040. There are numerous risk factors associated with AD, increasing age having the greatest impact.[28] According to the Baltimore Longitudinal Study of Aging, the prevalence of AD doubles every 5 years after the age of 65.[29] Recently, vascular risk factors have been associated with the incidence of AD.[30] There has been accumulating evidence that suggests AD is linked to midlife vascular risk factors such as hypercholesterolemia, hypertension,

diabetes mellitus, and obesity.[2,30-39] Other possible risk factors include physical inactivity, depression, smoking, and low educational attainment.[2]

The cause of AD is not fully understood, with the exception of the rare autosomal dominant FAD cases, which are caused by mutations in the APP, or presenilin 1 and 2 genes.[17] The "amyloid hypothesis" states that the accumulation of extracellular Aβ leads to the clinical outcomes observed in AD.[28] This hypothesis is based on the fact that the aberrant processing of APP is responsible for most forms of FAD.[40] Despite this, clinical trials that aim to remove Aβ from the brain have not been successful in reducing the incidence of AD.[41] It is likely that neuronal loss in AD may be due to indirect effects of Aβ accumulation, such as oxidative stress,[42] inhibition of anti-apoptotic pathways,[43,44] the deleterious effects of intracellular NFTs,[45] or a combination of any of these effects.[5]

Clinically, patients with probable AD typically present with an impaired ability to acquire and consolidate new memories, impaired reasoning, impaired visuospatial abilities, impaired language functions, or changes in personality and behavior such as agitation or aggression, psychosis, and insomnia.[46] These symptoms have a rather insidious onset, and in combination lead to the decline in the patient's autonomy by precluding them from participating in daily tasks such as handling finances, grooming, and decision-making.[28] Depression is often a comorbidity of AD and occurs in nearly 50% of all cases.[47] Of the behavioural changes seen in AD, aggression, depression, insomnia, anxiety, and psychosis may be treatable during the progression of the disease.

In order to diagnose AD in the clinic, physicians frequently rely on criteria set forth by the Diagnostic and Statistical Manual of Mental Disorders, fourth edition (DSM-IV-TR) and the

National Institute of Neurological Disorders and Stroke-Alzheimer Disease and Related Disorders (NINCDS-ADRDA) working group.[4] The DSM-IV-TR criteria require that the patient present with memory loss in addition to a decline in one other cognitive domain, and for those clinical features to interfere with normal everyday life. The NINCDS-ADRDA criteria supports a probabilistic diagnosis of AD if symptom onset appears to be insidious and if there are no other possible causes, either neural or systemic, of memory loss. Both criteria are evaluated using the patient's medical history, performance on cognitive tests such as the mini mental status exam (MMSE),[48] and in appropriate cases by excluding other causes of dementia using neuroimaging.[28] Newer research criteria for AD incorporate information based on neuroimaging biomarkers such as MRI and positron emission tomography (PET). [46] MRI can detect structural changes due to AD-related degeneration, such as hippocampal atrophy.[4] [^{18}F]fluorodeoxy glucose (FDG) PET shows a pattern of hypometabolism, indicative of decreased synaptic activity, in temporoparietal as well as the posterior cingulate gyrus in AD.[49] Pittsburgh compound B (PiB) and other beta-amyloid binding PET ligands provide *in vivo* imaging of neural amyloid deposition in areas associated with AD pathology. These neuroimaging markers are not sufficient to accurately diagnose AD on their own, but they can be combined with clinical findings to help physicians better diagnose the disease.[28] However, these supportive biomarkers are either expensive and not widely available (PET scanning) or not yet approved by Health Canada (beta-amyloid PET ligands) and therefore are not yet incorporated into routine clinical practice.

Currently, there is no cure for AD, but there are treatments designed to improve clinical symptoms of memory loss.[28] The acetylcholinesterase inhibitors donepezil, rivastigmine, and galantamine increase the amount of acetylcholine that is available for synaptic transmission in

cholinergic neurons of the hippocampus and neocortex.[50] These areas of the brain are highly affected by AD pathology and acetlycholinesterase inhibitors are effective in treating memory and attention deficits in patients with mild to moderate AD. Memantine is an N-methyl-D-aspartate (NMDA) receptor antagonist that is believed to protect glutamatergic neurons from sensitization due to aberrant increases in activity caused by AD pathology, resulting in impaired neuronal function. Clinical trial data support a role for memantine in moderate to severe dementia caused by AD. Lastly, the treatment of behavioural symptoms, such as aggression, psychosis, or agitation, could increase the quality of life for patients and caregivers, while reducing the economic and care burdens of AD on society. There are many unproven potential drug candidates for AD therapies including Aβ removal, secretase inhibition, and tau phosphorylation inhibition; however, none have been able to produce disease-modifying effects in clinical trials as of yet.[50]

1.3 Cerebral Amyloid Angiopathy – Clinical Characteristics

CAA is a common cause of hemorrhagic stroke. It is defined as the accumulation of beta-amyloid in the media and adventitia of the leptomeningeal and cortical arteries and arterioles of the brain.[8] Recently, CAA has been identified as an independent cause of cognitive impairment and dementia.[51] Currently, CAA can be probabilistically identified using the Boston Criteria[52,53] and characteristic biomarkers.[54]

In 1909, Gustav Oppenheim discovered vascular deposition of beta-amyloid for the first time, where he noticed areas of “gland-like necrosis” in the brain parenchyma adjacent to hyalinized capillary walls in 43% of the brains of individuals with dementia and AD pathology

that he had autopsied.[55] It was not until 1954 that Stefano Pantelakis first identified all of the hallmark pathological features of CAA that physicians are familiar with today.[18]

Cerebral amyloid angiopathy is present pathologically, to varying degrees, in 20-40% of the normal aged population and in 50-60% of the population afflicted by dementia.[56] In the elderly population, CAA-related intracerebral hemorrhages (ICHs) account for 5-20% of all hemorrhagic stoke.[18] The only identified risk factors for sporadic CAA are the presence of AD, increasing age, and the presence of the apolipoprotein E (APOE) ε2 and ε4 alleles. APOE is a cholesterol carrier; individuals that possess the APOE ε4 allele tend to produce an isoform of APOE that complexes with $A\beta_{(1-42)}$ and inhibits its removal.[57] A recent study has shown that mice expressing the human APOE ε4 allele have beta-amyloid deposits in the brain vasculature, and mice not expressing the allele do not.[58] APOE ε4 carriers have been implicated as having increased CAA severity, and APOE ε2 carriers have been implicated as having increased risk for CAA-related hemorrhage.[59] There are rare heritable forms of CAA, which are autosomal dominant disorders that present in selected families living in very specific geographical locations.[18] The presentation of CAA varies between different familial forms; however hereditary CAA often has a more severe clinical progression with earlier onset, as well as an earlier age of stroke or death compared to sporadic CAA.

Pathophysiologically, beta-amyloid deposits in the media and adventitia of the cerebral vasculature in CAA, without affecting non-cerebral vasculature.[8] Histologically, there are two types of CAA, CAA-Type 1 and CAA-Type 2.[60] CAA-Type 1, or pericapillary CAA, refers to beta-amyloid deposition in leptomeningeal or cortical arteries and arterioles, and in cortical capillaries; CAA-Type 2, or arteriolar CAA, does not affect the cortical capillaries. Originally, it

was thought that Aβ found in CAA deposits had a plasma origin, as it was found in circulation and there was a mechanism for transferring Aβ across the BBB in both directions.[18] However, this was unlikely, as transgenic mouse models that had several fold increases in circulating Aβ did not exhibit more vascular beta-amyloid deposition than mouse models with lower circulating Aβ concentrations. It was discovered that smooth muscle cells, pericytes, and endothelial cells within artery walls expressed APP and maintained the capacity to produce large amounts of Aβ, leading to an increase in vascular deposition.[22] This would explain the amyloidosis found in the arteries and arterioles, but does not explain deposition in the capillaries as they are devoid of smooth muscle cells. Most likely, Aβ of vascular origin contributes to the inhibition of neuronal Aβ perivascular drainage.

CAA pathology can occur as a result of decreases in Aβ proteolytic degradation, BBB transport, and perivascular clearance.[22] Neprilysin is an endopeptidase responsible for the degradation of Aβ.[19] As neprilysin activity decreases, CAA severity increases.[22] This is suggested by the fact that all familial forms of mutant APP produce Aβ that is resistant to degradation by neprilysin, which leads to the development of CAA. With age, the LRP-1 mediated Aβ transport across the BBB can be reduced. When Aβ degradation and BBB transport fail, Aβ is diverted to the perivascular spaces, which creates a bottleneck for Aβ clearance and thus a subsequent increase in vascular deposition. Pathological studies have shown there is preferential deposition of beta-amyloid at the branches of arteries and small arterioles, again likely due to the bottleneck in perivascular drainage caused by the morphology of the vasculature. Finally, the APOE ε4 allele is associated with down-regulated clearance of $A\beta_{(1-40)}$, thereby increasing the incidence of vascular deposition.[18]

Beta-amyloid deposition has a multitude of consequences for the affected vasculature. As Aβ accumulates in the perivascular spaces of the cerebral vasculature, it can alter the composition of the basement membranes, destroy artery walls, and induce inflammatory changes.[22] Beta-amyloid deposition in the arteries and capillaries decreases collagen IV, laminin, and perlecan content in the basement membranes. These proteins maintain the structure of the basement membranes of the arteries, so beta-amyloid deposition results in the weakening of the structure of its host vasculature. Beta-amyloid deposition can cause focal aneurysm formation, necrosis, and loss of smooth muscle cells, and can cause the outer vessel to separate from its inner layers. This effect is called double barreling as the vessels appear to be two concentric circles in the staining of pathological sections of brains exhibiting CAA. Finally, beta-amyloid deposition in the leptomeningeal arteries can induce the accumulation of macrophages causing inflammation. This type of inflammation can cause patients to present with headaches, changes in mental state, and in severe cases cause seizures.

A large portion of the aged population presents with some varying degree of CAA pathology without identifiable clinical consequences. Therefore, CAA appears to be completely asymptomatic in some individuals.[18] However, some individuals with moderate to severe CAA can have a number of clinical conditions. The most common of these conditions is the increased incidence of lobar intracerebral hemorrhage (ICH). The next common clinical feature is cognitive impairment, which presents as loss of memory, disturbances in consciousness, and focal neurological deficits.

In the elderly population, CAA-related ICH accounts for 5-20% of all ICH.[18] Due to beta-amyloid deposition being widespread and favoring the leptomeningial and cortical arteries, most

CAA-related ICHs occur in multiple or recurrent lobar locations. Beta-amyloid deposition weakens the walls of the blood vessels making them more prone to rupturing. Possession of the APOE ε2 allele has been shown to be associated with increased risk of CAA-related hemorrhage by encouraging fibrinoid necrosis and other vasculopathies associated with CAA.[61] In contrast to ICH caused by hypertension, the main alternative cause of ICH, patients with CAA-related ICH have a much higher risk of recurrence (approximately 10% per year vs. only 1-2% per year).[62]

The identification of CAA as an independent cause of cognitive impairment is a fairly recent discovery.[51] Along with weakening of the blood vessel walls, beta-amyloid deposition can completely destroy the lumen of the vessel, which leads to microinfarctions that affect surrounding brain tissues.[18] These microinfarctions can induce cognitive impairment, depression, and dementia.[63] The exact clinical profile of an individual with CAA has yet to be elucidated; however, clinical studies in humans have shown reductions in episodic memory and lower perceptual speed, with no effect on visuospatial skills, working memory, or executive function in moderate to severe CAA.[64]

Along with changes in cognition, CAA can present with transient focal neurological episodes (TFNE).[10] TFNE are classified as either positive symptoms, such as the perception of sensory stimuli that are not there, or as negative symptoms, such as numbness or weakening of the extremities. Both positive and negative TFNE can last up to 10 minutes per episode. A multicenter cohort study of 172 patients with CAA observed TFNE in 14.5% of the participants, and that these events were closely related to the identification of superficial cortical siderosis or convexity subarachnoid hemorrhages on neuroimaging.[10] TFNE have a high diagnostic value in CAA as it can be used to predict an early risk of symptomatic ICH.

A small subset of patients with CAA also presents with vasculitis, which is damage to the blood vessels due to inflammation.[65] CAA-related inflammation can present with seizures, subacute cognitive decline, white matter lesions, and headaches. CAA-related inflammation shows promise in responding to immunotherapeutic interventions.

Like many diseases related to dementia, a definite diagnosis of CAA is based only on autopsied pathological evidence. The Boston criteria are a pathologically validated and highly specific set of instructions used to diagnosis CAA during life (Table 1.1).[52,53] "Definite CAA" is defined as a full postmortem examination that shows evidence of lobar, cortical, or corticosubcortical hemorrhages, severe CAA with vasculopathy, and the absence of other diagnostic lesions. "Probable CAA with supporting pathology" is defined as biopsied tissue showing pathological evidence as described in the definite CAA diagnosis. A "Probable CAA" diagnosis relies on patients being 55 years of age or older and having clinical and MRI or computed tomography (CT) evidence of multiple lobar hemorrhages, or a single focal lobar ICH with one or more additional cerebral microbleeds restricted to lobar, cortical, or corticosubcortical regions. Cerebral microbleeds are evidence of microscopic hemorrhages that appear as signal void on T2*-weighted MR images (Figure 1.3). "Possible CAA" is similar to the probable CAA diagnosis, but only requires evidence of a single lobar, cortical, or corticosubcortical hemorrhage. In addition to the frequent presence of cerebral microbleeds, CAA patients often have a large burden of MRI white matter hyperintensities of presumed vascular origin (Figure 1.4). A recent revision of these criteria allow for the presence of cortical sulcal siderosis as additional MRI evidence of past bleeding episodes.[53]

Table 1.1 Boston Criteria for the diagnosis of cerebral amyloid angiopathy

Definite CAA	Full post-mortem examination showing severe CAA
Probable CAA with supporting pathology	Pathological tissue (evacuated hematoma or cortical biopsy) showing: • Lobar hemorrhage with some degree of CAA • Absence of other diagnostic lesions
Probable CAA	Clinical data and MRI or CT demonstrating: • Multiple hemorrhages restricted to lobar regions (cerebellar hemorrhage allowed) • Age ≥ 55 years • Absence of other causes of hemorrhage
Possible CAA	Clinical data and MRI or CT demonstrating single lobar hemorrhage in the absence of other causes of hemorrhage

These criteria have been validated in a neuropathological study.[52] The presence of cortical sulcul siderosis is also consistent with cerebral amyloid angiopathy.[53]

Currently, there are no treatments for CAA, except for the rare cases of CAA-associated inflammation where corticosteroid treatment can reduce vasogenic edema and improve clinical symptoms.[18] A recent randomized, placebo-controlled trial suggested that lowering blood pressure might protect against CAA-related ICH.[66] However, there are currently no proven disease-modifying treatments that reduce clinical symptoms by removing beta-amyloid plaques or preventing Aβ production. There is an early phase clinical trial of the anti-Aβ monoclonal antibody ponezumab (clinicaltrials.gov NCT01821118), which aims to clear vascular bound Aβ.[54] One of the barriers to more efficient research on treatments for CAA is the lack of validated surrogate outcome markers that change over a relatively short period of time. Our

group has previously shown that using fMRI, the amplitude of the blood oxygen level dependent (BOLD) measurements in response to a visual stimulus was reduced in the visual cortex of patients with CAA relative to controls.[67] However, there are no data on fMRI BOLD amplitude change over time in CAA. To be useful as a marker of disease progression, and potentially of response to therapy, the change over time must be measured. Therefore, one of the aims of this thesis is to determine if changes in blood flow regulation using fMRI, can be detected over a 1-year period in CAA.

1.4 Biomarkers of CAA

At present, the only way to definitively identify CAA is by histological evidence found from tissue extracted through highly invasive biopsies or by autopsy.[18] Therefore, less invasive or non-invasive methods of acquiring indicators of CAA pathology have been developed in an effort to aid in diagnosing CAA and determining its prognosis. Several neuroimaging biomarkers of CAA have been developed including identification of symptomatic ICH on CT and MRI,[54] the presence of cerebral microbleeds (CMBs) on gradient recalled echo (GRE) and susceptibility weighted images (SWI),[68] changes in white matter appearance such as white matter hyperintensities of presumed vascular origin (WMH) on T2-weighted fluid attenuated inversion recovery (FLAIR) images[69] and abnormal white matter microstructure on diffusion tensor imaging (DTI),[70] the detection of enlarged perivascular spaces (PVS) on T2-weighted MRI,[71] the presence of microinfarcts on diffusion weighted imaging (DWI),[72] the presence of beta-amyloid by PiB PET[73] and impaired vascular reactivity on fMRI.[67,74]

1.4.1 Hemorrhagic Markers

Intracerebral hemorrhage is defined as the accumulation of blood within the brain parenchyma or ventricular system, which occurs spontaneously and does not result from acute trauma.[75] CAA-related ICH is a result of vascular rupture due to weakening of cerebral vessels by beta-amyloid deposition.[18] ICH is reliably detected on CT, indicated by a bright signal mass of the hematoma within the parenchyma of the brain, and on MRI, represented chronically as heterogeneous signal surrounded by a border of hypointense signal on a T2*-weighted GRE image.[76]

Cerebral microbleeds are evidence of microscopic hemorrhages.[68] When these small bleeds occur, macrophages digest the hemoglobin; the heme iron of hemoglobin remains stored in macrophages and microglia as hemosiderin, near the hemorrhage site.[77] The iron in hemosiderin is ferromagnetic and leads to the local dephasing of the MR signal, appearing as small, signal voids on T2- and T2*-weighted MR sequences (Figure 1.3). CMBs are not specific to CAA, and can occur in other small vessel diseases too. However, there is a spatial pattern of CMB accumulation that is highly specific for CAA. When CMBs are spatially confined to lobar brain locations, excluding CMBs located in deep brain structures such as the basal ganglia or thalami, then they are a highly specific marker for CAA. CMBs located in the basal ganglia and thalami are predominantly caused by hypertension.[68] This spatially distinct pattern of hemorrhaging forms the basis for the pathologically validated Boston criteria. Patients with CAA that have more CMBs are at higher risk for symptomatic ICH and cognitive impairment.[68] Lobar CMBs are distributed with a posterior predominance in CAA; in other words, they are more prevalent in the occipital and temporal regions than in the parietal and frontal regions.[68] This matches the distribution of vascular beta-amyloid pathology seen in autopsy studies.[78]

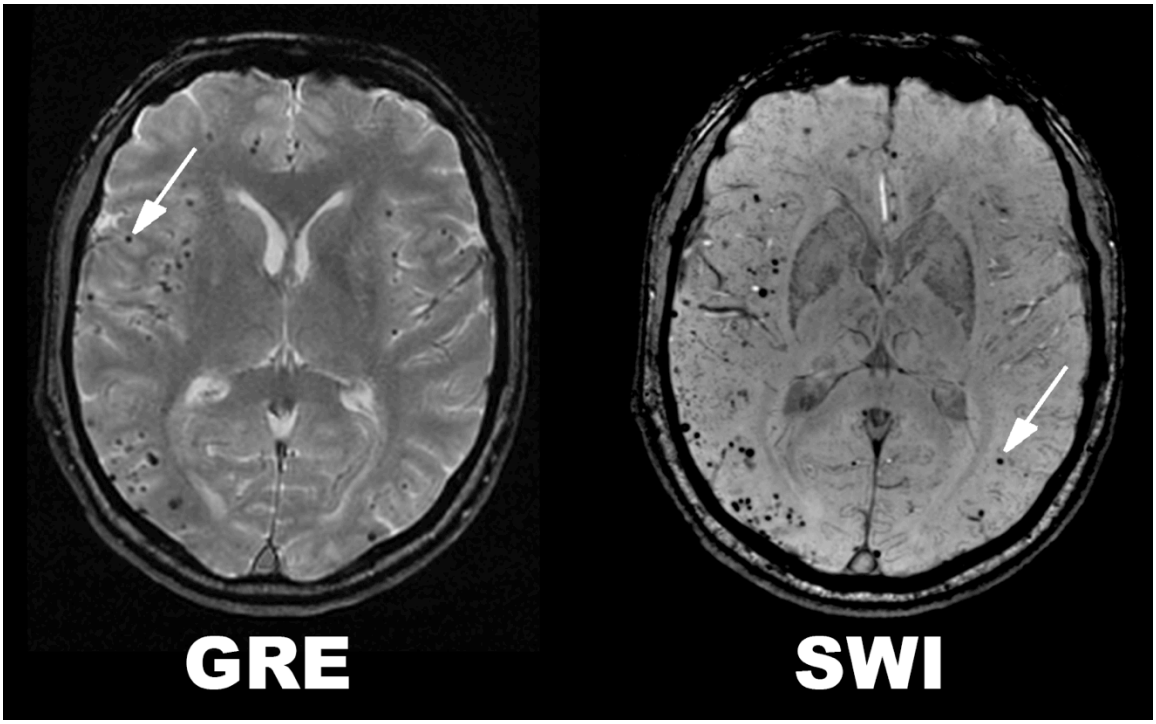

Figure 1.3 Cerebral microbleeds on T2*-weighted GRE and SWI axial images. Arrows indicate small, round signal voids classified as cerebral microbleeds. Images taken from a single patient with CAA from the study outlined in this thesis.

1.4.2 White Matter Change Markers

White matter hyperintensities are believed to be caused by the demyelination of axons due to poor blood supply to the white matter.[79] WMHs are named as such because they present as areas of hyperintense signal on T2-weighted FLAIR images, and as areas of hypointense signal on CT, in periventricular and subcortical white matter regions (Figure 1.4). [69] Over time, breakdown of the BBB and chronic ischemia can occur as a result of WMH accumulation.[80]

The LeukoAraiosis and DISability study (LADIS) was designed to determine if WMHs were independent contributors to disability in old age.[81] They provided a wealth of knowledge

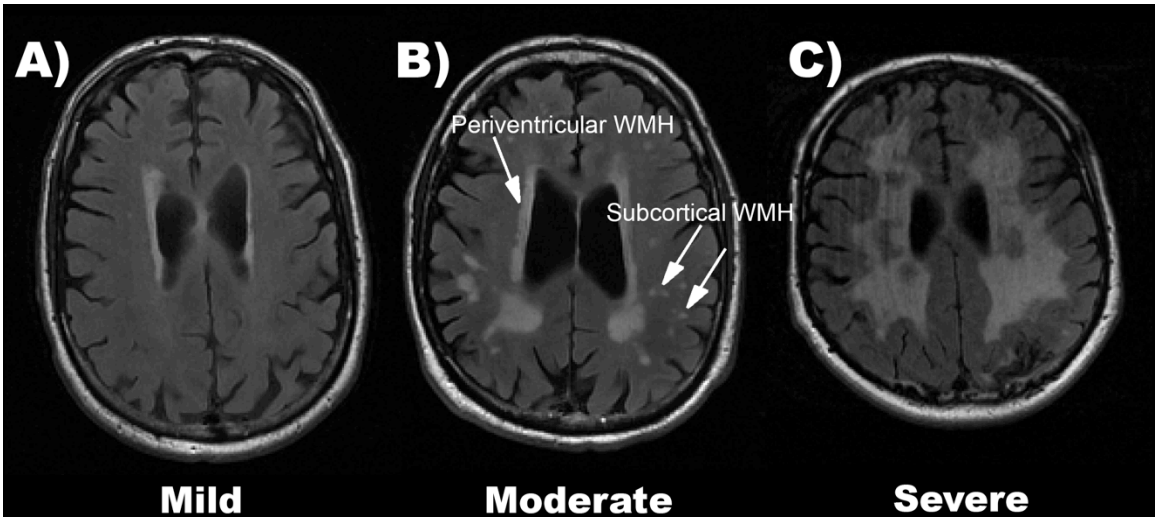

Figure 1.4 White matter hyperintensities as indicated by hyperintense signal on T2-weighted FLAIR axial images. Panels A, B, and C exhibit mild, moderate, and severe cases of WMH, respectively. Single arrow indicates periventricular lesions and double arrows indicate subcortical lesions. Images taken from 3 patients with CAA from the study outlined in this thesis.

regarding the methodology, neuroimaging, and especially the cognitive profile associated with WMHs. They determined that WMHs were associated with worse performance on tests for speed and motor control, attention, executive functions, and naming. The LADIS study was able to implicate WMH volume and WMH progression as predictors of depressive symptoms in the elderly population. WMHs were once thought of as innocuous neuroimaging findings but the LADIS group and others[82-84] have clearly exemplified that this is not the case.

WMHs occur in normal aging but are more prevalent in patients with small vessel disease.[85] CAA is one of a number of small vessel diseases associated with high WMH burden. However, in contrast to the specific lobar pattern of CMBs that discriminate CAA from other small vessel diseases, there is no easily discernible spatial pattern of WMH presentation in CAA.[54] Therefore the presence of WMHs is not useful for discriminating CAA from other

vascular diseases. However, WMH volume may be a marker of disease severity in CAA, as higher volumes are associated with worse cognitive impairment. WMH progression has been measured in CAA over a median time interval of 14 months.

The white matter microstructure can also be measured using DTI.[54] This method is used to determine how water diffuses throughout the brain, which provides information about the structure and organization of white matter tracts between connected cortical brain regions. DTI studies have shown that the microstructure of white matter in CAA is abnormal in the posterior corpus collosum and in the temporal white matter, and that these abnormalities seem to be linked to CAA-related cognitive impairment.[70,86]

1.4.3 Non-Hemorrhagic Markers

Perivascular spaces are the fluid-filled areas surrounding the penetrating vasculature of the cerebrum that allow for the clearance of interstitial fluid from the brain.[87] With increasing age, PVS become enlarged due to Aβ accumulation, which impedes efficient perivascular clearance.[71] These enlarged PVS can be seen as ovoid signal voids on axial T2-weighted GRE images. In CAA, enlarged PVS are most commonly seen in the centrum semiovale, which is consistent with the localization of CAA pathology.[54] The clinical consequences of enlarged PVS are unclear and require further study.[54]

Brain infarcts are defined as any neural cell death that is caused by ischemia.[75] Microinfarctions, defined as infarcts that are not grossly visible without the aid of a microscope, are frequently seen in patients with CAA at autopsy. These infarcts are typically <1 mm in diameter.[88] Such small infarcts are not visible on routine conventional MRI, but emerging evidence suggests they may be visible on MRI with a larger field strength (e.g., 7 Tesla).[89]

Additionally, a study of CAA patients found that 15.2% had incidentally detected small infarcts on diffusion weighted imaging (DWI), which may represent larger microinfarcts caught in evolution.[90] Microinfarcts are associated with CAA severity and may be responsible for causing the cognitive deficits seen in CAA.[54]

1.4.4 Molecular Imaging of Beta-Amyloid

Beta-amyloid peptides have an affinity for the radioligand Pittsburgh compound B (PiB), which allows for the localization and quantification of cerebral beta-amyloid *in vivo* using PET imaging.[49] Originally, PET amyloid imaging was designed to detect parenchymal amyloid plaques in AD; however, there have been several studies showing the efficacy of PiB PET in detecting vascular beta-amyloid in CAA.[73,91,92] PiB PET shows the aggregate total of both brain and vascular amyloid in a given tissue voxel, and cannot be used to discriminate vascular amyloid of CAA from the senile plaques of AD pathology.

1.4.5 Markers of Vascular Function

Vascular beta-amyloid deposition causes smooth muscle cell loss and thickening of the vascular walls, which impairs the vessels' ability to respond to physiological stimuli.[93] The cerebral vasculature's ability to respond to the environment, in order to regulate blood flow by constricting or relaxing arterioles, is called vascular reactivity. The physiological basis of vascular reactivity and experimental methods to measure it, including using fMRI blood oxygen-level dependent (BOLD) activity, are discussed in detail in subsequent sections (1.5 and 1.6, below). Recently, two independent studies have been able to detect abnormal BOLD responses to a visual stimulus task in CAA compared to healthy controls, suggesting that impaired vascular reactivity is an important feature of CAA (discussed in detail in section 1.7, below).[67,74]

Mouse models support the observations that there is impaired vascular reactivity in CAA. These models also suggest that impaired vascular reactivity due to amyloid deposition may be reversible.[54] Hence, unlike the other biomarkers of CAA severity, impaired BOLD amplitude may indicate a reversible pathogenic process of CAA, and could be used to demonstrate the efficacy of potential CAA treatments in early phase trials. However, the natural course of fMRI BOLD change over time in CAA is unknown. In this thesis, the author will provide the first data on fMRI BOLD amplitude change over time in CAA (Chapter 3)

1.5 Vascular reactivity

Vascular reactivity refers to the ability of arterioles to dilate or constrict in response to environmental changes, in order to regulate blood flow to desired levels. This principle underlies the ability to deliver nutrients, such as oxygen and glucose, to neurons as they require it.[94] In other words, neuronal activity signals the vasculature to dilate and shunt blood to its locale in order to meet the energy demands required by the activated neurons, in a process known as functional hyperemia. The exact mechanism that facilitates neurovascular coupling is not entirely understood. However, it is well established that the communication between the neuron and the vasculature, mediated by the astrocyte, is involved in the neurovascular coupling mechanism. The cerebral vasculature will also react to changes in intravascular pressure to maintain constant cerebral blood flow, in a process known as autoregulation,[95] as well as changes in arterial partial pressures of carbon dioxide.[20]

The brain receives 15% of the total cardiac output, despite its small size, as it has a high demand for energy in order to meet metabolic needs.[96] As a result, the brain has a very robust vascular system that ensures constant perfusion. Blood enters the brain through the carotid and

vertebral arteries that meet at the Circle of Willis at the base of the brain.[97] Arteries leave the Circle of Willis and travel along the surface of the brain, branch into smaller vessels, and penetrate the parenchyma. Penetrating arterioles are sheathed in endothelial cells covered in a layer of smooth muscle cells, which contain contractile elements responsible for the regulation of the diameter of the vessel.[94] As arterioles penetrate further into the parenchyma of the brain, they narrow into capillaries and contact astrocytic endfeet that envelope the diameter of the vessel.[98]

The central dogma of the neurovascular interaction is that neural activity causes local blood flow regulation.[99] When neurons are activated, they release neurotransmitters, such as glutamate and γ-aminobutyric acid (GABA), which spills out into perisynaptic spaces and binds to receptors on the astrocyte, thereby initiating intracellular waves of Ca^{2+}.[100] These Ca^{2+} waves have been shown to mediate the release of vasoactive factors, such as arachidonic acid metabolites, K^+, adenosine, and nitric oxide (NO).[100-102] In addition to the vasoactive factors released by the astrocyte, activated perivascular neurons release adenosine as a product of cellular metabolism.[103] Adenosine signals vascular smooth muscle cells to dilate through cyclic adenosine monophosphate (cAMP) and K^+ adenosine triphosphate (ATP) channels.[104] Endothelial cells are also capable of releasing vasodilators such as NO, prostacyclin, or carbon monoxide, and vasoconstrictors, such as endothelin or endothelium-derived constrictor. Smooth muscle cells dilate or constrict in response to vasoactive factors released by endothelial cells, neurons, and astrocytes.[99]

Neurovascular decoupling refers to the disruption of the neurovascular units' ability to maintain control of vascular reactivity.[99] Studies have shown that soluble Aβ can induce neurovascular decoupling, causing attenuated functional hyperemia, impaired autoregulation,

and impaired reactivity to global vasodilators such as carbon dioxide.[20] Specifically, laboratory studies have indicated that Aβ is disruptive to the survival and function of vascular endothelium.[105,106] Aβ is responsible for the production of reactive oxygen species (ROS) through its interaction with copper and zinc ions[42] and through nicotinamide adenine dinucleotide phosphate (NADPH) oxidase activation in astrocytes and microglia.[107,108] Multiple studies have demonstrated the consequence of Aβ on vascular reactivity in CAA. In a mouse model of severe CAA, there was a clear decrease in vasodilation in response to whisker barrel stimulation and carbon dioxide inhalation, two vasodilatory stimuli.[109] Exogenous $A\beta_{(1\text{-}40)}$ has been shown to cause endothelium-dependent vasoconstriction in transgenic mice overexpressing APP.[110] In patients with CAA, it has been shown that there were reductions in measured BOLD amplitudes in response to a visual stimulus.[67,74] These fMRI findings were interpreted as impairments of the hemodynamic response due to the deposition of amyloid in the cerebral vasculature.

1.6 Functional MRI and the Blood Oxygen Level Dependent Signal

Functional MRI is a non-invasive imaging technique used for measuring brain activation patterns in response to specific tasks. fMRI contrast relies on the BOLD signal, which is inversely proportional to the concentration of deoxyhemoglobin in venous blood.[111] BOLD signal amplitude changes as a function of time in response to changes in local blood flow associated with, for example, neural activity (Figure 1.5). When oxyhemoglobin unloads oxygen, the resulting deoxyhemoglobin molecule is paramagnetic,[112] altering the magnetic field experienced by the diamagnetic protons of intra and extravascular water. This attenuates the T2* signal as measured by fMRI. The temporal change in the MR signal, based on changes in deoxyhemoglobin concentration, results in the BOLD signal.

The BOLD signal in response to neural activity is characterized by the hemodynamic response function.[113] When neural activity is initiated by a brief stimulus, oxygen is consumed by the active neurons, the concentration of deoxyhemoglobin increases, and the MR signal intensity falls slightly below baseline in what is called the initial dip (Figure 1.5).[114] When the neurovascular unit signals vasodilation, an oversupply of oxygenated blood rushes to the area (i.e., functional hyperemia) and the relative decrease in deoxyhemoglobin concentration causes the MR signal intensity to reach a peak amplitude approximately five seconds after stimulus onset. It is thought that active tissue continues to deplete the source of oxyhemoglobin as local blood flow returns to normal.[115] The continuing generation of deoxyhemoglobin decreases the MR signal and the BOLD signal starts to drop towards baseline. As the BOLD signal approaches baseline, it enters a post-stimulus undershoot phase. This is thought to be due to the recovery of cerebral blood volume being slower than the process of the local blood flow returning to normal. As the vessel returns to its original diameter, the concentration of deoxyhemoglobin normalizes, and the MR signal intensity also returns to baseline.[116]

There is a clear relationship between BOLD signal amplitude increases and increases in cerebral blood flow. Animal experiments have shown high correlations (correlation coefficients 0.89-0.96) between the BOLD signal increase and cerebral blood flow increase when measured simultaneously in the visual cortex.[117,118]

The measurement of the BOLD signal has been thoroughly characterized in the primary visual cortex.[119] A study by Brewer *et al*. looked at the boundaries of retinotopically organized visual areas V1, V2, V3, V3A, V4, and MT/V5 as they appeared on fMRI activation maps in macaque monkeys.[120] Their results showed that areas of fMRI activation were in agreement with

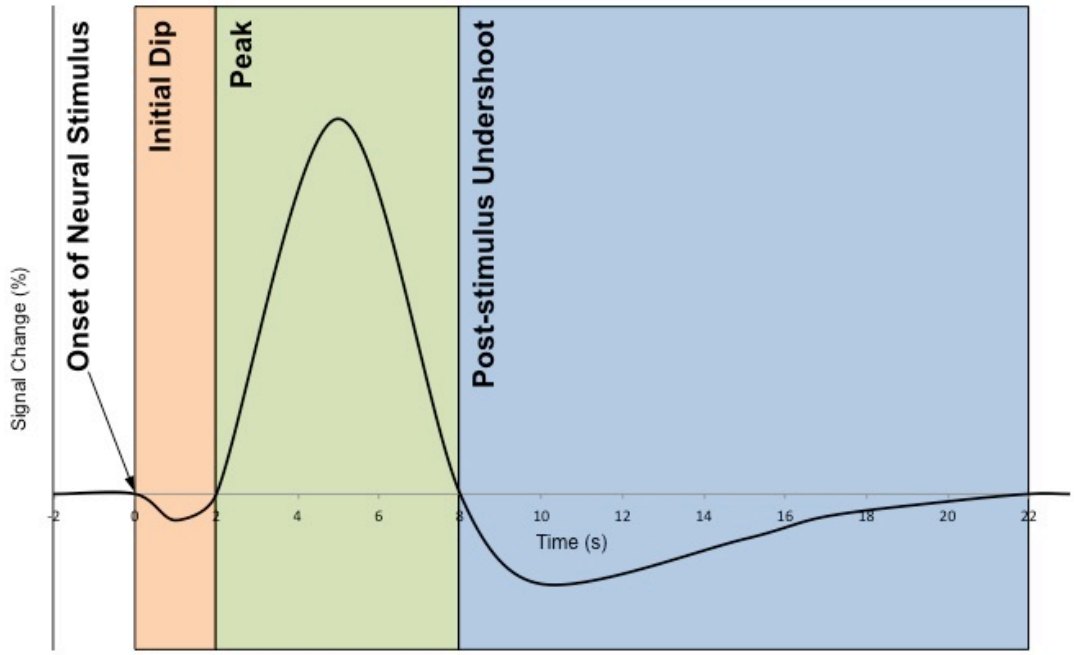

Figure 1.5 Blood oxygen level dependent signal in response to a brief neural stimulus.

their respective anatomically and physiologically defined regions. A study by Stiers *et al*. reproduced the same results in humans using a complex visual fMRI task that incorporated each area of the visual cortex.[121] These studies implicate the use of visual fMRI activation as being a highly robust and reproducible method for acquiring BOLD signal changes in specific visual areas such as the primary visual cortex.

1.7 Vascular Reactivity in CAA and AD

Histological studies have shown loss of smooth muscle cells, thickening of vascular walls, and hyalinization of the vascular media co-localized with vascular beta-amyloid deposits.[8] These findings indicate that beta-amyloid may be toxic to the smooth muscle cells of the brains small vessels.[93] Smooth muscle cells are important for regulating the tone of the brains vasculature in

response to increased neural activity.[104] Therefore, disruption of smooth muscle cell function by Aβ can cause impaired vascular reactivity.

There is accumulating evidence, both in animal models and in human studies, suggesting that impaired vascular reactivity in response to a vasodilatory response is an important feature of CAA. Two independent studies characterized the vascular reactivity impairment in two different mouse models of CAA.[109,122] In 2012, Dumas *et al*. were able to identify alterations in BOLD responses, indicative of impaired vascular reactivity, in CAA.[74] Peca *et al*. confirmed these results by showing that changes in BOLD responses occurred in the absence of reduced neural activity as determined by visual evoked potentials.[67] This section will review the findings linking impaired vascular reactivity and CAA, in detail.

Impaired vascular reactivity has been shown in both Tg2576 and Tg-SwDI mice, two models of severe human CAA.[109,122] In a study by Shin *et al.*, Tg2576 mice that exhibited cerebrovascular beta-amyloid deposition at 19-months were administered three vasodilatory stimuli: a hypercapnic challenge, whisker barrel stimulation, and cortical spreading depression.[109] The vasodilatory stimuli produced attenuated cerebral blood flow responses in 19-month-old Tg2576 mice compared to wild-types. A similar study by Park *et al.* used a Tg-SwDI mouse model that expressed both the Swedish and Dutch/Iowa mutations of the human APP, which exhibit vascular beta-amyloid deposition starting at 6-months.[122] Tg-SwDI mice were exposed to whisker barrel stimulation, superfusion of vasodilators, and a hypercapnic challenge, and blood flow responses were monitored using laser-Doppler flow imaging. As Tg-SwDI mice aged from 3-months-old to 24-months old, they showed an age-dependent decrease in

cerebrovascular function compared to wild-types. These results link increasing vascular beta-amyloid deposits to decreasing vascular reactivity in CAA.

A study by Dumas *et al*. suggested CAA-dependent vasoreactivity impairment in humans participating in a visual fMRI task.[74] Patients with CAA displayed a reduction in BOLD signal amplitude ($p<0.01$), as well as a longer time for the BOLD signal to reach its peak ($p<0.001$), and a prolonged time for the BOLD signal to return to its baseline ($p<0.001$) in patients with CAA compared to healthy controls. The change in the shape of the hemodynamic response indicates an alteration in cerebrovascular function in the CAA brain. In this study, they also showed that resting blood flow was similar in both patients with CAA and healthy controls, demonstrating that differences in BOLD responses were independent of blood flow delivered to the brain. These data suggest that lower BOLD responses in CAA were more likely due to impaired vascular reactivity.

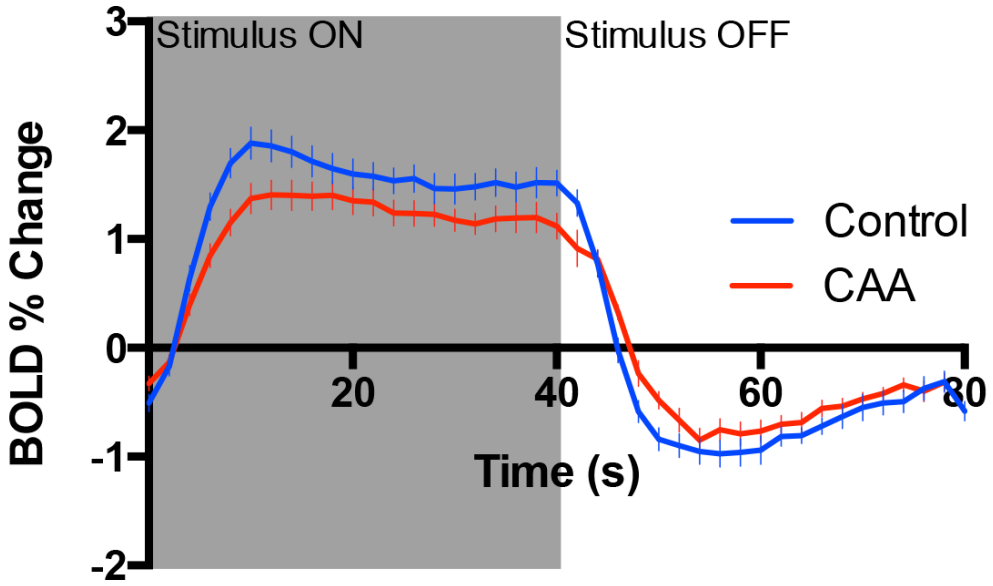

Figure 1.6 BOLD responses to a visual stimulus task in 31 patients with CAA and 27 healthy controls. Data was extracted from the baseline fMRI visits of participants in the study outlined in this thesis.

A more recent study conducted by Peca *et al.* in the Smith lab, measured the amplitude of BOLD signal responses to both visual and motor fMRI tasks. In the visual task, BOLD amplitudes were reduced by 28% in CAA compared to controls (p=0.01) (Figure 1.6),[67] but were similar in the motor task (p=0.22). These findings were consistent with the known posterior-anterior gradient of vascular beta-amyloid deposition in CAA. BOLD amplitudes in response to a visual task were negatively correlated with WMH volumes and microbleeds. Using visual evoked potentials (VEP), surface potentials were measured in the occipital lobe to monitor neural activity in response to a visual stimulus task, and it was found that there was no difference in neural activity between CAA and controls. These findings suggest that reduced BOLD amplitudes in CAA were most likely caused by impaired vascular reactivity and were not driven by decreased neuronal activity.

Vascular reactivity in AD has been measured in a number of studies, but it is unclear if these findings were driven by soluble Aβ or vascular Aβ. Animal model studies have shown that interactions between soluble Aβ and endothelial cells can result in the production of reactive oxygen species.[123] The change in the oxidative environment alters the structure and function of the endothelial cells, which impairs vascular reactivity. While soluble Aβ-mediated vascular dysfunction has been produced in animal models of AD, it was uncertain if these findings could be reproduced in humans.[20] In AD patients, neurodegeneration affects the temporal and parietal lobes, which is reflected by lower resting blood flow in those areas.[124] This is different than what is seen for CAA, in which vascular amyloid has the propensity to accumulate in the occipital and posterior temporal lobes as opposed to the parietal regions.[78] Despite the large number of studies regarding vascular reactivity in AD, there has been no consensus whether impaired vascular reactivity is a feature of AD,[125-127] or if it is not.[128-130] The reason for the variable results is not

entirely clear. None of the previous studies of AD considered whether their results might be driven by vascular amyloid (CAA), which frequently accompanies AD to a variable extent. For example, multiple lobar microbleeds consistent with CAA are detected in up to 25% of AD patients, yet none of the published AD studies included an assessment of microbleeds. Characterizing vascular reactivity in the occipital lobe of patients with mild AD, MCI and CAA may elucidate whether AD-related vascular impairment is driven by soluble Aβ or by vascular Aβ.

The aims of this thesis are: 1) to determine whether vascular reactivity, as inferred from the BOLD response amplitude to a visual task, is impaired in CAA as well as in MCI and AD; and 2) to determine whether a decrease in BOLD response amplitude can be detected in CAA longitudinally over a 1-year period. The results from this thesis will show whether visual task BOLD changes are a unique feature of CAA or are also observed in other beta-amyloid diseases (AD) or syndromes where patients are at risk for having prodromal AD (i.e. MCI). Additionally, if we can detect visual task BOLD changes over time in CAA, future work might demonstrate that it is a useful marker of progression in CAA.

1.8 Hypotheses

Supported by our previous results and background literature, we hypothesize that: 1) BOLD signal amplitudes in response to a visual fMRI task will be highest in healthy controls, followed by MCI, then AD, and lowest in CAA, reflecting the presumed severity of vascular amyloid deposition; and 2) patients with CAA will exhibit a reduced amplitude of the BOLD signal at 1-year follow-up compared to baseline, while controls will exhibit no change, and that this CAA-

related reduction will be associated with the progression of CAA severity as indicated by progressive increase in WMH volume and increased number of CMBs.

1.8.1 Specific Aims

1. To compare BOLD response amplitude between patients with AD, MCI, and CAA, and healthy controls. We anticipate that BOLD response amplitude will be lowest (i.e. most abnormal) in patients with CAA, followed by AD, followed by MCI, and highest in healthy controls.

2. To compare BOLD amplitude in response to a visual stimulus task longitudinally over 1 year in patients with CAA. We hypothesize that BOLD response amplitude will be lower at 1-year follow-up compared to initial scan, and that this difference will be greater in patients with CAA than in healthy controls.

3. To compare longitudinal measures of BOLD response amplitudes with WMH progression and CMB counts. We anticipate that BOLD response amplitudes will decrease over time in CAA subjects and that this will be correlated with an increase in WMH volume over time and an increase in the number of CMBs.

1.9 Scientific Contributions and Publication Record

I am responsible for all written portions of this thesis, which were edited by my supervisors Dr. Eric Smith and Dr. Brad Goodyear. Dr. Eric Smith and I devised the research aims of this thesis based on previous cross-sectional work done by a former postdoctoral fellow in Dr. Smith's lab, Dr. Stefano Peca. Dr. Peca and Dr. Goodyear developed the methods pertaining to the fMRI analyses done in this thesis, which were slightly modified to better fit the longitudinal aim of my study.

For the fMRI analyses in Chapters 2 and 3, I analyzed data from patients recruited for the Functional Assessment of Vascular Reactivity (FAVR) study. Dr. Smith designed the FAVR study, which aimed to determine the vascular reactivity profile of the occipital lobe in healthy controls, and in patients with MCI, AD, and CAA. All VEP measurements were supervised and analyzed by Dr. Neelan Pillay. Dr. Cheryl McCreary acquired all MR images used in my thesis. I retrieved the MR data from a local database and performed all analyses pertinent to the fMRI and WMH studies. Dr. Smith trained me in the identification and quantification of WMH volumes. Using in-house designed software, I quantified WMH volumes for all subjects in my thesis. Cerebral microbleed identification required the expertise of a trained radiologist; as such, Dr. Saima Batool and Dr. Smith were responsible for counting the microbleed data used in my thesis. I was responsible for conducting all univariate statistics pertaining to my thesis and Dr. Smith was responsible for conducting all multivariate analyses. Dr. Smith acted as the expert statistician for my study, and the findings were interpreted by myself with the help of Dr. Smith.

I received guidance and input from other scientists working in the Seaman Family Magnetic Resonance Research Centre. Dr. Smith, my primary supervisor, provided mentorship and support throughout my project. Dr. Goodyear, my co-supervisor, also provided guidance and feedback for my research. Dr. McCreary and Dr. Paolo Federico, members of my supervisory committee, provided help with analysis, as well as invaluable feedback for improvements of my research. Other graduate students and staff in the Seaman Family MR Centre, such as Ali Sojoudi, Filomeno Cortese, Ismael Gaxiola, Kristine Woodward, and Craig Beers, were instrumental in helping me learn how to use the FSL software used in my fMRI analyses.

Work in Chapter 3 was presented at the International Stroke Conference 2014 in San Diego California. Chapter 3 is being prepared for submission to the *Neuroimage: Clinical* journal. Chapter 2 is being prepared for publication and will be submitted when more participants are added to the study by the end of 2014.

Chapter Two: **Cross-sectional Differences in fMRI Blood Oxygen Level Dependent Signal in Cerebral Amyloid Angiopathy and Alzheimer's Disease**

2.1 Introduction

Alzheimer's disease and CAA are two diseases caused by the deposition of beta-amyloid. AD is characterized by the accumulation of beta-amyloid in the parenchyma of the brain as senile plaques, contributing to cognitive decline and memory loss.[24] CAA is marked by beta-amyloid deposition in the media and adventitia of the leptomeningeal and cortical small arteries of the brain, leading to increased risk of hemorrhagic stroke and cognitive impairment.[10] CAA is also present, to varying degrees, in 90% of patients with AD, as observed through autopsy;[131] however, most AD patients do not develop symptomatic hemorrhages. Conversely, most cases of clinically recognized CAA do not have AD or dementia, even though both diseases are marked by beta-amyloid accumulation. Both CAA and AD pathologies exist on a spectrum, where one end represents predominantly parenchymal amyloid deposition with AD-dementia, and the other end represents predominantly vascular beta-amyloid deposition with CAA-related symptomatic hemorrhaging and vascular cognitive impairment.[131]

Our lab has recently demonstrated there is impaired blood flow regulation in patients with CAA.[67] BOLD amplitude responses to a visual task were reduced in CAA relative to similarly-aged controls, adjusting for age and vascular risk factors. Visual evoked potential responses did not differ between groups, suggesting that the reduced BOLD responses seen in patients with CAA, were the result of impaired vasodilation, not decreased metabolic activity. However, BOLD responses in AD were not assessed in that study.

Because AD and CAA exist on a spectrum, it is possible that impaired blood flow regulation may be a feature of AD, as well. The concept that blood flow regulation may be impaired in AD is not new. Experimental work in animal and tissue models has previously shown that soluble Aβ increases vascular oxidative stress and impairs vascular reactivity.[20] Several previous cross-sectional studies have measured blood flow regulation in AD in response to a vasodilatory stimulus such as carbon dioxide inhalation; however, there was variance in the conclusions of these studies where some detected impaired vascular reactivity,[125-127] and others did not.[128-130] These studies had shortcomings: they were small, none had a CAA comparison group, and they only measured global vascular reactivity, mostly using carbon dioxide inhalation even though blood flow regulation in response to neural activity provides the most sensitive measure of vascular compliance.[132] Therefore, BOLD responses to a visual stimulus task would be ideal for determining occipital blood flow abnormalities in AD and may contribute to distinguishing CAA from AD and MCI.

The present study aimed to compare the BOLD response to a visual stimulus in patients with vascular (CAA) and parenchymal (AD) beta-amyloid deposits compared to healthy controls. An MCI comparison group was also included because MCI represents an at-risk state for dementia, and many patients with MCI have AD pathology.[6] We hypothesized that BOLD signal change in response to a visual fMRI task would be lowest (that is, most abnormal) in CAA, followed by AD, followed by MCI, and highest in healthy controls based on the estimated distribution of amyloid pathology in each group.

Methods

2.1.1 Study Population

Study participants included 30 patients with CAA, 10 patients with AD, 10 patients with MCI, and 27 healthy controls recruited as part of a prospective longitudinal study. Detailed inclusion and exclusion criteria are outlined in Table 2.1. Patients with CAA were recruited from an outpatient cognitive assessment clinic or an inpatient stroke service. Patients with CAA presented with MRI evidence of lobar intracerebral hemorrhage, microbleeds, or superficial siderosis without other evident cause, consistent with the diagnosis of probable CAA by the validated Boston criteria (refer to Table 1.1).[52,53] AD was diagnosed using the clinical National Institute of Aging (NIA) criteria[46] and had early stage mild dementia, as defined by a Clinical Dementia Rating scale (CDR) score of 0.5 or 1.0[133] and Folstein Mini Mental Status examination

Table 2.1 Study inclusion and exclusion criteria

A. Inclusion Criteria: Diagnosis of CAA, AD, MCI, or healthy controls (see section 2.1.1 for more details).
B. Exclusion Criteria (relevant to all participants) • Residence in a nursing home or long term care facility • Moderate to severe dementia (defined here as a CDR scale total score > 1.0). Mild dementia is allowed (CDR score total 0.5 or 1.0), and must be present in AD • Other significant neurological or psychiatric disease (e.g. multiple sclerosis) • Known diagnosis of stenosis of the large intracranial or extracranial arteries perfusing the brain • Corrected visual acuity <20/50 • Non-English speaking (to avoid confounding neuropsychological test performance • History of photic-induced seizure • Presence of pacemaker or other MRI contraindication • Recent (<60 days) changes in antihypertensive or vasoactive medications • Recent (<90 days) symptomatic stroke (relevant to CAA only) • Neurological impairment expected to impair compliance with study procedures • Patients with AD that had lobar microbleeds on SWI (relevant to AD only)
These exclusion criteria (B) are applicable to all four study groups (CAA, AD, MCI, and controls) unless otherwise indicated.

score ≥20.[134] Patients with MCI were diagnosed by NIA criteria.[135] AD and MCI groups were recruited from a Cognitive Neuroscience Clinic, which sees approximately 200 new referrals per year. Healthy controls, recruited from the community by advertising in a newsletter or poster, did not have a history of stroke or dementia as determined by neurologist assessment.

2.1.2 Measurements

2.1.2.1 MRI Parameters

MRI measurements were made on a 3.0 T scanner (either GE Signa VH/I or Discovery 750) with an 8-channel phased-array head coil (GE Healthcare, Wi). Because of a scanner upgrade, there were 22/77 study subjects scanned on the Signa VH/I scanner and the remaining on the Discovery 750 scanner. All fMRI scans were T2*-weighted images using a gradient-recalled echo, echo planar imaging (GRE-EPI) sequence (TR/TE = 2000 ms/30 ms, flip angle = 70°, in-plane voxel size 3.75 x 3.75 mm, 34 slices, 4 mm gaps between slices, field of view = 240 x 240 mm). Three-dimensional T1-weighted inversion-recovery spoiled gradient recalled (IR-SPGR) images (TR/TE = 6 ms/2.4 ms, flip angle = 8°, in-plane voxel size 1 x 1 mm, 206 slices, 1 mm slice thickness, acquired and reconstructed matrix = 256 x 256) and 2-dimensional T1-weighted multi-slice spoiled gradient echo (TR/TE = 225 ms/approx. 2.5 ms, flip angle = 18°, voxel size 0.9375 x 0.9375 x 4 mm, acquired matrix = 128 x 128, reconstructed matrix = 256 x 256) images were collected to improve the registration of the fMRI data to the standard Montreal Neurological Institute (MNI) template. T2-weighted FLAIR images were used to measure the volume of WMHs of presumed vascular origin (TR/TE/TI = 9000 ms/149 ms/2250 ms, in-plane voxel size 0.9 x 0.9 mm, 39 slices,3.5 mm slice thickness, acquired and reconstructed matrix = 256 x 256). SWI was used to detect the presence of cerebral microbleeds (TR/TE = 30 ms/20 ms, flip angle = 15°, in-plane voxel size 0.9 x 0.9 mm, 120 slices, 2 mm slice thickness, acquired

matrix = 256 x 256, reconstructed matrix = 512 x 512). The entire imaging protocol took approximately 1 hour and included DTI and ASL images that were not used in this study.

2.1.2.2 Visual Task

The fMRI study used a visual stimulus task consisting of a block design employing the passive viewing of an 8-Hz contrast reversing checkerboard stimulus (Figure 2.1) to activate the primary visual cortex in the occipital lobe. Participants watched the stimulus for 40 seconds followed by viewing a fixation cross in the middle of a grey screen for 40 seconds; this was repeated for 4 blocks.

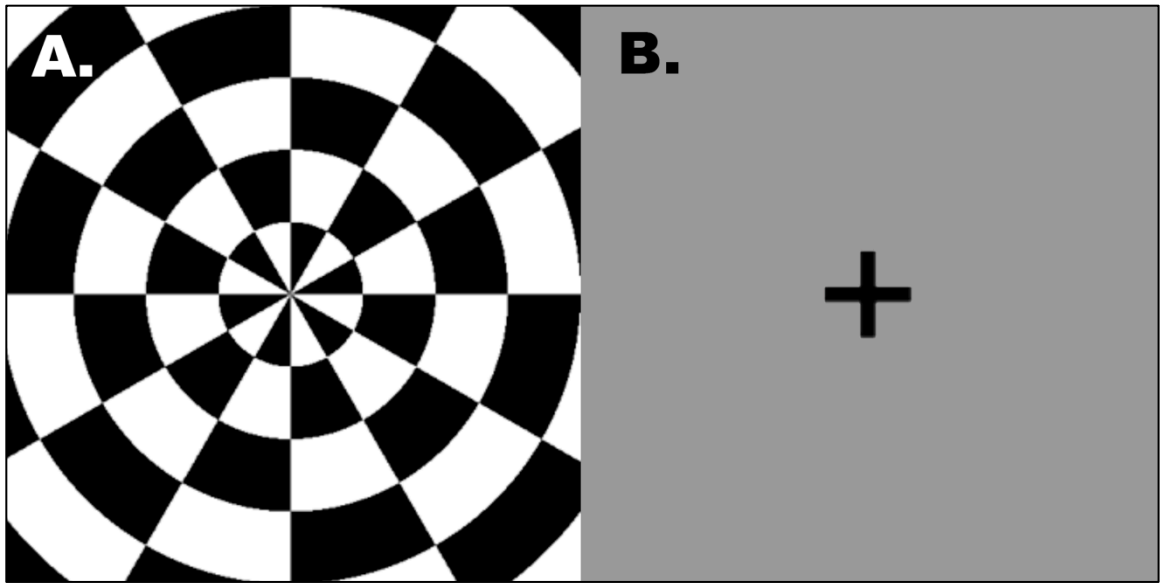

Figure 2.1 fMRI visual stimulus task. A. 8-Hz contrast reversing checkerboard stimulus for 40 seconds. B. Fixation cross for 40 seconds.

2.1.2.3 Visual Evoked Potentials

Visual evoked potentials (VEP) were measured to assess cortical neuronal activity in the occipital lobe using the Queen's Square standard electrode placement, consistent with American Clinical Neurophysiology Society guidelines.[136] Study participants were seated 1.5 m away from

a monitor that presented a 2-Hz contrast reversing checkerboard stimulus. One hundred responses were averaged and repeated 1-3 times to ensure reproducibility. A typical VEP wave, in response to a pattern stimulus, contains a negative peak 75 ms after stimulus onset (N75), a positive peak 100 ms after stimulus onset (P100), followed by a negative peak 145 ms after stimulus onset (Figure 2.2).[137] Using the difference between the N75 and P100 peaks, the amplitude of the P100 potential (μV) was calculated. VEP P100 amplitudes have been shown to correlate well with fMRI measurements of metabolic activity.[138,139] Measuring the latency of the P100 peak has been shown to vary among disease groups and with age.[140] These measurements were recorded as the time of the P100 peak following the stimulus onset (ms).

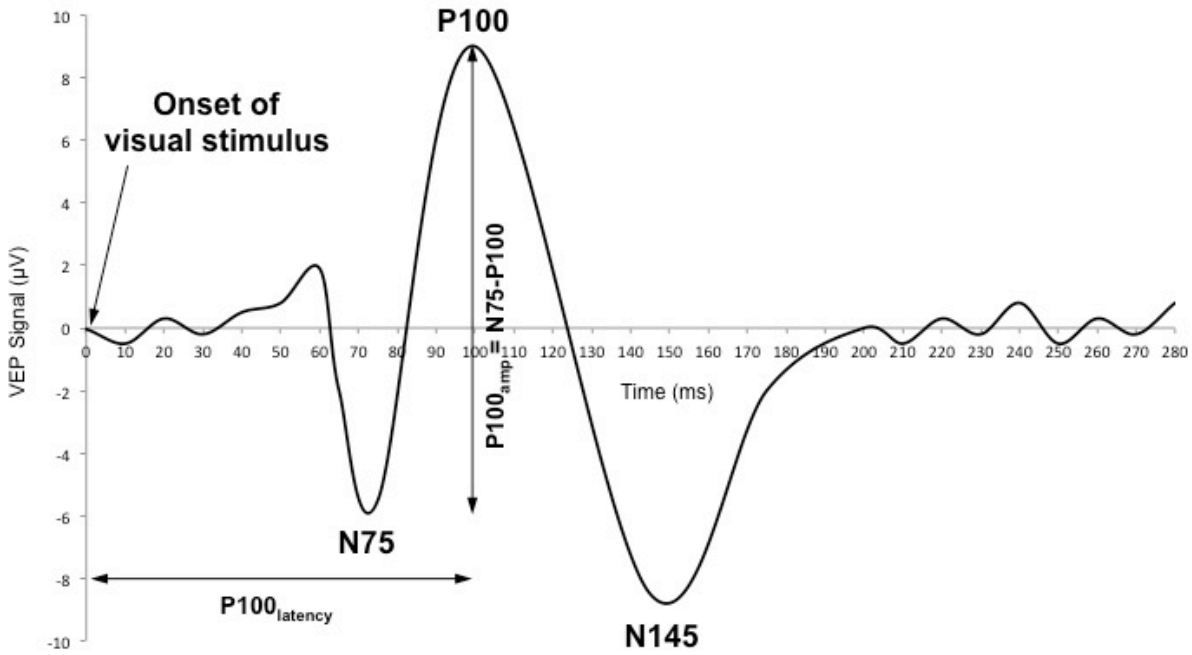

Figure 2.2 Typical VEP waveform. The letter N refers to a negative trough and the letter P refers to a positive peak. There are 2 N troughs at 75 ms (N75) and 145 ms (P145) following stimulus onset, and 1 P peak 100 ms (P100) following stimulus onset. The difference between the N75 and P100 signal values is defined as the P100 amplitude ($P100_{amp}$). The time between the stimulus onset and the peak of P100 is defined as the P100 latency ($P100_{latency}$)

2.1.3 Image Processing

2.1.3.1 fMRI Preprocessing

fMRI data were preprocessed using FSL (FMRIB Software Library version 5.0.1, Oxford, UK) to correct for non-physiological variability in the data. Using FSLs brain extraction tool (BET) all non-brain tissues (the skull, scalp, and eyes) were removed from the T1-weighted high-resolution and anatomical images.[141] Brain extraction improved the registration of the fMRI data to standard MNI space. The fMRI Expert Analysis Tool (FEAT) was used for the preprocessing and statistical analysis of the fMRI data. Slices of the fMRI data were acquired in an interleaved fashion to avoid cross slice excitation. Because each slice was acquired at a different time within one TR, the temporal fMRI signal from each voxel was interpolated to the center image of the TR using Fourier-space time-series phase-shifting. The fMRI data were motion corrected using the Motion Correction: FMRIB's Linear Image Registration Tool (MCFLIRT),[142] which minimizes the effect of head movements on the fMRI signal using a rigid-body transformation. The fMRI data were spatially smoothed to increase the signal-to-noise ratio. This was performed using a 5 mm full width half maximum (FWHM) Gaussian kernel. Scanner drift, or the gradual change in the scanners magnetic field, can contribute to non-physiological low frequency signal to the data. This was removed by temporal filtering using a Gaussian-weighted least squares straight line fitting with sigma equal to 100 s.

2.1.3.2 First-Level fMRI Analysis

The preprocessed fMRI data were registered to the standardized space of the MNI brain (using the 2-dimensional and 3-dimensional anatomical images) using FLIRT to allow for statistical comparisons in a common coordinate system. Statistical activation maps were generated for each participant's fMRI data using FEAT[143] in a first-level analysis. The visual stimulus paradigm

was modeled to represent the expected fMRI signal for active voxels in the brain. This model, or block design, was a square function with a 40 second OFF period followed by a 40 second ON period repeated four times. The block design was convolved with the hemodynamic response function (refer to Figure 1.5) in order to better represent the measured BOLD signal in each voxel (Figure 2.3). The next step of the analysis was to fit the predicted BOLD signal to the time course of every voxel of the fMRI data using a general linear model (GLM). There were two regressors used to model the fMRI data: the predicted BOLD signal and the temporal derivative. The temporal derivative was used to account for small differences in the latency of the fMRI response.[144] The GLM equation that represented the first-level analysis is written in Equation 2.1.

$$y(t) = \beta_1 \cdot x(t) + \beta_2 \cdot z(t) + \varepsilon \qquad \text{Equation 2.1}$$

Where y(t) is the observed BOLD signal time-course from a single voxel, x(t) is the expected BOLD regressor, z(t) is the temporal derivative regressor, and β_1 and β_2 are parameter estimates used to minimize the residual error or noise ε and to achieve the best fit possible. β_1 was standardized into z-scores using the mean and standard deviation of the parameter estimation.

2.1.3.3 Isolating the 200 Most Active Voxels and BOLD % Signal Change Calculation

Following the first-level analysis, a mask of the occipital lobe in native fMRI space was generated by manually drawing a region of interest (ROI) over the occipital lobe using anatomical landmarks on the filtered fMRI data. The occipital mask was multiplied with the z-statistic map and the 200 voxels (11.3 cm^3) exhibiting the greatest z-scores were selected as the ROI. BOLD % signal change within this mask was calculated for each voxel using:

$$BOLD\ \%\ Signal\ Change = \frac{\beta_1 \cdot x_{(p-p)}}{\bar{S}_{filtered_func}} \cdot 100 \qquad \text{Equation 2.2}$$

where β_1 is the parameter estimate of the expected response, $x_{(p-p)}$ is the peak to peak, or height, of the expected BOLD regressor, and $\bar{S}_{filtered_func}$ is the mean signal over time in the voxel from the filtered fMRI data. BOLD % signal change was averaged over the 200 most active voxels. BOLD amplitudes were compared between groups using a one-way ANOVA.

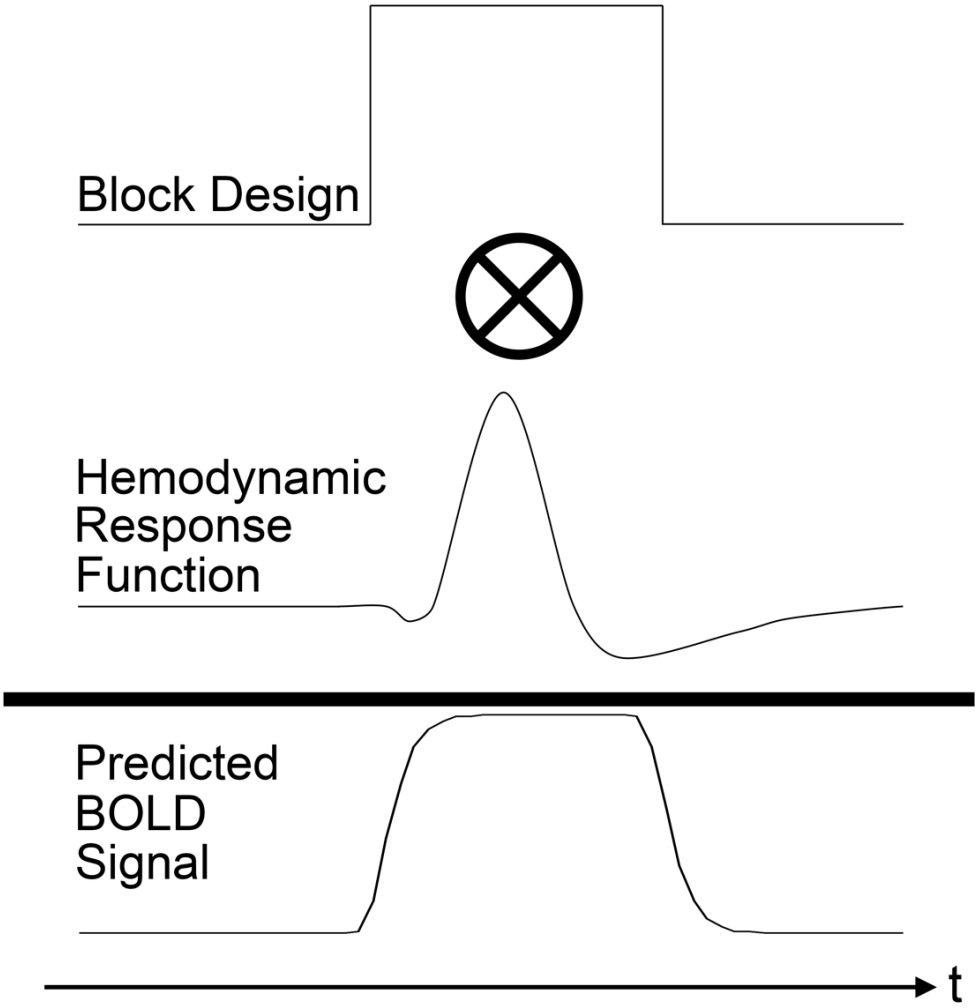

Figure 2.3. fMRI convolution. The block design representing the neural stimulus based on the fMRI paradigm is convolved with the hemodynamic response function and results in the predicted BOLD signal.

2.1.3.4 Higher-level fMRI Analysis

Higher-level analyses were used to generate mean activation maps for each group based on β_1 for each individual subject within the group. Higher-level analyses were carried out in FSL using a General Linear Mixed Model within FEAT.[145] FMRIB's Local Analysis of Mixed Effects (FLAME) was used for modeling and estimating the random-effects between subjects.[145] FLAME takes into account session and participant variability, which allows for inferences to be made about populations as opposed to the study sample only.

The next step of the higher-level analysis was to determine differences in activation between groups by creating β_1 contrasts. Specifically, a 1-level 4-factor GLM was used to determine which voxels exhibited significant differences in response magnitudes between each patient group and the healthy control group.

Z-statistic maps were generated to represent the voxels with statistically different activation between groups. The z-statistic maps were thresholded at $z>2.3$ and cluster corrected to a significance of $p=0.05$, using ALPHASIM,[146] a program designed to correct for family-wise errors.

2.1.3.5 Quantification of WMH Volumes

T2-weighted FLAIR images were analyzed to calculate WMH volumes for each participant by a single rater using Quantamo, a custom-designed software application (Cybertrails Inc; Calgary, AB, Canada). The Quantamo application uses a semi-automated threshold-based seed-growing algorithm to detect the volume of hyperintense signal (defined as ≥2 SD above the mean signal intensity) by a trained rater[147]. WMH volumes were measured on FLAIR images blinded to

fMRI results. WMH volumes were classified and reported according to the standards for reporting vascular changes on neuroimaging (STRIVE).[87]

2.1.3.6 Classification of Microbleeds

Cerebral microbleeds were identified on SWI images by a trained radiologist. Because many subjects with CAA had very large numbers of microbleeds, it was not feasible to count each microbleed separately as they were visually indistinguishable. Therefore, the rater instead categorized each subject based on the number of microbleeds: 0) 0 Microbleeds, 1) 1 Microbleed, 2) 2-4 Microbleeds, 3) 5-20 Microbleeds, 4) ≥20 Microbleeds. The rater was blinded to clinical information and fMRI results. One CAA patient was excluded from CMB analyses due to the low quality of their SWI.

2.1.4 Statistical Analysis

BOLD amplitudes were approximately normally distributed and were compared between each group by one-way ANOVA with a Tukey's multiple comparison correction.[148] Multivariable-adjusted GLMs with least squares means were used to determine whether group status was an independent predictor of BOLD responses, controlling for age, hypertension, and WMH volume. In these models, BOLD response was the dependent (outcome) variable, with group status, age, and history of hypertension as covariates. Within-group pairwise comparisons with 95% confidence intervals were calculated using least squares means, with Tukey's method to control for multiple comparisons. To determine whether the association between group status and BOLD response was mediated by WMH volume, we then performed a second multivariable adjusted model including WMH volume as an additional covariate. WMH volume had a right-skewed distribution and therefore values were log-transformed to a more normal distribution for analysis

with parametric tests, as has been done in another study.[149] Statistical analyses were performed using SAS version 9.3 (Cary, NC). Patients with CAA were separated into two groups: those with <20 microbleeds and those with ≥20 microbleeds. The BOLD amplitudes were compared between CMB groups by two-sample t-test. For all statistical tests a p-value less than 0.05 was considered to be significant.

2.2 Results

2.2.1 Demographics

Clinical characteristics of 30 patients with CAA, 10 patients with MCI, 10 patients with AD, and 27 healthy controls are provided in Table 2.2. Patients with CAA were 66.9 ± 8.0 years old, patients with MCI were 72.4 ± 7.8 years old, and patients with AD were 67.0 ± 5.7 years old. Across all groups, there were differences in age and history of hypertension, but there were similar distributions of coronary artery disease, atrial fibrillation, hypercholesterolemia, diabetes mellitus, and tobacco use.

Table 2.2 Clinical features of the study populations.

Characteristics	Control (n=27),n	MCI (n=10),n	AD (n=10),n	CAA (n=30),n	P value
Age (mean±SD)	66.9±8.0	72.4±7.8	67.0±5.7	74.0±7.0	0.002
Female sex	14	6	3	11	0.37
Hypertension	4	1	4	23	<0.001
Coronary artery disease	2	2	0	3	0.46
Hypercholesterolemia	11	3	1	15	0.11
Diabetes	1	2	1	7	0.18
Smoker - None	15	6	4	15	
Past	11	4	5	13	0.93
Current	1	0	1	2	
WMH volume (median [25th and 75th percentiles]; mL)	3.7 [17, 5.3]	12.6 [2.2, 22.3]	9.4 [5.0, 11.3]	33.1 [8.7, 46.7]	<0.001
VEP P100 (mean±SD)	6.2±3.9	5.5±3.3	4.4±2.7	4.8±2.2	0.31

P value by ANOVA or chi-square test, as appropriate.

2.2.2 BOLD Amplitude Responses

BOLD amplitude responses to a visual stimulus are displayed graphically for healthy controls, AD, MCI, and CAA in Figure 2.4. In univariate analyses, BOLD amplitudes differed significantly across the four groups ($F(3,73)=5.76$, $p=0.001$). Tukey post-hoc comparisons between each group indicated that CAA BOLD amplitudes were 30% lower than healthy controls (1.93±0.81% vs. 2.76±0.66%, $p=0.001$) and that MCI BOLD amplitudes were 29% lower than healthy controls (1.97±0.97% vs. 2.76±0.66%, $p=0.04$). AD BOLD amplitudes were non-significantly 12% lower than healthy controls (2.43±0.94% vs. 2.76±0.66%, $p=0.67$) and non-significantly 12% higher than patients with CAA (1.93±0.81% vs. 2.43±0.94%, $p=0.33$).

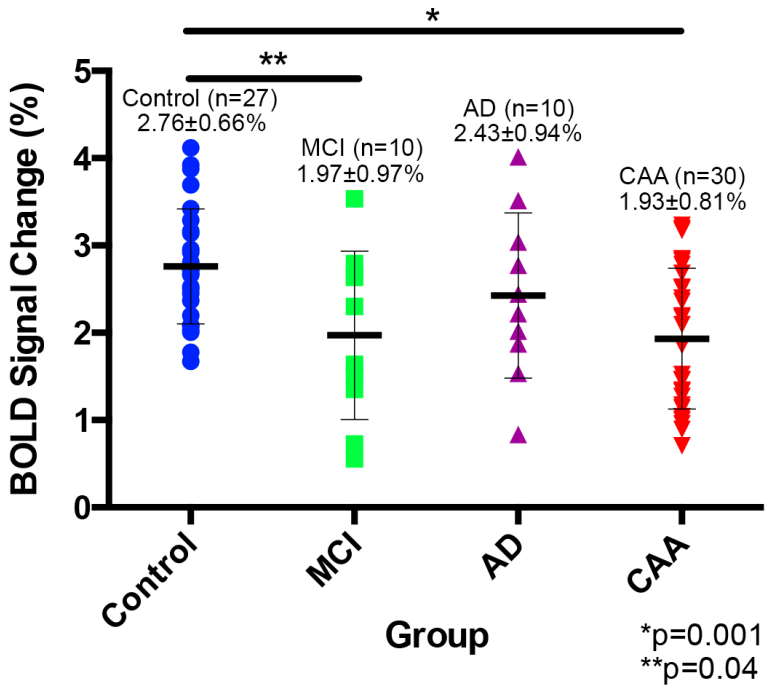

Figure 2.4 BOLD amplitudes for healthy controls, MCI, AD, and CAA. CAA BOLD amplitudes were significantly lower than healthy controls. MCI BOLD amplitudes were significantly lower than healthy controls. AD BOLD amplitudes were not lower than healthy controls or higher than CAA. Error bars indicate standard deviation.

BOLD amplitudes were not significantly different based on the scanner they were acquired on (2.21±0.22% vs. 2.23±0.11%, p=0.59). The mean amplitude (F(3,69)=1.22, p=0.31) and latency (F(3,71)=0.60, p=0.62) of the VEP P100 potentials were the same across all groups.

2.2.3 Higher-level fMRI Analysis

Voxel-wise group contrast analyses showed that fMRI activation was significantly lower in the primary visual cortex of each patient group compared to healthy controls (Figure 2.5). For patients with CAA, primary visual cortex activation was significantly lower than healthy controls in a volume of 35.9 cm^3. For patients with MCI, primary visual cortex activation was significantly lower than healthy controls in a volume of 13.3 cm^3. For patients with AD, primary visual cortex activation was significantly lower than healthy controls in a volume of 6.6 cm^3.

2.2.4 WMH Volumes and Cerebral Microbleed Counts

WMH volumes are displayed graphically for healthy controls, AD, MCI, and CAA (Figure 2.6). WMH volumes differed significantly across the three groups (F(3,73)=17.99, p<0.0001). Tukey post-hoc comparisons between each group indicated that CAA WMH volumes were significantly higher than healthy controls (36.03±31.61 mL vs. 3.95±2.97 mL, p<0.0001), MCI WMH volumes were significantly higher than healthy controls (14.86±13.68 mL vs. 3.95±2.97 mL, p=0.031), and AD WMH volumes were borderline significantly higher than healthy controls (8.43±3.17 mL vs. 3.95±2.97 mL, p=0.05) and borderline significantly lower than CAA (8.43±3.17 mL vs. 36.03±31.61 mL, p=0.05).

Cerebral microbleed categories are tabulated for patients with CAA in Figure 2.7A. For patients with CAA, those with ≥20 microbleeds exhibited significantly lower BOLD amplitudes compared to those with <20 microbleeds (2.32±0.18% vs. 1.51±0.19%, p=0.005) (Figure 2.7B).

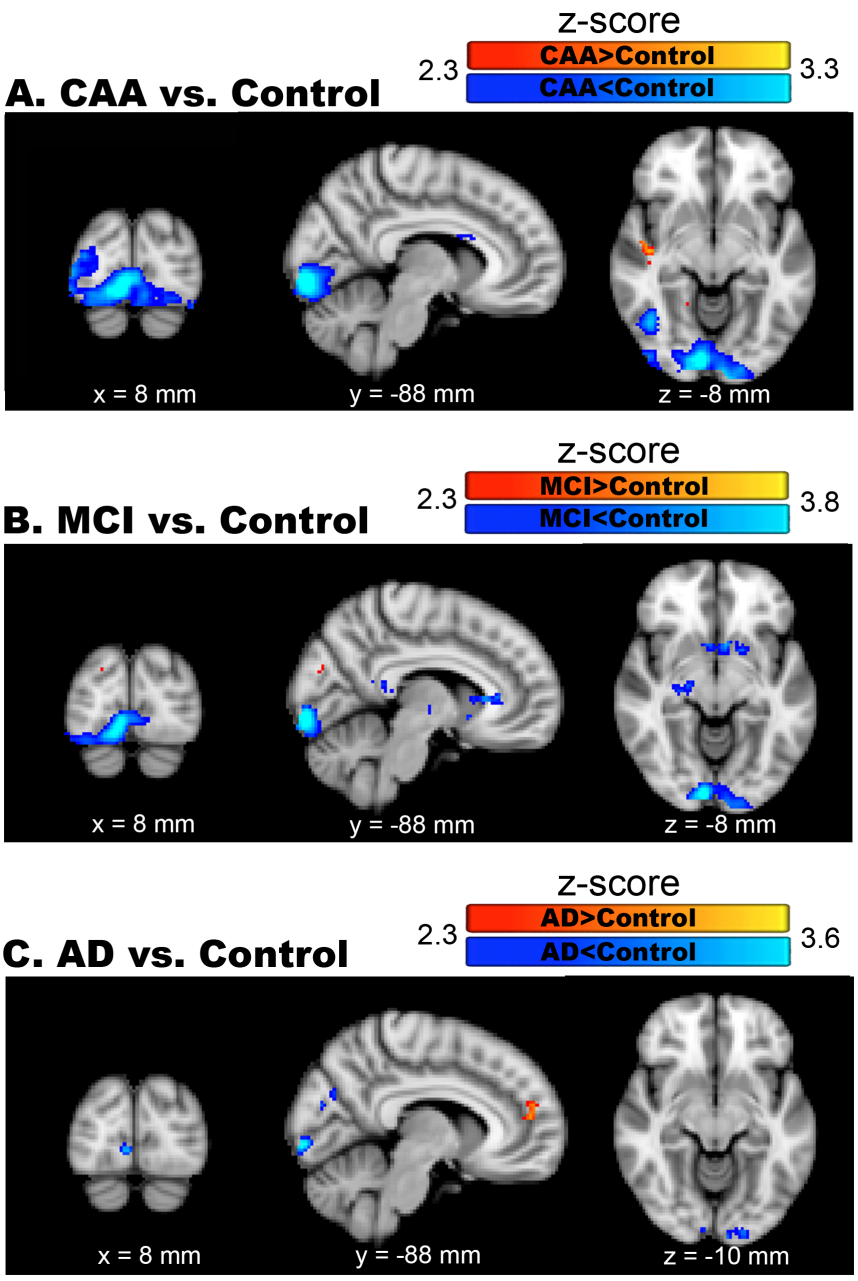

Figure 2.5 Differences in BOLD activation between each patient group and healthy controls. A) For patients with CAA, fMRI activation was significantly lower in a 35.9 cm^3 volume of the primary visual cortex, compared to healthy controls. B) For patients with MCI, fMRI activation was significantly lower in a 13.3 cm^3 volume of the primary visual cortex, compared to healthy controls. C) For patients with AD, fMRI activation was significantly lower in a 6.6 cm^3 volume of the primary visual cortex, compared to healthy controls. Areas of activation were cluster corrected to $z>2.3$ with a significance of $p<0.05$.

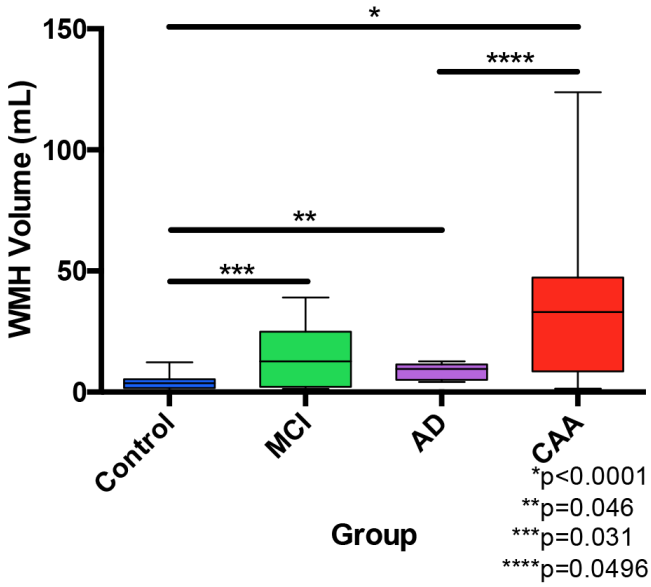

Figure 2.6 Differences in WMH volumes between healthy controls, MCI, AD, and CAA. CAA WMH volumes were significantly higher than controls, MCI WMH volumes were significantly higher than healthy controls, and AD WMH volumes were borderline significantly higher than healthy controls and borderline significantly lower than CAA. Error bars represent 5% and 95% confidence intervals. For statistical tests, WMH volumes were log transformed and group differences were determined using an ANOVA with Tukey's post-hoc test.

A. Microbleed categories for CAA	
0 CMBs	2
1 CMB	1
2-4 CMBs	5
5-20 CMBs	6
≥20 CMBs	15

CMBs = cerebral microbleeds

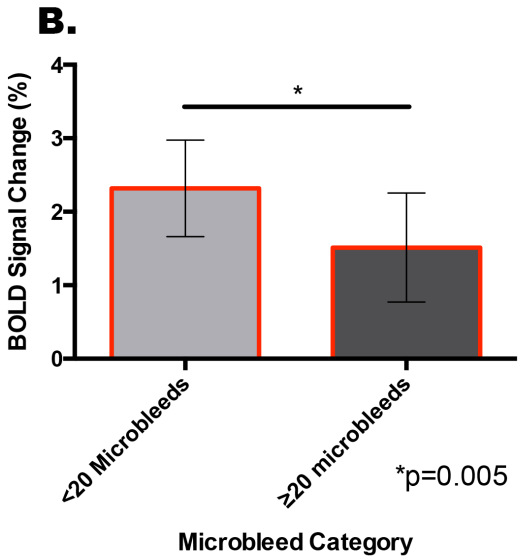

Figure 2.7 BOLD amplitude and microbleed analyses in patients with CAA. A) Cerebral microbleed categories in patients with CAA. B) BOLD amplitudes were significantly lower when patients had higher microbleed counts in CAA. Error bars represent standard deviation. Statistical differences were determined using an un-paired t-test.

2.2.5 Multivariable-adjusted Analyses of the Association between Group Status and fMRI BOLD Amplitude, Controlling for Other Factors

In a multivariable-adjusted analysis, controlling for hypertension and age (Table 2.3), the overall group differences in BOLD amplitudes remained significant ($F(3,71)=6.89$, $p<0.001$). There was a significant hypertension effect ($F(1,71)=5.61$, $p=0.02$) but not an age effect ($F(1,71)=0.02$, $p=0.90$). Using a Tukey's post-hoc test, the model predicted that CAA BOLD amplitudes were significantly lower than healthy controls (difference -1.15%, 95% CI 1.48 to -0.13, $p=0.0002$), MCI BOLD amplitudes showed a non-significant trend towards being lower than healthy controls (difference -0.76%, 95% CI -0.025 to 1.54, $p=0.06$), while AD BOLD amplitudes were the same compared to healthy controls (difference -0.47%, CI -1.23 to 0.30, $p=0.39$). Differences between CAA and AD ($p=0,13$) and CAA and MCI ($p=0.62$) were not significant.

Next, we added WMH volumes to the same fully adjusted model (Table 2.4). In this model, the group differences in BOLD remained significant ($F(3,70)=3.28$, $p=0.03$) even when accounting for differences in WMH volume between the groups. WMH ($F(1,70)=13.18$, $p<0.001$) and hypertension ($F(1,70)=9.72$, $p=0.003$) were also independently associated with BOLD amplitude, but not age ($F(1,70)=0.01$, $p=0.92$). BOLD amplitudes remained significantly lower in CAA compared to healthy controls ($p=0.03$), even after accounting for the higher WMH volumes seen in that group (Table 2.4). After accounting for differences in WMH volume, BOLD amplitudes were not different in MCI ($p=0.14$) or AD ($p=0.39$) compared to controls.

2.3 Discussion

We hypothesized that BOLD amplitudes would be lowest in patients with CAA, followed by AD, followed by MCI, and highest in healthy controls. Our results confirmed that BOLD amplitudes were lower in CAA than in controls; however BOLD amplitudes also tended to be

Table 2.3 General linear model results controlling for group, age, and hypertension

	Adjusted BOLD Amplitude (Mean, 95% confidence limits)	Difference compared to controls	CI for difference compared to controls	P value (difference compared to controls)
CAA	1.75%, 1.42 to 2.08	-1.15%	-1.83 to -0.46	0.0002
MCI	2.14%, 1.63 to 2.66	-0.76%	-1.48 to -0.13	0.06
AD	2.43%, 1.93 to 2.93	-0.47%	-1.23 to 0.30	0.39
Controls	2.90%, 2.57 to 3.23	N/A	N/A	N/A

Table 2.4 General linear model results controlling for group age, hypertension, and WMH volume

	Adjusted BOLD amplitude (Mean, 95% confidence intervals)	Difference compared to controls	CI for differences compared to controls	P value (difference compared to controls)
CAA	1.96%, 1.63 to 2.29	-0.76%	-1.45 to -0.065	0.03
MCI	2.12%, 1.65 to 2.60	-0.60%	-1.33 to 0.13	0.14
AD	2.29%, 1.82 to 2.76	-0.43%	-1.15 to 0.28	0.39
Controls	2.72%, 2.40 to 3.04	N/A	N/A	N/A

low in MCI, a finding that did not quite reach significance in this small dataset, while BOLD amplitudes were similar between AD and healthy controls. Differences in BOLD amplitudes occurred despite normal underlying neural activity across groups as detected by VEP. Impaired vascular reactivity findings in CAA were consistent with previous literature linking reduced BOLD amplitudes to CAA.[67,74] The present study suggests that occipital blood flow regulation is also impaired in MCI, but larger sample sizes will be needed to confirm or refute this possible finding. In this small study, BOLD amplitude was not different in AD compared to healthy controls.

Our fMRI results for patients with CAA are consistent with previous cross-sectional studies that first implicated impaired vascular reactivity as a novel characteristic of CAA.[67,74] Our lab's previous study of 18 participants showed that decreased fMRI BOLD amplitudes occurred despite normal neuronal function as measured by VEP. The present study, with 12 more CAA participants (total n=30), confirms the previous findings of decreased BOLD response with normal VEP.

As expected, we found that WMH volumes were highest in patients with CAA.[150] We were able to confirm statistically significant relationships between WMH volumes or microbleed counts and BOLD amplitudes in CAA, as was found in our previous study.[67] We also found that WMH volumes were associated with lower BOLD amplitude independent of group status, suggesting that the association between higher WMH volume and lower BOLD amplitudes may be a general phenomenon not limited to CAA. WMH is associated with arteriolosclerosis pathologically,[151] and therefore may be a marker of vessel wall changes that also impair vascular reactivity. To see whether the association between CAA and BOLD amplitude could be accounted for by the higher burden of WMH in CAA, we ran another model that included WMH as an additional covariate. In this model, BOLD amplitudes in patients with CAA remained lower than in healthy controls, despite controlling for WMH. Therefore, it seems likely that unmeasured characteristics of CAA, independent of WMH volume, may contribute to the impaired vascular reactivity in CAA. This suggests that fMRI may be a unique, complementary biomarker for CAA, reflecting CAA-related dysfunction that cannot be predicted by current markers such as WMH.

We confirmed our a priori hypothesis that BOLD amplitude would be lowest in CAA compared to controls. However, contrary to our expectations the BOLD amplitude response in MCI showed a non-significant trend toward being lower than healthy controls. This was somewhat surprising as we expected that some, but not all, of the MCI patients would have AD and that these patients would exhibit impaired vascular reactivity due to the presumed effects of soluble Aβ. One explanation for our results is that the MCI group may have contained patients with non-AD, non-CAA pathologies that also cause impaired vascular reactivity. Non-CAA vascular pathology may cause subcortical ischemic vascular MCI, even in the absence of symptomatic stroke, and could have accounted for our results. This would be consistent with our finding of higher WMH of presumed vascular origin in MCI compared to AD. Larger sample sizes will be needed to determine whether the 29% lower BOLD amplitude in MCI is significantly different than controls. In the future, the supervisor's lab intends to recruit a total of 20 patients with MCI to test this hypothesis.

Our study did not examine resting tissue perfusion; however previous literature suggests lower resting cerebral blood flow (CBF) in posterior brain regions such as the occipital, precuneus, and posterior cingulate cortical areas in patients with MCI using arterial spin labeling[152] and single photon emission computed tomography.[153] Because lower resting perfusion has been linked to decreased BOLD responses in a prior study,[154] it is possible that lower BOLD responses in MCI and AD could have been due to lower resting perfusion. We did not examine resting perfusion as part of this study. Future studies should consider employing a measure of resting CBF to better understand the nature of vascular reactivity in MCI.

Vascular reactivity in AD was lower than healthy controls but higher than patients with CAA but these differences were not significant, possibly due to the small sample size. If this observation is confirmed with a larger sample size, it would be consistent with our hypothesis that vascular reactivity would be impaired in AD, related to the effects of accompanying "silent" CAA as well as effects of soluble Aβ, but not as impaired as in clinically diagnosed CAA where autopsy validation studies show severe vascular changes related to vascular amyloid deposition, including complete destruction and replacement of the vascular media with beta-amyloid in some vessel segments.[155] In previous studies that measured global vascular reactivity using carbon dioxide inhalation, some studies were able to detect vascular reactivity impairment,[125-127] and some were not.[128-130] In this study, BOLD amplitudes were not significantly different from either healthy controls or CAA. Future studies should consider using larger sample sizes to determine the relationship between occipital blood flow regulation and AD.

The voxel-based primary visual cortical activation differences between each patient group and controls were consistent with the BOLD amplitude data. Patients with CAA exhibited the largest volume of reduced primary visual cortex activation compared to controls, which was consistent with lower BOLD amplitudes and the known distribution of vascular amyloid deposits in posterior brain regions in CAA.[156] Next, there was a smaller volume of the primary visual cortex affected by reduced activation in MCI compared to controls, which was concordant with the trend in lower MCI BOLD amplitudes. Finally, the smallest volume of the primary visual cortex was affected by reduced activation in AD compared to controls.

The principal limitation of our study was the small sample size in the AD and MCI populations. This analysis was done on an interim basis, because the final targeted sample sizes

of 30 AD and 20 MCI could not be recruited during the time period of this thesis. However, even with the smaller than anticipated sample sizes, we were able to detect significant differences in BOLD amplitudes in CAA compared to controls, and a trend toward lower BOLD amplitudes in MCI. Larger studies are required to determine the profile of occipital vascular reactivity in AD. The present study did not look at the relationship between BOLD amplitudes and the results of neuropsychological testing due to the insufficient power of the study. Finally, PET amyloid imaging could have been useful in determining associations between the amount of vascular amyloid deposition and the degree of vascular reactivity impairment; however, PET amyloid imaging is not available at our center.

2.4 Conclusion

We measured BOLD amplitudes in response to a visual stimulus to determine the occipital vascular reactivity profile of patients with CAA, MCI, and AD. Our results indicated that vascular reactivity was lowest in CAA compared to similarly-aged controls and that this reduction was related to greater WMH and microbleed burdens. BOLD amplitudes were also lower than healthy controls in patients with MCI but not when corrected for age, hypertension, and WMH volumes; however, more research is required for understanding this difference. We did not observe a significant difference in BOLD amplitudes between patients with AD and healthy controls, most likely due to the small AD population studied. Neural activity was consistent across all groups, as measured by VEP, suggesting that differences in BOLD amplitudes were due to vascular impairment rather than neuronal dysfunction. While the results presented here are preliminary, we have been able to suggest that CAA, MCI, and AD may exhibit varying impairments in vascular reactivity. These findings may implicate a possible future therapeutic target for improving the outcomes of these amyloid-related syndromes.

Chapter Three: **Longitudinal Decrease in fMRI Blood Oxygen Level Dependent Signal in Cerebral Amyloid Angiopathy**

3.1 Introduction

Recently, two independent studies have demonstrated that BOLD amplitudes, in response to a visual stimulus, were reduced in patients with CAA.[67,74] In one study, clinical tests of visual function and occipital surface evoked potentials were normal despite the reduced BOLD amplitude, suggesting the contribution of impaired vascular reactivity.[2] These modifications of blood flow responses were also independent of resting blood flow,[74] and were correlated with neuroimaging markers of CAA severity. In Chapter 2, it was shown that BOLD amplitudes in response to a visual stimulus in CAA were lower than controls.

Despite the accumulating evidence to suggest there is vascular reactivity impairment in patients with CAA, there have been no studies investigating if vascular reactivity decreases over time. Animal models have shown that vascular amyloid accumulates longitudinally and is associated with progressive reduction of vascular reactivity.[4] However, the timing and rate of cerebral hemodynamic impairment in patients with CAA is unknown because there are no published longitudinal studies. Understanding the temporal course of blood flow regulation impairment in CAA will help our understanding of CAA-related vascular changes. Showing that BOLD amplitudes change over a clinically feasible follow-up of 1 year could support the applicability of BOLD amplitude as a viable surrogate marker of CAA.

The study described in this Chapter aimed to track the progression of vascular reactivity impairment over 1 year in CAA as part of a prospective longitudinal study. We hypothesized that blood flow responses to a visual fMRI task would decrease over 1 year in CAA, and remain unchanged in healthy similarly-aged controls.

3.2 Methods

3.2.1 Study Population

Study participants included 22 patients with CAA and 16 non-cognitively impaired, stroke-free, healthy controls recruited as a part of a prospective longitudinal study, described previously in Chapter 2 but reviewed briefly here (refer to Table 2.1). Patients with CAA were recruited from an outpatient cognitive assessment clinic or an inpatient stroke service. Patients presented with MRI evidence of lobar intracerebral hemorrhages, microbleeds, or superficial siderosis without other evident cause, consistent with the diagnosis of probable CAA by the validated Boston criteria (refer to Table 1.1).[52,53] Patients were excluded if they resided in a nursing home or long term care facility, had moderate to severe dementia (defined as a Clinical Dementia Rating (CDR) score >1.0),[133] presented with ICH affecting the occipital pole, had abnormal visual acuity (<20/50), or were not fluent in English (because English language cognitive testing was part of the study). Patients with recent symptomatic stroke (<90 days) were excluded to avoid any acute effects of ICH. Healthy controls were recruited from the community by advertising in a newsletter or poster, and did not have a history of stroke or dementia as determined by neurologist assessment. Each participant had a repeat study visit and MRI at 1 year.

3.2.2 Measurements

The MRI scan sequence protocols were described in section 2.2.2. In brief, a 3.0 T scanner (either GE Signa VH/i or Discovery 750) with an 8-channel phased-array head coil (GE Healthcare, Wi) was used to acquire both structural and functional images. Because of a scanner upgrade, 9/22 CAA and 10/16 controls had their baseline scan on a GE Vi/H Signa scanner and their follow-up on a GE Discovery 750 scanner, while the remaining CAA and controls had both baseline and follow-up on the same GE Discovery 750 scanner. All fMRI scans were T2*-

weighted images using a GRE-EPI sequence. Both 3-dimensional and 2-dimensional T1 images were acquired to aid the registration of the fMRI data to the standard MNI template. T2-weighted FLAIR images were used to measure the volume of WMH of presumed vascular origin. SWI was used to detect the presence of cerebral microbleeds. The entire imaging protocol took approximately 1 hour and included DTI and ASL images that were not used in this study. The fMRI study incorporated a visual stimulus task that was described in section 2.2.2.2.

3.2.3 Image Processing

3.2.3.1 fMRI Preprocessing

fMRI data were processed using FSL (FMRIB Software Library version 5.0.1, Oxford, UK). The image preprocessing steps were completed to minimize non-physiological contributions to the data as described in section 2.2.3.1. The preprocessed fMRI data were registered to the standard space of the MNI brain to allow for group statistical comparisons in a common coordinate system.

3.2.3.2 Isolating the 200 Most Active Voxels and BOLD % Signal Change Calculation

Statistical activation maps were generated for each participant's fMRI data using FEAT[143] as described in section 2.2.3.2. The 200 most active voxels (11.3 cm^3) in the primary visual cortex were selected as the ROI, and the amplitude of the BOLD response from baseline (expressed as percent change in the signal) was calculated using Equation 2.1 and compared longitudinally within both the CAA group and the healthy control group.

3.2.3.3 Higher Level Analysis

Contrast activation maps between each session within the CAA group were generated using the FEAT higher-level analysis explained in section 2.2.3.4. Using a paired t-test, statistical

activation maps within groups were compared longitudinally using a higher-level FEAT analysis in MNI space. The z-statistic maps were thresholded at z>2.3 and cluster corrected to a significance of p=0.05 using ALPHASIM.[146]

3.2.3.4 DICE Coefficient of Overlap

We noticed that the anatomical area of activation differed over time between the baseline and follow-up scans within patients because we were sampling the most active voxels. This could bias our results by always selecting the healthiest voxels as opposed to measuring how BOLD amplitudes change over 1 year in a single anatomical location. To measure this, the 200 most active voxels mask from each individual's functional space, at each time point (i.e. baseline and follow-up), was transformed into standard MNI space using the transformation matrix calculated in the FLIRT registration. A threshold of 0.5 was applied to the transformed mask in order to correct for interpolation and preserve the original size of the mask. The anatomical similarity between the two masks over time was calculated using the DICE coefficient (Equation 3.1).

$$DICE = \frac{2N_{overlap}}{N_{Baseline} + N_{Follow-up}} \bullet 100 \qquad \text{Equation 3.1}$$

Where N denotes the number of voxels in the mask from baseline, the mask from follow-up, and the area where the two masks overlap. The DICE coefficient was represented as a percentage of the overlapping areas between the two masks in standard MNI space (Figure 3.1).

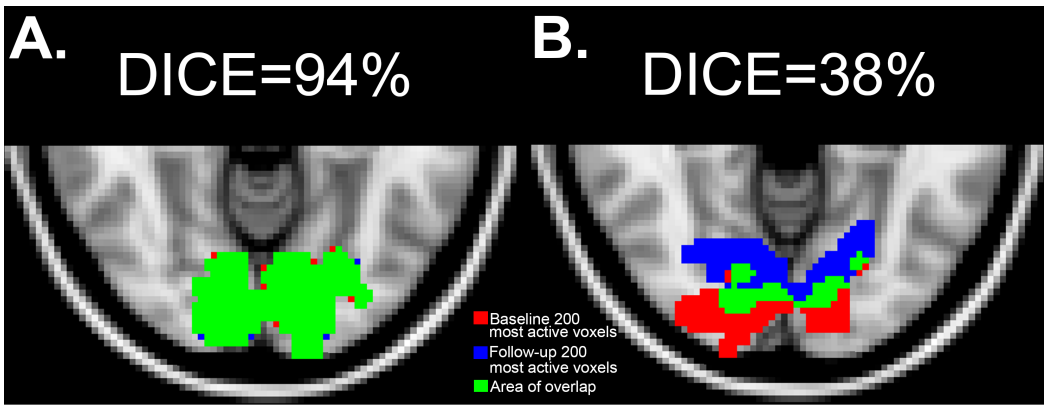

Figure 3.1 Examples of DICE coefficient overlap analyses. A) The 200 most active voxels mask from each time point almost overlapped completely showing that the anatomical area of activation was relatively consistent across time in a healthy control. B) The 200 most active voxels mask from each time point did not overlap completely showing that the anatomical area of activation varied over time in a patient with CAA.

3.2.3.5 Calculating BOLD Amplitudes with an Anatomical ROI

Based on the results from the DICE analysis, we performed a sensitivity analysis where we analyzed the BOLD amplitude changes in a pre-specified anatomically defined ROI. This ROI was centered on the primary visual cortex, which is the brain region most heavily affected by vascular amyloid deposition. The anatomically defined visual cortex V1 ROI[157] was extracted from the Juelich Histological Atlas structures within FSL, and encompassed a 21.7 cm^3 area of the primary visual cortex in MNI space (Figure 3.2). The anatomically defined ROI was transformed into the fMRI space of each individual and the BOLD amplitude was calculated as the average of all voxels within the ROI.

3.2.3.6 Calculating WMH Volumes and Counting Cerebral Microbleeds

T2-weighted FLAIR images were analyzed to calculate WMH volumes for each participant by a single rater using Quantomo, a custom-designed software application (Cybertrials Inc; Calgary, AB, Canada[147]) as described in section 2.2.3.5. FLAIR images from baseline and follow-up were

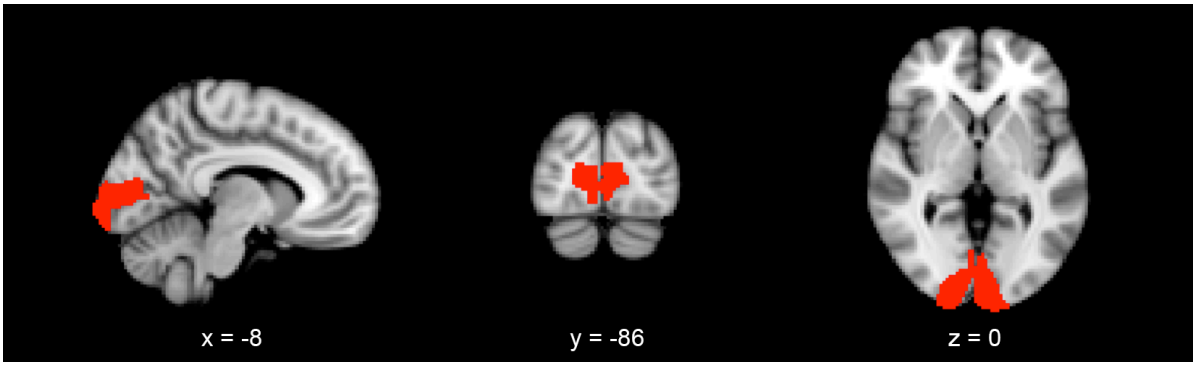

Figure 3.2 Anatomically defined ROI for sensitivity analysis. The ROI was a modified version of the Visual Cortex V1 structure from the Juelich Histological atlas. Mean BOLD amplitudes were extracted from all voxels within the anatomical ROI to normalize the longitudinal sampling of voxels.

viewed side by side and the threshold of detection was set by visually selecting a WMH that did not appear to change volume over time. This was done in an attempt to normalize for varying MR signal values over time. WMH volumes were calculated on baseline and follow-up FLAIR images and the difference between the follow-up and baseline volumes were determined to be the WMH change over time. The analyses were performed blinded to fMRI results.

SWI sequences were interpreted for the presence of cerebral microbleeds by a trained rater. Microbleed counts were categorized as described in section 2.2.3.6. Rater was blinded to clinical information and fMRI results. One subject was excluded from the microbleed analysis due to the poor quality of their SWI.

Microbleeds and WMH were classified and reported according to the standards for reporting vascular changes on neuroimaging (STRIVE).[87]

3.2.4 Statistical Analysis

BOLD amplitudes were approximately normally distributed and were compared within each group by paired t-test. The absolute difference between BOLD amplitudes at follow-up and

baseline were compared between CAA and healthy control groups by unpaired t-test. Due to the difference in prevalence of hypertension between the groups, and the variation in MR scanner used between subjects, a mixed-model linear regression was used to determine whether association between CAA and longitudinal BOLD amplitude change over time was independent of age, sex, hypertension, or MR scanner. Because of the small sample size, we used forward selection to serially enter and retain covariates significantly associated with the outcome, retaining only covariates with $p<0.05$ or where there was evidence for confounding of the CAA group effect (defined as a 20% shift in the model beta-coefficient). WMH volumes had right-skewed distributions and were log transformed to allow for longitudinal comparison by paired t-test as described in section 2.2.4. Among patients with CAA, the associations between longitudinal BOLD amplitude change over time and WMH volume at baseline or change over time was determined using the Spearman correlation coefficient. Because of the low numbers of subjects in microbleed categories 1-4, they were collapsed into one category resulting in 2 categories <20 microbleeds and ≥20 microbleeds. This was done in order to facilitate comparisons between microbleed counts and BOLD amplitude changes by unpaired t-test. Statistical analyses were performed using SAS version 9.3 (Cary, NC). For all statistical tests a p-value less than 0.05 was considered to be significant.

3.3 Results

3.3.1 Demographics

Clinical characteristics of each group are provided in Table 3.1. Patients with CAA were 72.6 ± 6.9 years old, were more likely to have hypertension than the healthy controls ($p<0.001$), but had similar distributions of coronary artery disease, hypercholesterolemia, diabetes mellitus, and tobacco use.

Table 3.1 Clinical features of the study populations.

Characteristics	Control (n=16),n	CAA (n=22),n	P value
Age (mean±SD)	68.4±5.9	72.6±6.9	0.06
Female	9	7	0.19
Hypertension	1	18	<0.001
Coronary Artery Disease	1	2	0.99
Hypercholesterolemia	12	8	0.99
Diabetes	0	5	0.06
Smoker	1	2	0.99
WMH volume change[1] (mL)	0.82	4.6	0.03

[1]WMH volume change, MRI white matter hyperintensity volume at follow-up subtracted by volume at baseline

3.3.2 BOLD Amplitude Changes

BOLD amplitude responses at baseline and follow-up are displayed graphically for healthy controls and CAA (Figure 3.3). In healthy controls, mean BOLD amplitude was the same at baseline and follow-up (2.54 ± 0.58% vs. 2.76 ± 0.59%, p=0.08) (Figure 3.3A), while in patients with CAA, the mean BOLD amplitude at 1-year follow-up was less than at baseline (1.98 ± 0.87% vs. 1.64 ± 0.77%, p=0.04) (Figure 3B). Scatterplots of the difference between baseline and follow-up, for patients with CAA and healthy controls (difference -0.34 ± 0.71% vs. 0.21 ± 0.48% respectively, p=0.007), are shown in Figure 3.4.

Mixed-model linear regression (Table 3.2) showed that there was a significant decrease in BOLD amplitudes over 1 year in CAA, from 1.98% to 1.64% (difference -0.55%, 95% CI -0.97 to -0.14, p=0.01) but no significant change in healthy controls, from 2.54% to 2.76% (difference +0.21%, 95% CI -0.10 to +0.53, p=0.18). The change over time in CAA was greater than in controls (p<0.001).

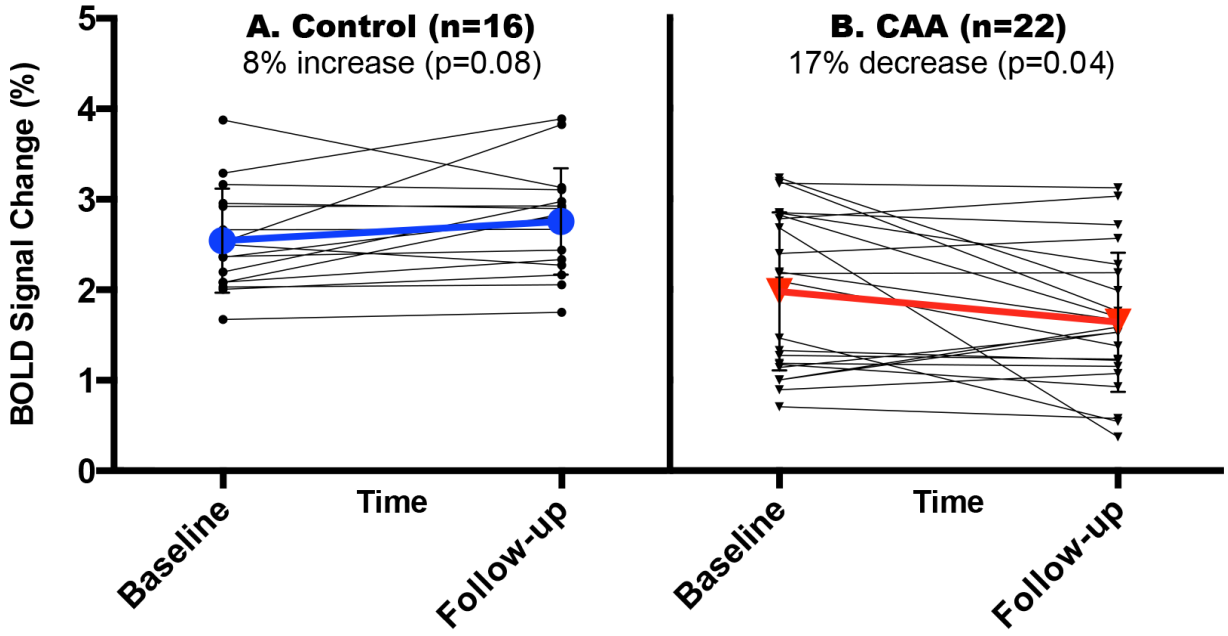

Figure 3.3 Longitudinal BOLD amplitude changes in response to a visual fMRI task. A) BOLD amplitudes did not change over time in healthy controls (2.54 ± 0.58% vs. 2.76 ± 0.59%, p=0.08). B) BOLD amplitudes decreased over time in CAA (1.98 ± 0.87% vs. 1.64 ± 0.77%, p=0.04). Coloured markers denote mean BOLD amplitude and error bars represent standard deviations. Significance was determined by paired t-test.

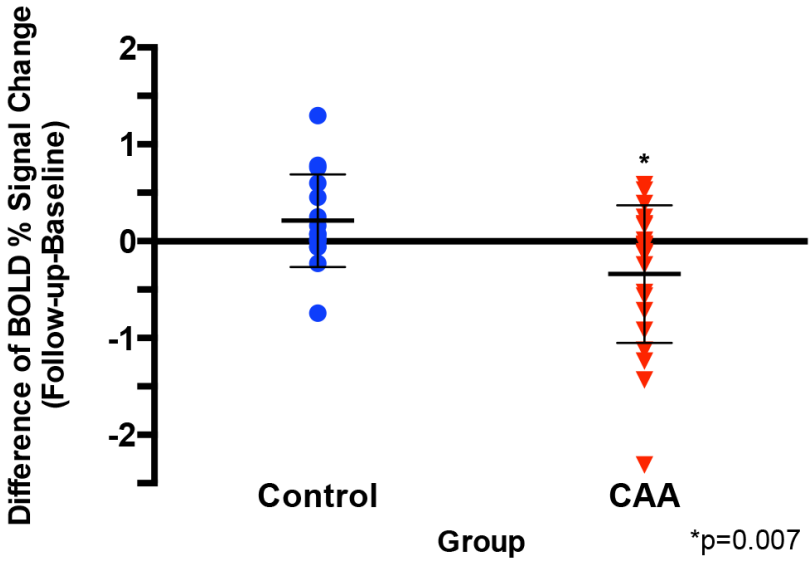

Figure 3.4 Absolute longitudinal difference in BOLD amplitude. There was a significant difference between patients with CAA and healthy controls in BOLD (difference -0.34 ± 0.71% vs. 0.21 ± 0.48% respectively, p=0.007). Error bars represent standard deviations. Significance was determined by unpaired t-test.

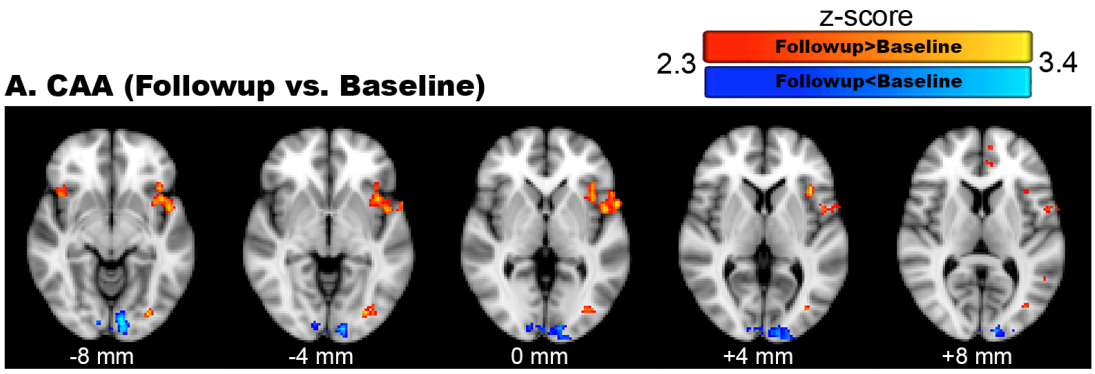

Figure 3.5 Longitudinal change in BOLD activation. fMRI activation was significantly lower at follow-up within the primary visual cortex in patients with CAA and are shown in blue. fMRI activation was significantly higher in the peri-insular regions, shown in red, which was unexpected and may be due to data outliers. Areas of activation were cluster corrected to z>2.3 with a significance of p<0.05.

Group contrast analyses showed that fMRI activation was significantly lower at follow-up within the primary visual cortex in patients with CAA (Figure 3.5), which was concordant with the calculated BOLD amplitude data. There was also increased fMRI activation at follow-up within the left anterior insular region. Upon investigating the individual z-scores for each subject and session, it was found that several patients had sub-threshold negative scores during the baseline session and sub-threshold positive scores at follow-up. This resulted in a significant difference between sessions. Hence, the insular activity difference between baseline and follow-up was most likely not physiologically meaningful. The difference observed in the visual cortex was more likely to be meaningful, as significant activation was observed at each time point.

To assess for potential confounders we repeated the model in Table 3.2, serially adding additional covariates for age, sex, hypertension and scanner effect. In the model controlling for CAA group status, there was no effect of age (p=0.15), sex (p=0.06), hypertension (p=0.87), or scanner model (p=0.19) on BOLD amplitude over time.

Table 3.2 Mixed model linear regression results.

	Baseline (Mean)	Follow-up (Mean)	Difference (Baseline minus follow-up)	P value for difference from baseline to follow-up	P value (Baseline difference between CAA and Control)	P value (Difference between slopes)
CAA	1.98%	1.68%	-0.34%	0.01		
					<0.001	0.01
Control	2.54%	2.76%	+0.21%	0.18		

The change from baseline to follow-up was significant for CAA (p=0.01) but not for controls (p=0.18)

The area of overlap between the 200 most active voxel masks from each time point was low for controls (average DICE±SD: 62±12%) and even lower for CAA (51±15%). In light of this information, we proceeded with the sensitivity analysis. The longitudinal decrease in BOLD amplitudes in patients with CAA remained significant in sensitivity analyses that employed an anatomically defined ROI as opposed to the 200 most active voxels for extracting BOLD amplitudes (Baseline: 1.27±0.56% vs. 1.01±0.51, p=0.027).

3.3.3 Longitudinal WMH Volume and Cerebral Microbleed Count Changes

In patients with CAA, WMH volumes increased over time (median 1.44 mL, interquartile range -0.56 to 9.25 mL, p=0.017) (Figure 3.6A). In patients with CAA, 2/4 subjects that had 2-4 microbleeds at baseline moved into the 5-20 microbleeds category at follow-up (Table 3.3). Longitudinal decrease in BOLD amplitude in the visual cortex was not correlated with higher baseline WMH volume (r=-0.15, p=0.36) or WMH volume increase over time (r=0.08, p=0.72) by Spearman correlation (Figure 3.6B). Patients with CAA that had more microbleeds at baseline had lower BOLD amplitudes at baseline (1.57±0.78% vs. 2.54±0.69%, p=0.009) (Figure 3.7A).

However, patients with CAA that had more microbleeds at baseline did not show greater BOLD amplitude loss over time (difference -0.19±0.74%, p=0.56) (Figure 3.7B).

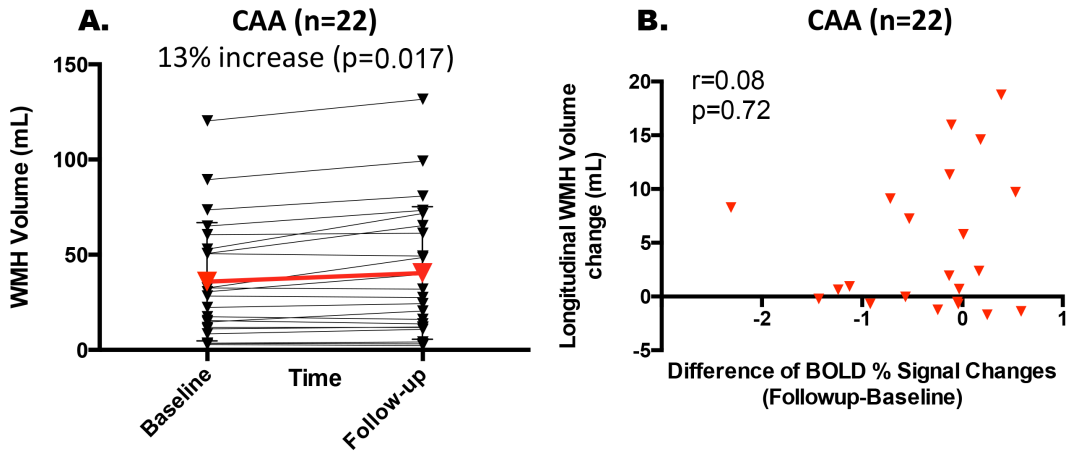

Figure 3.6 Relationships between WMH volumes and time or BOLD amplitude change in CAA. A) Longitudinal changes in WMH volumes. WMH volume increased over time (median 1.44 mL, interquartile range -0.56 to 9.25 mL, p=0.017). Triangles denote mean BOLD amplitude and error bars represent standard deviations. B) Relationship between absolute longitudinal difference in BOLD amplitudes and WMH volume progression in CAA. Longitudinal decrease in BOLD amplitude in the visual cortex was not correlated with WMH volume increase over time (r=0.08, p=0.72). WMH volume data was log transformed and significance was determined by Spearman correlation coefficient.

3.4 Discussion

Lower BOLD amplitudes at follow-up compared to baseline in patients with CAA but not in healthy controls imply that progressive impairment of vascular reactivity is a distinct feature of CAA, and is detectable even over a relatively short 1-year period of time. Our results confirm previous literature showing that BOLD responses to visual fMRI stimuli do not decrease in an aged, healthy control population, and therefore would not be expected to change over a 1-year period.[158] The present study provided new evidence to indicate that blood flow responses to visual tasks worsen over time in CAA; however, we did not find correlations between baseline or incident, WMH or microbleeds and change in BOLD amplitude.

Table 3.3 Microbleeds at baseline and follow-up in CAA.

Baseline microbleed category	Follow-up microbleed category: 0 CMBs	1 CMBs	2-4 CMBs	5-20 CMBs	≥20 CMBs
0 CMBs	1	0	0	0	0
1 CMBs	0	1	0	0	0
2-4 CMBs	0	0	2	2	0
5-20 CMBs	0	0	0	2	0
≥20 CMBs	0	0	0	0	13

CMBs = cerebral microbleeds

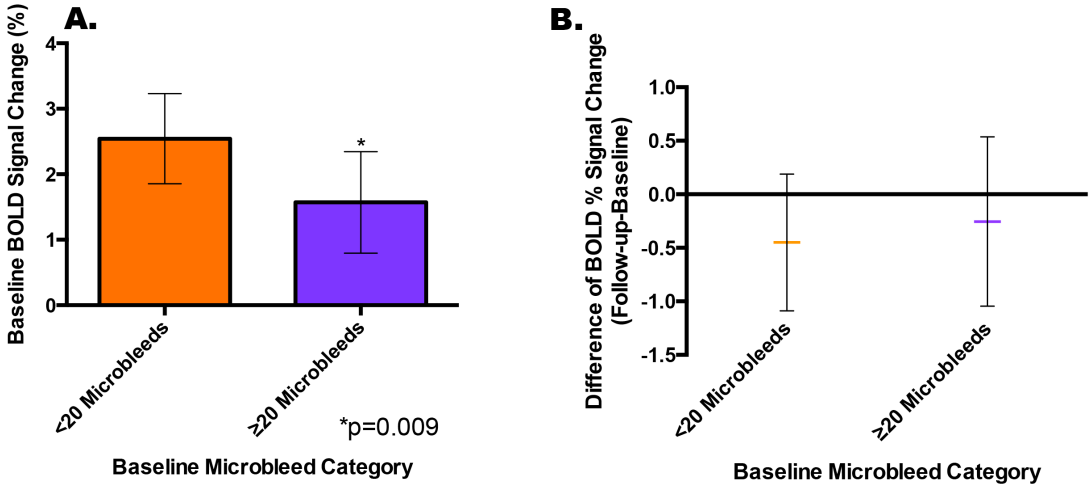

Figure 3.7 Relationships between baseline microbleed counts and baseline BOLD amplitude or BOLD change over time in CAA. A) Patients with more microbleeds at baseline had low BOLD amplitudes at baseline (2.54 ± 0.69% vs. 1.57 ± 0.78%, p=0.009). B) Patients with more microbleeds at baseline was not associated with greater BOLD loss over time (difference -0.19 ± 0.74%, p=0.56). Error bars represent standard deviations.

The results presented here are consistent with previous cross-sectional studies suggesting impaired visual task driven vascular reactivity as a novel characteristic of CAA.[67,74] Previous studies suggested that lower BOLD amplitudes in response to a visual stimulus task were a result of vascular impairment and not neuronal dysfunction in CAA.[67] Further, another study showed reduced blood flow responses to a visual task in patients with CAA compared to healthy controls, despite no difference in resting blood flow in both populations.[74] These findings suggest that decreased BOLD amplitudes in CAA result from impaired vascular reactivity rather than reduced blood flow delivery due to decreased neuronal activity or abnormal cerebral blood supply. While the two previous cross-sectional studies have provided evidence for impaired vascular reactivity as an important feature of CAA, the present study is the first to detect the progression of this feature over time in CAA. A previous study showed that vascular reactivity was impaired in a patient with pre-symptomatic hereditary CAA;[132] the present study showed that impaired vascular reactivity was not limited to early stages of the disease and was progressively worsening even in patients with more advanced symptomatic CAA.

BOLD activation differences over 1 year for CAA were concordant with the BOLD amplitude differences over time. Within the primary visual cortex, there was lower BOLD activation seen at follow-up compared to baseline. These data indicated that the primary visual cortex may have been affected by vascular reactivity impairment, which was expected based on the known distribution of vascular amyloid deposition in CAA.[156] Conversely, the data showed that there was increased activation over time in the left anterior insular cortex in response to a visual stimulus. It was determined that the activity differences seen in the insular cortex were not physiologically meaningful, and instead were driven by several outliers having sub-threshold negative scores at baseline and sub-threshold positive scores at follow-up. The difference

between these scores were significant, however, there was no significant insular activity seen at either session. The differences observed in the visual cortex across sessions were more likely to be physiologically meaningful as there was significant activation present at both baseline and follow-up scans.

In our primary analysis we defined the ROI based on the most active voxels on each scan, analogous to the approach in our cross-sectional study.[67] However, we acknowledged that the anatomical area represented by the most activated voxels might change over time due to progressive disease activity as well as normal non-physiological variation in fMRI signal.[159,160] We tested this using the DICE coefficient of overlap analysis described in section 3.2.3.2 and discovered that the 200 most active voxels masked different anatomical areas over time. In light of this information, we performed a sensitivity analysis where we determined the BOLD response in an anatomically defined region, selected independently of voxel activation. This sensitivity analysis, showing lower BOLD amplitudes at follow up compared to baseline in the region of the primary visual cortex, was concordant with our primary analysis.

WMH of presumed vascular origin are seen in normal elderly, but the volume is much higher in patients with CAA or other vascular diseases.[150] WMH are considered a marker of CAA severity,[54] and WMH progression has been detected in CAA patients over a median 14 month period.[161] Our results confirm that WMH progression can be detected in CAA over a short time interval. However, we did not find a correlation between either baseline WMH or WMH progression and the decrease in BOLD amplitudes. Similarly, we did not find a correlation between baseline microbleed count, and BOLD amplitude change. We were not able to determine a relationship between increasing microbleed count and greater BOLD amplitude loss

over time because the categorical method of classifying microbleeds was not sensitive enough to detect changes in the appearance of microbleeds over time. Obtaining accurate microbleed counts for each patient and time point was not feasible because some patients with CAA had many microbleeds and counting each one was too arduous of a task for the rater. Currently, software for computer-aided microbleed counting is under development at Calgary Image Processing and Analysis Center (CIPAC) to be used in future studies. Future studies would benefit from obtaining accurate microbleed counts in order to help discern a relationship with BOLD amplitude loss over time. The reasons for the lack of correlations between these CAA markers is unclear, but could be related to the small study sample size, or could indicate that impaired vascular reactivity is a feature of CAA but that impaired vascular reactivity is not directly causative of WMH or microbleeds.

The principle limitation of our study was the small sample size; however, we were able to detect a significant decrease in BOLD amplitudes over time in CAA. These results act as important preliminary data that should be further investigated in larger studies. It was possible that we were unable to determine a correlation between impaired vascular reactivity and increasing WMH volume burden over time because of the low sample size, and therefore future larger studies will be needed to thoroughly investigate this relationship. Because of the small sample size, we had insufficient power to investigate associations between BOLD amplitude signal change and cognitive decline or recurrent ICH. Finally this study is limited by the short, 1-year follow-up; although a significant longitudinal decrease in vascular reactivity was detected, a longer follow-up with 1-year intervals could be helpful in determining the time course of vascular reactivity impairment in CAA, including the identification of stages in CAA severity, and how it can be used to predict brain injury and CAA-related ICH.

3.5 Conclusions

We measured BOLD amplitudes in response to a visual stimulus task longitudinally in CAA to detect a change in vascular reactivity over a short follow-up period, and to see if this change was associated with other markers of CAA severity. Our results showed that lower BOLD responses were seen after 1 year in the CAA group but not in similarly-aged controls, and these findings supported the utility of visual fMRI task-related BOLD amplitude as a biomarker representing vascular function in CAA. We did not determine any relationships between the decreasing BOLD amplitude and progression of other CAA biomarkers, which may suggest that impaired vascular reactivity is not causally related to the formation of WMHs and microbleeds. While this study was preliminary, we have been able to suggest that BOLD fMRI may be a useful surrogate outcome marker for early phase clinical trials where it would not be feasible to recruit the large numbers of patients needed to detect outcomes such as symptomatic recurrent ICH.

Chapter Four: **Conclusion and Future Directions**

This final chapter includes a summary of the results regarding BOLD amplitudes as a surrogate marker for vascular reactivity in CAA and AD. Secondly, this chapter will provide overarching conclusions based on the discussion of the cross-sectional comparisons of BOLD amplitudes across patients with CAA, AD, MCI, and healthy controls (Chapter 2) and the longitudinal change in BOLD amplitudes over time in CAA (Chapter 3).

4.1 Summary of Results

Previous fMRI studies have implicated BOLD amplitudes in response to a visual stimulus task as a surrogate marker of vascular reactivity in CAA.[67,74] Based on these studies, we aimed to assess the vascular reactivity profiles of patients with AD and MCI, based on measured BOLD amplitudes, as well as to characterize the change in BOLD amplitudes over a 1-year period in patients with CAA. In Chapter 2, we hypothesized that BOLD amplitudes in response to a visual stimulus would be highest in healthy controls, followed by MCI, then AD, and lowest in CAA, based on the estimated severity of amyloid deposition in each condition. In Chapter 3, we hypothesized that BOLD amplitudes would decrease over time in patients with CAA but remain unchanged in the healthy control population. As secondary aims, we assessed the relationships between the cross-sectional or longitudinal differences in BOLD amplitudes, and the severity or progression of WMH volumes and microbleed counts, other markers of CAA severity.

The original research presented in Chapter 2 demonstrated differences in BOLD amplitudes in response to a visual stimulus task between patients with mild AD, MCI, CAA, and healthy controls. However, these differences were not exactly as we hypothesized. It was demonstrated that BOLD amplitudes were significantly lower in patients with CAA compared to

healthy controls, which was concordant with previous literature,[67,74] and expected to been seen as hypothesized. Contrarily, patients with MCI also exhibited a trend toward lower BOLD amplitudes compared to healthy controls, which was not expected. Patients with AD displayed BOLD amplitudes that were not significantly different than patients with CAA or healthy controls, again contrary to our hypotheses. WMH volume differences between the groups followed similar trends seen in the BOLD amplitude differences, where patients with MCI and CAA had significantly higher WMH volumes compared to healthy controls and patients with AD had WMH volumes that were significantly higher than healthy controls and significantly lower than patients with CAA. Cerebral microbleeds were present in the CAA population in varying quantities. Higher WMH volumes and more microbleeds were associated with lower BOLD amplitudes in CAA, as shown in a previous study;[67] but there were no associations between either WMH volumes and BOLD amplitudes in patients with AD or MCI.

The results shown in Chapter 3 indicated that BOLD amplitudes in response to a visual stimulus decreased over time in patients with CAA but did not change in healthy controls. The finding in CAA was consistent regardless of whether the BOLD amplitudes were extracted from the most active areas of the primary visual cortex or from an anatomically defined region. Longitudinal changes in BOLD amplitudes in CAA were also independent of age, sex, the presence of hypertension, or the MRI scanner the subject was scanned in. In patients with CAA, WMH volumes increased over time. Neither WMH volumes at baseline, longitudinal increases in WMH volumes, or the number of microbleeds at baseline were associated with the longitudinal decrease in BOLD amplitudes seen in CAA.

4.2 Overall Conclusions

Results from Chapter 2 failed to show that BOLD amplitudes in response to a visual stimulus task could be used to effectively distinguish between patients with CAA, MCI, and AD. However, the results did suggest some unexpected findings regarding vascular reactivity in MCI. Patients with MCI possess the potential to develop into AD, vascular dementia, or revert to normal aging,[162] so we reasoned that BOLD amplitudes would have been higher than AD and CAA. Contrarily, the results from Chapter 2 indicated that vascular reactivity in patients with MCI may be more impaired than in patients with AD, which was not expected. One possible explanation for this finding was that patients with MCI exhibited higher WMH burden than the healthy control or AD groups. Higher WMH burden is indicative of more severe cerebral small vessel disease,[163] so it would follow that some of the MCI patients may have had vascular cognitive impairment. Because vascular cognitive impairment may be associated with lower resting brain perfusion, future studies should look at resting CBF in MCI to determine if the change in BOLD amplitude is associated with lower perfusion. Future studies should also examine whether MCI patients with lower BOLD amplitude responses are more likely to convert to dementia.

With the current sample size we were unable to detect any significant differences in BOLD amplitudes between patients with AD and the healthy control or CAA groups. Larger studies with greater statistical power are required for establishing the vascular reactivity profile in patients with AD. After completion of this thesis, our lab plans to recruit 20 more AD and 10 more MCI patients to provide a total sample size of 30 CAA, 30 AD and 20 MCI.

Results from Chapter 3 extend our knowledge of blood flow regulation disturbances in CAA by showing that changes in BOLD amplitude responses to a visual task can be detected over 1 year, with lower BOLD responses seen at 1 year in the CAA group but not in similarly-aged controls. However, it remains unclear how vascular reactivity impairment is related to other biomarkers of CAA severity. The longitudinal decrease in BOLD amplitude in patients with CAA occurred independently of age, sex, scanner, or the presence of coexisting hypertension, which further validates its use as a biomarker of CAA vascular health. A previous study had shown that lower BOLD amplitudes were associated with higher WMH volumes[67] so it would have followed that increasing WMH volumes over time would correlate with decreasing BOLD amplitudes. Unfortunately, we failed to determine a relationship between these two biomarkers. It was possible that the incidence of WMH volume growth over time could have been a process independent of vascular reactivity impairment as it has been previously suggested that WMHs may have a nonvascular etiology.[164] Similarly, we were unable to determine a relationship between increasing cerebral microbleed counts and decreasing BOLD amplitudes in CAA. This was most likely a product of using categories to characterize the amount of microbleeds across time, which was not sensitive enough to detect longitudinal changes between categories. Future studies are required to further characterize the relationship between CAA-related vascular reactivity impairment and progression of other markers of CAA severity.

The two principal limitations of the research presented in this thesis are small sample sizes and a short duration between baseline and follow-up scans. The small sample sizes for the MCI and AD groups limit our statistical confidence in the group differences in BOLD amplitudes. However, we were able to show a significant difference in BOLD amplitudes between the healthy control and CAA groups because the difference was large. Because of small

sample sizes we chose not to assess the relationship between lower BOLD amplitudes and cognitive decline. We made this decision because the neuropsychiatric data tends to show larger variances; therefore, we expected that larger sample sizes would be needed to determine statistically significant results. The short 1-year follow-up limited our longitudinal study. Despite the short follow-up, we were able to detect a significant decrease in BOLD amplitudes over time in patients with CAA. Larger studies with longer follow-up will be needed to better define the shape of decreasing BOLD amplitude responses over time (e.g. whether it linear or whether it asymptotically approaches a floor value), and whether changing responses predict CAA-related ICH, which has an incidence of about 10% per year.

Overall, the results from this thesis provide support for the use of BOLD amplitudes in response to a visual task for assessing vascular reactivity in CAA. However, more work is required to determine how BOLD amplitudes change in patients with MCI and AD. Future work is also required to determine how vascular reactivity changes over time in CAA and how the impairment relates to other pathological changes associated with CAA, such as the incidence of CAA-related ICH or changes in cognition.

4.3 Future Directions

The next step in researching the utility of BOLD amplitudes in response to a visual task would be to have larger studies with longer follow-up periods. Such studies could potentially determine how vascular reactivity impairment is associated with Aβ-related diseases such as MCI and mild AD, as well as help to elucidate the temporal course of vascular reactivity impairment in patients with CAA.

Another role for future studies would be to determine the relationship between the amount of deposited vascular amyloid and the degree to which vascular reactivity is impaired. Amyloid PET imaging is a modality that is capable of identifying the distribution of aggregated, fibrillar beta-amyloid deposits in the brain antemortem (refer to Section 1.4.4).[165] Amyloid PET tracers appear to bind both parenchymal and vascular deposits of beta-amyloid with strong affinity.[73,91,92] Using amyloid PET studies in conjunction with fMRI studies could identify whether the degree of amyloid binding in the occipital cortex is correlated with the BOLD amplitude in response to a visual task. Additionally, amyloid PET imaging could be used to distinguish MCI caused by AD from MCI caused by other factors, to see if BOLD amplitude responses differ in those two groups. Unfortunately, amyloid PET imaging was not feasible for our study because the University of Calgary did not have cyclotron facility and we did not have access to PET tracers from other sources.

As previously mentioned, we were unable to determine any associations between global WMH volumes or cerebral microbleeds and the change in task-related BOLD amplitudes over time in a specific region, the occipital cortex. It is possible that occipital BOLD changes might correlate more closely with occipital microbleed count or posterior WMH, than with total microbleed count or total WMH. Planned future studies, to be completed after the thesis, will test this hypothesis. However, we consider it unlikely that stronger associations will emerge, because we expect that local microbleed count and WMH volume will correlate strongly with total microbleed count and global WMH volume.

Several fMRI studies have used inhaled carbon dioxide to induce a global vasodilation in the brain that is useful for assessing cerebrovascular reactivity.[166-172] Hypercapnic BOLD studies

would provide a global measure of vascular reactivity that would allow investigation of regional correlations between impaired reactivity and other markers of small vessel disease severity.

4.4 Implications for Clinical Care

Presently, this research is too preliminary to directly transfer to physician use in clinical care. However, the results presented in this thesis show promise for the use of BOLD amplitudes as a marker of *in vivo* cerebrovascular function. By showing that BOLD amplitude change over time can be detected during a clinically feasible follow-up period of 1 year, these findings support the utility of visual fMRI task-related BOLD amplitude as one of a growing number of biomarkers in CAA. Because BOLD amplitude change is a continuous measure of vascular function, it could potentially be improved in the short term by treatments that restore more normal vascular function. This offers a potential advantage over other biomarkers, such as MRI evidence of hemorrhage or WMH, that represent non-modifiable and slowly accruing irreversible structural changes. Therefore, BOLD fMRI may be a useful surrogate outcome marker for early phase clinical trials where it would not be feasible to recruit the large numbers of patients needed to detect outcomes such as symptomatic recurrent ICH.[54] An early phase clinical trial of the anti-Aβ monoclonal antibody ponezumab for treatment of CAA (clinicaltrials.gov NCT01821118) incorporates BOLD fMRI as the principal surrogate outcome measure, and will provide the first evidence for whether CAA-associated vascular dysfunction is potentially modifiable. The present study showed that progressively impaired vascular reactivity was detectable in CAA; whether modifying vascular reactivity is possible and beneficial to the patient awaits the development of effective treatments for CAA, for which there are currently none.

References:

1 Seshadri, S. & Wolf, P. A. Lifetime risk of stroke and dementia: current concepts, and estimates from the Framingham Study. *The Lancet Neurology* **6**, 1106-1114, doi:http://dx.doi.org/10.1016/S1474-4422(07)70291-0 (2007).

2 Barnes, D. E. & Yaffe, K. The projected effect of risk factor reduction on Alzheimer's disease prevalence. *The Lancet Neurology* **10**, 819-828, doi:http://dx.doi.org/10.1016/S1474-4422(11)70072-2 (2011).

3 Alzheimer's Society of Canada. Rising Tide: Impact of Dementia on Canadian Society. <http://www.alzheimer.ca/en/Get-involved/Raise-your-voice/Rising-Tide/Rising-tide-summary> (2009).

4 Dubois, B. *et al.* Research criteria for the diagnosis of Alzheimer's disease: revising the NINCDS–ADRDA criteria. *The Lancet Neurology* **6**, 734-746, doi:http://dx.doi.org/10.1016/S1474-4422(07)70178-3 (2007).

5 Huang, H.-C. & Jiang, Z.-F. Accumulated Amyloid-β Peptide and Hyperphosphorylated Tau Protein: Relationship and Links in Alzheimer's Disease. *Journal of Alzheimer's Disease* **16**, 15-27, doi:10.3233/jad-2009-0960 (2009).

6 Britt, W. G. *et al.* Mild Cognitive Impairment: Prodromal Alzheimer's Disease or Something Else? *Journal of Alzheimer's Disease* **27**, 543-551, doi:10.3233/JAD-2011-110740 (2011).

7 Mitchell, A. J. & Shiri-Feshki, M. Rate of progression of mild cognitive impairment to dementia – meta-analysis of 41 robust inception cohort studies. *Acta Psychiatrica Scandinavica* **119**, 252-265, doi:10.1111/j.1600-0447.2008.01326.x (2009).

8 Vinters, H. V. Cerebral amyloid angiopathy. A critical review. *Stroke* **18**, 311-324, doi:10.1161/01.str.18.2.311 (1987).

9 Smith, E. E. & Eichler, F. Cerebral amyloid angiopathy and lobar intracerebral hemorrhage. *Archives of Neurology* **63**, 148-151, doi:10.1001/archneur.63.1.148 (2006).

10 Charidimou, A. *et al.* Spectrum of Transient Focal Neurological Episodes in Cerebral Amyloid Angiopathy: Multicentre Magnetic Resonance Imaging Cohort Study and Meta-Analysis. *Stroke* **43**, 2324-2330 (2012).

11 Cupino, T. & Zabel, M. Alzheimer's Silent Partner: Cerebral Amyloid Angiopathy. *Transl. Stroke Res.*, 1-8, doi:10.1007/s12975-013-0309-7 (2013).

12 Perez, R. G., Zheng, H., van der Ploeg, L. H. T. & Koo, H. K. The beta-Amyloid Precursor Protein of Alzheimer's Disease Enhances Neuron Viability and Modulates Neuronal Polarity. *The journal of Neuroscience* **17**, 9407-9414 (1997).

13 Huang, H.-C. & Jiang, Z.-F. Amyloid-β Protein Precursor Family Members: A Review from Homology to Biological Function. *Journal of Alzheimer's Disease* **26**, 607-626, doi:10.3233/jad-2011-110335 (2011).

14 Thinakaran, G. & Koo, E. H. Amyloid Precursor Protein Trafficking, Processing, and Function. *Journal of Biological Chemistry* **283**, 29615-29619 (2008).

15 Zhang, X. & Song, W. The role of APP and BACE1 trafficking in APP processing and amyloid-β generation. *Alzheimer's Research & Therapy* **5**, doi:10.1186/alzrt211 (2013).

16 Schmidt, M. *et al.* Comparison of Alzheimer Aβ(1–40) and Aβ(1–42) amyloid fibrils reveals similar protofilament structures. *Proceedings of the National Academy of Sciences* **106**, 19813-19818 (2009).

17 Zhang, S., Zhang, M., Cai, F. & Song, S. Biological function of Presenilin and its role in AD pathogenesis. *Translational Neurodegeneration* **2**, 1-13 (2013).
18 Biffi, A. & Greenberg, S. Cerebral Amyloid Angiopathy: A Systematic Review. *The Journal of Clinical Neurology* **7**, 1-9, doi:10.3988/jcn.2011.7.1.1 (2011).
19 Tanzi, R. E., Moir, R. D. & Wagner, S. L. Clearance of Alzheimer's Aβ Peptide: The Many Roads to Perdition. *Neuron* **43**, 605-608, doi:http://dx.doi.org/10.1016/j.neuron.2004.08.024 (2004).
20 Smith, E. E. & Greenberg, S. M. β-Amyloid, Blood Vessels, and Brain Function. *Stroke* **40**, 2601-2606, doi:10.1161/strokeaha.108.536839 (2009).
21 Dash, P. in *Neuroscience Online: An Electronic Textbook for Neurosciences* (ed J H Bryne) Ch. 11, (The University of Texis Medical School at Houston (UTHealth), 1997).
22 Weller, R. O., Subash, M., Preston, S. D., Mazanti, I. & Carare, R. O. Clearance of Aβ from the Brain in Alzheimer's Disease: Perivascular Drainage of Amyloid-β Peptides from the Brain and Its Failure in Cerebral Amyloid Angiopathy and Alzheimer's Disease. *Brain Pathology* **18**, 253-266, doi:10.1111/j.1750-3639.2008.00133.x (2008).
23 Benilova, I., Karran, E. & De Strooper, B. The toxic A[beta] oligomer and Alzheimer's disease: an emperor in need of clothes. *Nat Neurosci* **15**, 349-357, doi:http://www.nature.com/neuro/journal/v15/n3/abs/nn.3028.html - supplementary-information (2012).
24 Dubois, B. *et al.* Revising the definition of Alzheimer's disease: a new lexicon. *The Lancet Neurology* **9**, 1118-1127, doi:http://dx.doi.org/10.1016/S1474-4422(10)70223-4 (2010).
25 Tanzi, R. E. The synaptic Aβ hypothesis of Alzheimer disease. *Nat Neurosci* **8**, 977-979 (2005).
26 Berrios, G. E. Alzheimer's disease: A conceptual history. *International Journal of Geriatric Psychiatry* **5**, 355-365, doi:10.1002/gps.930050603 (1990).
27 *Information about Alzheimer's and related dementias*, <http://www.cihr-irsc.gc.ca/e/45554.html> (2011).
28 Yaari, R. & Corey-Bloom, J. Alzheimer's Disease. *Seminars in Neurology* **27**, 32-41 (2007).
29 Kawas, C., Gray, S., Brookmeyer, R., Fozard, J. & Zonderman, A. Age-specific incidence rates of Alzheimer's disease: the Baltimore Longitudinal Study of Aging. *Neurology* **54**, 2072-2077 (2000).
30 Hayden, K. M. *et al.* Vascular Risk Factors for Incident Alzheimer Disease and Vascular Dementia: The Cache County Study. *Alzheimer disease and associated disorders* **20**, 93-100 (2006).
31 Skoog, I. *et al.* 15-year longitudinal study of blood pressure and dementia. *The Lancet* **347**, 1141-1145, doi:http://dx.doi.org/10.1016/S0140-6736(96)90608-X (1996).
32 Skoog, I. *et al.* A population study on blood-brain barrier function in 85-year-olds Relation to Alzheimer's disease and vascular dementia. *Neurology* **50**, 966-971 (1998).
33 Launer, L. J. *et al.* Midlife blood pressure and dementia: the Honolulu–Asia aging study ☆ . *Neurobiology of Aging* **21**, 49-55, doi:http://dx.doi.org/10.1016/S0197-4580(00)00096-8 (2000).

34 Sparks, D. L., Martin, T. A., Gross, D. R. & Hunsaker, J. C. Link between heart disease, cholesterol, and Alzheimer's disease: A review. *Microscopy Research and Technique* **50**, 287-290, doi:10.1002/1097-0029(20000815)50:4<287::AID-JEMT7>3.0.CO;2-L (2000).
35 Miia, K. *et al.* Midlife vascular risk factors and Alzheimer's disease in later life: longitudinal, population based study. *BMJ* **322** (2001).
36 Kivipelto, M. *et al.* Apolipoprotein E ε4 Allele, Elevated Midlife Total Cholesterol Level, and High Midlife Systolic Blood Pressure Are Independent Risk Factors for Late-Life Alzheimer Disease. *Annals of Internal Medicine* **137**, 149-155, doi:10.7326/0003-4819-137-3-200208060-00006 (2002).
37 Peila, R., Rodriguez, B. L. & Launer, L. J. Type 2 diabetes, APOE gene, and the risk for dementia and related pathologies The Honolulu-Asia Aging Study. *Diabetes* **51**, 1256-1262 (2002).
38 Gustafson, D., Rothenberg, E., Blennow, K., Steen, B. & Skoog, I. AN 18-year follow-up of overweight and risk of alzheimer disease. *Archives of Internal Medicine* **163**, 1524-1528, doi:10.1001/archinte.163.13.1524 (2003).
39 Puglielli, L., Tanzi, R. E. & Kovacs, D. M. Alzheimer's disease: the cholesterol connection. *Nat Neurosci* **6**, 345-351 (2003).
40 Hardy, J. & Selkoe, D. J. The Amyloid Hypothesis of Alzheimer's Disease: Progress and Problems on the Road to Therapeutics. *Science* **297**, 353-356 (2002).
41 Liu, Y.-H. *et al.* Clearance of Amyloid-Beta in Alzheimer's Disease: Shifting the Action Site from Center to Periphery. *Mol Neurobiol*, 1-7, doi:10.1007/s12035-014-8694-9 (2014).
42 Barnham, K. J., Masters, C. L. & Bush, A. I. Neurodegenerative diseases and oxidative stress. *Nat Rev Drug Discov* **3**, 205-214 (2004).
43 Wang, H.-Y., Lee, D. H. S., Davis, C. B. & Shank, R. P. Amyloid Peptide Aβ1-42 Binds Selectively and with Picomolar Affinity to α7 Nicotinic Acetylcholine Receptors. *Journal of Neurochemistry* **75**, 1155-1161, doi:10.1046/j.1471-4159.2000.0751155.x (2000).
44 Tagami, S. *et al.* Involvement of apoptosis and cholinergic dysfunction in Alzheimer's disease. *Psychogeriatrics* **6**, S57-S63, doi:10.1111/j.1479-8301.2006.00172.x (2006).
45 Iqbal, K. & Grundke-Iqbal, I. Metabolic/signal transduction hypothesis of Alzheimer‚Äôs disease and other tauopathies. *Acta Neuropathol* **109**, 25-31, doi:10.1007/s00401-004-0951-y (2005).
46 McKhann, G. M. *et al.* The diagnosis of dementia due to Alzheimer's disease: Recommendations from the National Institute on Aging-Alzheimer's Association workgroups on diagnostic guidelines for Alzheimer's disease. *Alzheimer's & Dementia* **7**, 263-269, doi:http://dx.doi.org/10.1016/j.jalz.2011.03.005 (2011).
47 Lyketsos, C. G. & Olin, J. Depression in Alzheimer's disease: overview and treatment. *Biological psychiatry* **52**, 243-252 (2002).
48 Galasko, D. *et al.* The mini-mental state examination in the early diagnosis of Alzheimer's disease. *Archives of Neurology* **47**, 49-52, doi:10.1001/archneur.1990.00530010061020 (1990).
49 Edison, P. *et al.* Amyloid, hypometabolism, and cognition in Alzheimer disease: An [11C]PIB and [18F]FDG PET study. *Neurology* **68**, 501-508 (2007).
50 Blennow, K., de Leon, M. J. & Zetterberg, H. Alzheimer's disease. *The Lancet* **368**, 387-403, doi:http://dx.doi.org/10.1016/S0140-6736(06)69113-7 (2006).

51 MRC CFAS. Pathological correlates of late-onset dementia in a multicentre, community-based population in England and Wales. *The Lancet* **357**, 169-175, doi:http://dx.doi.org/10.1016/S0140-6736(00)03589-3 (2001).
52 Knudsen, K. A., Rosand, J., Karluk, D. & Greenberg, S. M. Clinical diagnosis of cerebral amyloid angiopathy: Validation of the Boston Criteria. *Neurology* **56**, 537-539 (2001).
53 Linn, J. *et al.* Prevalence of superficial siderosis in patients with cerebral amyloid angiopathy. *Neurology* **74**, 1346-1350 (2010).
54 Greenberg, S. M. *et al.* Outcome markers for clinical trials in cerebral amyloid angiopathy. *The Lancet Neurology* **13**, 419-428, doi:http://dx.doi.org/10.1016/S1474-4422(14)70003-1 (2014).
55 Oppenheim, G. Über "drusige Nekrosen" in der Grosshirnrinde. *Neural. Centralbl.* **28**, 410-413 (1909).
56 Charidimou, A. & Werring, D. J. Cerebral microbleeds and cognition in cerebrovascular disease: An update. *Journal of the Neurological Sciences* **322**, 50-55, doi:http://dx.doi.org/10.1016/j.jns.2012.05.052 (2012).
57 Liu, C., Kanekiyo, T., Xu, H. & Bu, G. Apolipoprotein E and Alzheimer disease: risk, mechanisms, and therapy. *Nat Rev Neurol* **9**, 106-118 (2013).
58 Hawkes, C. A. *et al.* Disruption of Arterial Perivascular Drainage of Amyloid-β from the Brains of Mice Expressing the Human APOE ε4 Allele. *PLoS ONE* **7**, e41636, doi:10.1371/journal.pone.0041636 (2012).
59 Chen, Y.-W., Lee, M.-J. & Smith, E. E. Reviews: Cerebral amyloid angiopathy in East and West. *International Journal of Stroke* **5**, 403-411, doi:10.1111/j.1747-4949.2010.00466.x (2010).
60 Thal, D. R. G., Estifanos; Rub, Udo; Yamaguchi, Haruyasa; Tredici, Kelly Del; Braak, Heiko. Two Types of Sporadic Cerebral Amyloid Angiopathy. *Journal of Neuropathology & Experimental Neurology* **61**, 282-293 (2002).
61 McCarron, M. O. *et al.* The Apolipoprotein E [epsilon]2 Allele and the Pathological Features in Cerebral Amyloid Angiopathy-related Hemorrhage. *Journal of Neuropathology & Experimental Neurology* **58** (1999).
62 A, V. *et al.* Antiplatelet use after intracerebral hemorrhage. *Neurology* **66**, 206-209 (2006).
63 Gahr, M., Nowak, D. A., Connemann, B. J. & Schönfeldt-Lecuona, C. Cerebral amyloidal angiopathy—A disease with implications for neurology and psychiatry. *Brain Research* **1519**, 19-30, doi:http://dx.doi.org/10.1016/j.brainres.2013.04.052 (2013).
64 Arvanitakis, Z. *et al.* Cerebral amyloid angiopathy pathology and cognitive domains in older persons. *Annals of Neurology* **69**, 320-327, doi:10.1002/ana.22112 (2011).
65 Kinnecom, C. L., M H.; Wendell, L; Smith, E E.; Rosand, J; Frosch, M P.; Greenberg, S M. Course of cerebral amyloid angiopathy–related inflammation. *Neurology* **68**, 1411-1416, doi:10.1212/01.wnl.0000260066.98681.2e (2007).
66 Arima, H. *et al.* Effects of Perindopril-Based Lowering of Blood Pressure on Intracerebral Hemorrhage Related to Amyloid Angiopathy: The PROGRESS Trial. *Stroke* **41**, 394-396 (2010).
67 Peca, S. *et al.* Neurovascular Decoupling is Associated with Severity of Cerebral Amyloid Angiography. *Neurology* **81**, 1659-1665 (2013).

68 Charidimou, A., Krishnan, A., Werring, D. & Rolf Jäger, H. Cerebral microbleeds: a guide to detection and clinical relevance in different disease settings. *Neuroradiology* **55**, 655-674, doi:10.1007/s00234-013-1175-4 (2013).
69 Maillard, P. *et al.* FLAIR and Diffusion MRI Signals Are Independent Predictors of White Matter Hyperintensities. *American Journal of Neuroradiology* **34**, 54-61 (2013).
70 Salat, D. H. *et al.* White Matter Alterations in Cerebral Amyloid Angiopathy Measured by Diffusion Tensor Imaging. *Stroke* **37**, 1759-1764 (2006).
71 Charidimou, A. *et al.* White matter perivascular spaces: An MRI marker in pathology-proven cerebral amyloid angiopathy? *Neurology* **82**, 57-62 (2014).
72 Gregoire, S. M. *et al.* Acute ischaemic brain lesions in intracerebral haemorrhage: multicentre cross-sectional magnetic resonance imaging study. *Brain* **134**, 2376-2386 (2011).
73 Greenberg, S. M. *et al.* Detection of isolated cerebrovascular β-amyloid with pittsburgh compound B. *Annals of Neurology* **64**, 587-591, doi:10.1002/ana.21528 (2008).
74 Dumas, A. *et al.* Functional magnetic resonance imaging detection of vascular reactivity in cerebral amyloid angiopathy. *Annals of Neurology* **72**, 76-81, doi:10.1002/ana.23566 (2012).
75 Sacco, R. L. *et al.* An updated definition of stroke for the 21st century: a statement for healthcare professionals from the American Heart Association/American Stroke Association. *Stroke* **44**, 2064-2089, doi:10.1161/STR.0b013e318296aeca (2013).
76 Kidwell, C. S., Chalela, J. A., Saver, J. L. & et al. Comparison of MRI and CT for detection of acute intracerebral hemorrhage. *JAMA* **292**, 1823-1830, doi:10.1001/jama.292.15.1823 (2004).
77 Fazekas, F. *et al.* Histopathologic Analysis of Foci of Signal Loss on Gradient-Echo T2*-Weighted MR Images in Patients with Spontaneous Intracerebral Hemorrhage: Evidence of Microangiopathy-Related Microbleeds. *American Journal of Neuroradiology* **20**, 637-642 (1999).
78 Vinters, H. V. & Gilbert, J. J. Cerebral amyloid angiopathy: incidence and complications in the aging brain. II. The distribution of amyloid vascular changes. *Stroke* **14**, 924-928 (1983).
79 Pantoni, L. & Garcia, J. H. Pathogenesis of Leukoaraiosis: A Review. *Stroke* **28**, 652-659 (1997).
80 Grinberg, L. T. & Thal, D. R. Vascular pathology in the aged human brain. *Acta Neuropathol* **119**, 277-290, doi:10.1007/s00401-010-0652-7 (2010).
81 The LADIS Group. 2001–2011: A Decade of the LADIS (Leukoaraiosis And DISability) Study: What Have We Learned about White Matter Changes and Small-Vessel Disease? *Cerebrovascular Diseases* **32**, 577-588 (2011).
82 Fang, M. *et al.* Microbleeds and Silent Brain Infarctions Are Differently Associated with Cognitive Dysfunction in Patients with Advanced Periventricular Leukoaraiosis. *J Med Sci* **10**, 1307-1313 (2013).
83 Schulz, U. G., Grüter, B. E., Briley, D. & Rothwell, P. M. Leukoaraiosis and Increased Cerebral Susceptibility to Ischemia: Lack of Confounding by Carotid Disease. *Journal of the American Heart Association* **2** (2013).
84 Tveiten, A., Ljøstad, U., Mygland, Å. & Naess, H. Leukoaraiosis is Associated with Short- and Long-term Mortality in Patients with Intracerebral Hemorrhage. *Journal of*

Stroke and Cerebrovascular Diseases, doi:http://dx.doi.org/10.1016/j.jstrokecerebrovasdis.2013.01.017 (2013).
85 Gurol, M. E. *et al.* Cerebral amyloid angiopathy burden associated with leukoaraiosis: A positron emission tomography/magnetic resonance imaging study. *Annals of Neurology* **73**, 529-536, doi:10.1002/ana.23830 (2013).
86 Viswanathan, A. *et al.* Tissue Microstructural Changes Are Independently Associated With Cognitive Impairment in Cerebral Amyloid Angiopathy. *Stroke* **39**, 1988-1992 (2008).
87 Wardlaw, J. M. *et al.* Neuroimaging standards for research into small vessel disease and its contribution to ageing and neurodegeneration. *The Lancet Neurology* **12**, 822-838, doi:http://dx.doi.org/10.1016/S1474-4422(13)70124-8 (2013).
88 Smith, E. E., Schneider, J. A., Wardlaw, J. M. & Greenberg, S. M. Cerebral microinfarcts: the invisible lesions. *The Lancet Neurology* **11**, 272-282, doi:http://dx.doi.org/10.1016/S1474-4422(11)70307-6 (2012).
89 van Veluw, S. J. *et al.* In vivo detection of cerebral cortical microinfarcts with high-resolution 7T MRI. *J Cereb Blood Flow Metab* **33**, 322-329, doi:http://www.nature.com/jcbfm/journal/v33/n3/suppinfo/jcbfm2012196s1.html (2013).
90 Auriel, E. *et al.* Characteristic distributions of intracerebral hemorrhage–associated diffusion-weighted lesions. *Neurology* **79**, 2335-2341 (2012).
91 Johnson, K. A. *et al.* Imaging of amyloid burden and distribution in cerebral amyloid angiopathy. *Annals of Neurology* **62**, 229-234, doi:10.1002/ana.21164 (2007).
92 Ly, J. V. *et al.* 11C-PIB binding is increased in patients with cerebral amyloid angiopathy–related hemorrhage. *Neurology* **74**, 487-493 (2010).
93 Davis-Salinas, J., Saporito-Irwin, S. M., Cotman, C. W. & Van Nostrand, W. E. Amyloid β-Protein Induces Its Own Production in Cultured Degenerating Cerebrovascular Smooth Muscle Cells. *Journal of Neurochemistry* **65**, 931-934, doi:10.1046/j.1471-4159.1995.65020931.x (1995).
94 Iadecola, C. & Nedergaard, M. Glial regulation of the cerebral microvasculature. *Nat Neurosci* **10**, 1369-1376 (2007).
95 Prewitt, R. L., Rice, D. C. & Dobrian, A. D. Adaptation of Resistance Arteries to Increases in Pressure. *Microcirculation* **9**, 295-304, doi:10.1038/sj.mn.7800143 (2002).
96 Williams, L. R. & Leggett, R. W. Reference values for resting blood flow to organs of man. *Clinical Physics and Physiological Measurement* **10**, 187 (1989).
97 Hossmann, K.-A. Pathophysiology and Therapy of Experimental Stroke. *Cellular and Molecular Neurobiology* **26**, 1055-1081, doi:10.1007/s10571-006-9008-1 (2006).
98 Peters, A., Palay, S. & Webster, H. D. *The Fine Structures of the Nervous System*. 494 (Oxford University Press, 1991).
99 Iadecola, C. Neurovascular regulation in the normal brain and in Alzheimer's disease. *Nat Rev Neurosci* **5**, 347-360 (2004).
100 Nedergaard, M., Ransom, B. & Goldman, S. A. New roles for astrocytes: Redefining the functional architecture of the brain. *Trends in Neurosciences* **26**, 523-530, doi:http://dx.doi.org/10.1016/j.tins.2003.08.008 (2003).
101 Paulson, O. B. & Newman, E. A. Does the Release of Potassium from Astrocyte Endfeet Regulate Cerebral Blood Flow? *Science* **237**, 896-898 (1987).

102 Harder, D. R., Zhang, C. & Gebremedhin, D. Astrocytes Function in Matching Blood Flow to Metabolic Activity. *Physiology* **17**, 27-31 (2002).
103 Rubio, R., Berne, R. M., Bockman, E. L. & Curnish, R. R. Relationship between adenosine concentration and oxygen supply in rat brain. *American Journal of Physiology -- Legacy Content* **228**, 1896-1902 (1975).
104 Faraci, F. M. & Heistad, D. D. Regulation of the Cerebral Circulation: Role of Endothelium and Potassium Channels. *Physiological Reviews* **78**, 53-97 (1998).
105 Wang, Z., Natté, R., Berliner, J. A., van Duinen, S. G. & Vinters, H. V. Toxicity of Dutch (E22Q) and Flemish (A21G) Mutant Amyloid-β Proteins to Human Cerebral Microvessel and Aortic Smooth Muscle Cells. *Stroke* **31**, 534-538, doi:10.1161/01.str.31.2.534 (2000).
106 Herzig, M. C., Van Nostrand, W. E. & Jucker, M. Mechanism of Cerebral β-Amyloid Angiopathy: Murine and Cellular Models. *Brain Pathology* **16**, 40-54, doi:10.1111/j.1750-3639.2006.tb00560.x (2006).
107 Della Bianca, V., Dusi, S., Bianchini, E., Dal Prà, I. & Rossi, F. β-Amyloid Activates the O2 Forming NADPH Oxidase in Microglia, Monocytes, and Neutrophils: A Possible Inflammatory Mechanism of Neuronal Damage in Alzheimer's Disease. *Journal of Biological Chemistry* **274**, 15493-15499 (1999).
108 Abramov, A. Y., Canevari, L. & Duchen, M. R. β-Amyloid Peptides Induce Mitochondrial Dysfunction and Oxidative Stress in Astrocytes and Death of Neurons through Activation of NADPH Oxidase. *The Journal of Neuroscience* **24**, 565-575 (2004).
109 Shin, H. K. *et al.* Age-dependent cerebrovascular dysfunction in a transgenic mouse model of cerebral amyloid angiopathy. *Brain* **130**, 2310-2319, doi:10.1093/brain/awm156 (2007).
110 Niwa, K., Carlson, G. A. & Iadecola, C. Exogenous Aβ1-40 Reproduces Cerebrovascular Alterations Resulting From Amyloid Precursor Protein Overexpression in Mice. *J Cereb Blood Flow Metab*\ **20**, 1659-1668 (2000).
111 Ogawa, S., Lee, T. M., Kay, A. R. & Tank, D. W. Brain magnetic resonance imaging with contrast dependent on blood oxygenation. *Proceedings of the National Academy of Sciences* **87**, 9868-9872 (1990).
112 Pauling, L. & Coryell, C. D. The Magnetic Properties and Structure of Hemoglobin, Oxyhemoglobin and Carbonmonoxyhemoglobin. *Proceedings of the National Academy of Sciences* **22**, 210-216 (1936).
113 Heeger, D. J. & Ress, D. What does fMRI tell ys about neuronal activity? *Nature Reviews Neuroscience* **3**, 142-151, doi:10.1038/nrn730 (2002).
114 Hu, X. & Yacoub, E. The story of the initial dip in fMRI. *NeuroImage* **62**, 1103-1108, doi:http://dx.doi.org/10.1016/j.neuroimage.2012.03.005 (2012).
115 Devor, A. *et al.* Stimulus-Induced Changes in Blood Flow and 2-Deoxyglucose Uptake Dissociate in Ipsilateral Somatosensory Cortex. *The Journal of Neuroscience* **28**, 14347-14357 (2008).
116 Buxton, R. B. Dynamic models of BOLD contrast. *NeuroImage* **62**, 953-961, doi:http://dx.doi.org/10.1016/j.neuroimage.2012.01.012 (2012).
117 Zhu, X.-H. *et al.* Simultaneous oxygenation and perfbsion imaging study of functional activity in primary visual cortex at different visual stimulation frequency: Quantitative

correlation between BOLD and CBF changes. *Magnetic Resonance in Medicine* **40**, 703-711, doi:10.1002/mrm.1910400510 (1998).

118 Silva, A. C., Lee, S.-P., Yang, G., Iadecola, C. & Kim, S.-G. Simultaneous Blood Oxygenation Level-Dependent and Cerebral Blood Flow Functional Magnetic Resonance Imaging During Forepaw Stimulation in the Rat. *J Cereb Blood Flow Metab* **19**, 871-879 (1999).

119 Kwong, K. K. *et al.* Dynamic magnetic resonance imaging of human brain activity during primary sensory stimulation. *Proceedings of the National Academy of Sciences* **89**, 5675-5679 (1992).

120 Brewer, A. A., Press, W. A., Logothetis, N. K. & Wandell, B. A. Visual Areas in Macaque Cortex Measured Using Functional Magnetic Resonance Imaging. *The Journal of Neuroscience* **22**, 10416-10426 (2002).

121 Stiers, P., Peeters, R., Lagae, L., Van Hecke, P. & Sunaert, S. Mapping multiple visual areas in the human brain with a short fMRI sequence. *NeuroImage* **29**, 74-89, doi:http://dx.doi.org/10.1016/j.neuroimage.2005.07.033 (2006).

122 Park, L. *et al.* Age-Dependent Neurovascular Dysfunction and Damage in a Mouse Model of Cerebral Amyloid Angiopathy. *Stroke* (2014).

123 Thomas, T., Thomas, G., McLendon, C., Sutton, T. & Mullan, M. β-Amyloid-mediated vasoactivity and vascular endothelial damage. *Nature* **380**, 168-171 (1996).

124 Alsop, D. C., Detre, J. A. & Grossman, M. Assessment of cerebral blood flow in Alzheimer's disease by spin-labeled magnetic resonance imaging. *Annals of Neurology* **47**, 93-100, doi:10.1002/1531-8249(200001)47:1<93::aid-ana15>3.0.co;2-8 (2000).

125 Bär, K.-J. *et al.* Influence of Galantamine on Vasomotor Reactivity in Alzheimer's Disease and Vascular Dementia Due to Cerebral Microangiopathy. *Stroke* **38**, 3186-3192 (2007).

126 Gucuyener, D. O. *et al.* An Analysis of Changes in Cerebral Blood Flood Velocities in Depressive Pseudo-Dementia and Alzheimer Disease Patients. *Neurologist* **16**, 358-363 (2010).

127 Cantin, S. *et al.* Impaired cerebral vasoreactivity to CO2 in Alzheimer's disease using BOLD fMRI. *NeuroImage* **58**, 579-587, doi:http://dx.doi.org/10.1016/j.neuroimage.2011.06.070 (2011).

128 Yamaguchi, F., Meyer, J. S., Yamamoto, M., Sakai, F. & Shaw, T. Noninvasive regional cerebral blood flow measurements in dementia. *Archives of Neurology* **37**, 410-418, doi:10.1001/archneur.1980.00500560040003 (1980).

129 Jagust, W. J., Eberling, J. L., Reed, B. R., Mathis, C. A. & Budinger, T. F. Clinical Studies of Cerebral Blood Flow in Alzheimer's Disease. *Annals of the New York Academy of Sciences* **826**, 254-262, doi:10.1111/j.1749-6632.1997.tb48477.x (1997).

130 Zazulia, A. R., Videen, T. O., Morris, J. C. & Powers, W. J. Autoregulation of cerebral blood flow to changes in arterial pressure in mild Alzheimer's disease. *J Cereb Blood Flow Metab* **30**, 1883-1889, doi:http://www.nature.com/jcbfm/journal/v30/n11/suppinfo/jcbfm2010135s1.html (2010).

131 Weller, R., Boche, D. & Nicoll, J. R. Microvasculature changes and cerebral amyloid angiopathy in Alzheimer's disease and their potential impact on therapy. *Acta Neuropathol* **118**, 87-102, doi:10.1007/s00401-009-0498-z (2009).

132 Smith, E. E. *et al.* Impaired visual evoked flow velocity response in cerebral amyloid angiography. *Neurology* **71**, 1424-1430, doi:10.1212/01.wnl.0000327887.64299.a4 (2008).
133 Morris, J. C. The Clinical Dementia Rating (CDR): current version and scoring rules. *Neurology* **43**, 2412-2414 (1993).
134 Mungas, D. Iii-office mental status testing: A practical guide. *Geriatrics* **46** (1991).
135 Albert, M. S. *et al.* The diagnosis of mild cognitive impairment due to Alzheimer's disease: Recommendations from the National Institute on Aging-Alzheimer's Association workgroups on diagnostic guidelines for Alzheimer's disease. *Alzheimer's & Dementia* **7**, 270-279, doi:http://dx.doi.org/10.1016/j.jalz.2011.03.008 (2011).
136 Society, A. C. N. Guidline 9B: Guidlines on visual evoked potentials. *journal of Clinical Neurophysiology* **23**, 138-156 (2006).
137 Odom, J., Leys, M. & Weinstein, G. in *Duane's Opthalmology* (eds W Tasman & EA Jaegar) Ch. 5, (Lippincott Williams & Wilkins, 2006).
138 Bonmassar, G. A., K; Ives, J; Belliveau, J W. Visual evoked potentials (VEP) measured by simultaneous 64-channel EEG and 3T fMRI. *Neuroreport* **10**, 1893-1897 (1999).
139 Zaletel, M. S., M; Pretnar-Oblak, J; Zvan, B. Age-related changes in the relationship between visual evoked potentials and visually evoked cerebral blood flow velocity responses. *Functional Neurology* **20**, 115-120 (2005).
140 Walsh, P., Kane, N. & Butler, S. The clinical role of evoked potentials. *Journal of Neurology, Neurosurgery & Psychiatry* **76**, ii16-ii22 (2005).
141 Smith, S. M. Fast robust automated brain extraction. *Human Brain Mapping* **17**, 143-155 (2002).
142 Jenkinson, M., Bannister, P., Brady, J. M. & Smith, S. M. Improved Optimisation for the Robust and Accurate Linear Registration and Motion Correction of Brain Images. *NeuroImage* **17**, 825-841 (2002).
143 Worsley, K. J. in *Functional MRI: An Introduction to Methods* (eds P. Jezzard, P.M. Matthews, & S.M. Smith) Ch. 14, (Oxford University Press, 2001).
144 Hensen, R. in *Human Brain Function* (eds J Ashburner, K Friston, & W Penny).
145 Jenkinson, M., Beckmann, C. F., Behrens, T. E. J., Woolrich, M. W. & Smith, S. M. FSL. *NeuroImage* **62**, 782-790, doi:http://dx.doi.org/10.1016/j.neuroimage.2011.09.015 (2012).
146 Ward, B. D. in *Biophysics Research Institute Medical College of Wisconsin* (2000).
147 Kosior, J. C. *et al.* Quantomo: validation of a computer-assisted methodology for the volumetric analysis of intracerebral haemorrhage. *International Journal of Stroke* **6**, 302-305, doi:10.1111/j.1747-4949.2010.00579.x (2011).
148 Zar, J. H. in *Biostatistical Analysis* Ch. 11, (Pearson Prentice Hall, 2009).
149 Smith, E. E., Egorova, S., Blacker, D. & et al. MAgnetic resonance imaging white matter hyperintensities and brain volume in the prediction of mild cognitive impairment and dementia. *Archives of Neurology* **65**, 94-100, doi:10.1001/archneurol.2007.23 (2008).
150 Holland, C. M. *et al.* Spatial Distribution of White-Matter Hyperintensities in Alzheimer Disease, Cerebral Amyloid Angiopathy, and Healthy Aging. *Stroke* **39**, 1127-1133 (2008).

151 Gebeily, S. *et al.* Cerebral white matter hyperintensities (WMH): an analysis of cerebrovascular risk factors in Lebanon. *International Journal of Neuroscience* **0**, null, doi:doi:10.3109/00207454.2014.884087.
152 Chao, L. L. *et al.* Patterns of cerebral hypoperfusion in amnestic and dysexecutive MCI. *Alzheimer disease and associated disorders* **23**, 245 (2009).
153 Nobili, F. *et al.* Amnestic mild cognitive impairment in Parkinson's disease: A brain perfusion SPECT study. *Movement Disorders* **24**, 414-421, doi:10.1002/mds.22381 (2009).
154 Vazquez, A. L. *et al.* Vascular dynamics and BOLD fMRI: CBF level effects and analysis considerations. *NeuroImage* **32**, 1642-1655, doi:http://dx.doi.org/10.1016/j.neuroimage.2006.04.195 (2006).
155 Chalmers, K., Wilcock, G. K. & Love, S. APOEε4 influences the pathological phenotype of Alzheimer's disease by favouring cerebrovascular over parenchymal accumulation of Aβ protein. *Neuropathology and Applied Neurobiology* **29**, 231-238, doi:10.1046/j.1365-2990.2003.00457.x (2003).
156 Vinters, H. V. & Gilbert, J. J. Cerebral amyloid angiopathy: incidence and complications in the aging brain. II. The distribution of amyloid vascular changes. *Stroke* **14**, 924-928 (1983).
157 Amunts, K., Malikovic, A., Mohlberg, H., Schormann, T. & Zilles, K. Brodmann's Areas 17 and 18 Brought into Stereotaxic Space—Where and How Variable? *NeuroImage* **11**, 66-84, doi:http://dx.doi.org/10.1006/nimg.1999.0516 (2000).
158 Stefanova, I. *et al.* Age-related changes of blood-oxygen-level–dependent signal dynamics during optokinetic stimulation. *Neurobiology of Aging* **34**, 2277-2286, doi:http://dx.doi.org/10.1016/j.neurobiolaging.2013.03.031 (2013).
159 Bennett, C. M. & Miller, M. B. How reliable are the results from functional magnetic resonance imaging? *Annals of the New York Academy of Sciences* **1191**, 133-155, doi:10.1111/j.1749-6632.2010.05446.x (2010).
160 Raemaekers, M., du Plessis, S., Ramsey, N. F., Weusten, J. M. H. & Vink, M. Test-retest variability underlying fMRI measurements. *NeuroImage* **60**, 717-727, doi:http://dx.doi.org/10.1016/j.neuroimage.2011.11.061 (2012).
161 Chen, Y. W. *et al.* Progression of white matter lesions and hemorrhages in cerebral amyloid angiopathy. *Neurology* **67**, 83-87 (2006).
162 Gabryelewicz, T. *et al.* The rate of conversion of mild cognitive impairment to dementia: predictive role of depression. *International Journal of Geriatric Psychiatry* **22**, 563-567, doi:10.1002/gps.1716 (2007).
163 Rost, N. *et al.* White matter hyperintensity volume is increased in small vessel stroke subtypes. *Neurology* **75**, 1670-1677 (2010).
164 Wardlaw, J. M. *et al.* Vascular risk factors, large-artery atheroma, and brain white matter hyperintensities. *Neurology* **82**, 1331-1338 (2014).
165 Klunk, W. E. *et al.* Imaging brain amyloid in Alzheimer's disease with Pittsburgh Compound-B. *Annals of Neurology* **55**, 306-319, doi:10.1002/ana.20009 (2004).
166 Kastrup, A., Krüger, G., Neumann-Haefelin, T. & Moseley, M. E. Assessment of cerebrovascular reactivity with functional magnetic resonance imaging: comparison of CO2 and breath holding. *Magnetic Resonance Imaging* **19**, 13-20, doi:http://dx.doi.org/10.1016/S0730-725X(01)00227-2 (2001).

167 van der Zande, F. H. R., Hofman, P. A. M. & Backes, W. H. Mapping hypercapnia-induced cerebrovascular reactivity using BOLD MRI. *Neuroradiology* **47**, 114-120, doi:10.1007/s00234-004-1274-3 (2005).
168 Stefanovic, B., Warnking, J. M., Rylander, K. M. & Pike, G. B. The effect of global cerebral vasodilation on focal activation hemodynamics. *NeuroImage* **30**, 726-734, doi:http://dx.doi.org/10.1016/j.neuroimage.2005.10.038 (2006).
169 Wise, R. G. *et al.* Dynamic forcing of end-tidal carbon dioxide and oxygen applied to functional magnetic resonance imaging. *J Cereb Blood Flow Metab* **27**, 1521-1532 (2007).
170 Mandell, D. M. *et al.* Mapping Cerebrovascular Reactivity Using Blood Oxygen Level-Dependent MRI in Patients With Arterial Steno-occlusive Disease: Comparison With Arterial Spin Labeling MRI. *Stroke* **39**, 2021-2028 (2008).
171 Bright, M. G., Bulte, D. P., Jezzard, P. & Duyn, J. H. Characterization of regional heterogeneity in cerebrovascular reactivity dynamics using novel hypocapnia task and BOLD fMRI. *NeuroImage* **48**, 166-175, doi:http://dx.doi.org/10.1016/j.neuroimage.2009.05.026 (2009).
172 Yezhuvath, U. S., Lewis-Amezcua, K., Varghese, R., Xiao, G. & Lu, H. On the assessment of cerebrovascular reactivity using hypercapnia BOLD MRI. *NMR in Biomedicine* **22**, 779-786, doi:10.1002/nbm.1392 (2009).